CALIFORNIA ENERGY COMMISSION

Energy Research and Development Division

FINAL PROJECT REPORT

Performance-Based Earthquake Engineering Assessment Tool for Natural Gas Storage and Pipeline Systems

Task D – Seismic Response of Pipeline and Gas Storage Surface Infrastructure

Gavin Newsom, Governor

July 2022

PREPARED BY:

Primary Authors:
Elide Pantoli, Tara C. Hutchinson

University of California, San Diego
9500 Gilman Drive, La Jolla (CA) 92093
(858) 822-2273
https://se.ucsd.edu

Sherif Elfass, David McCallen

University of Nevada Reno
1664 N. Virginia Street, Reno, NV 89557
(775) 784-1110
https://www.unr.edu/cee

Contract Number: PIR-18-003

PREPARED FOR:
California Energy Commission

Yahui Yang
Project Manager

Laurie ten Hope
Deputy Director
ENERGY RESEARCH AND DEVELOPMENT DIVISION

Drew Bohan
Executive Director

ACKNOWLEDGEMENTS

The Performance-Based Earthquake Engineering Assessment Tool for Natural Gas Storage and Pipeline Systems project is led by Professor Jonathan Bray at the University of California Berkeley, with partners at the University of California Berkeley, University of Nevada Reno (UNR), Lawrence Berkeley National Laboratories (LBNL), University of California (UC) San Diego, NHERI SimCenter at UC Berkeley, and Slate Geotechnical Consultants and its subcontractors Lettis Consultants International (LCI) and Thomas O'Rourke. The authors are grateful for the technical input and advice from all members of the project team, and especially Professor Thomas O'Rourke of Cornell University. The authors are also grateful for the support of the staff at the UC San Diego and UNR Laboratories; donations of materials by University Mechanical and Engineering Contractors (UMEC) of El Cajon, California and SoCalGas; and fabrication and delivery of the component specimens tested at UC San Diego by UMEC.

This research study was funded by the California Energy Commission, under Contract No. PIR 18-003. The opinions, findings, conclusions, and recommendations expressed in this publication are those of the authors and do not necessarily reflect the view of California Energy Commission and its employees, the State of California, the Pacific Earthquake Engineering Research (PEER) Center, and the Regents of the University of California.

PREFACE

The California Energy Commission's (CEC) Energy Research and Development Division manages the Natural Gas Research and Development Program, which supports energy-related research, development, and demonstration not adequately provided by competitive and regulated markets. These natural gas research investments spur innovation in energy efficiency, renewable energy and advanced clean generation, energy-related environmental protection, energy transmission and distribution and transportation.

The Energy Research and Development Division conducts this public interest natural gas-related energy research by partnering with RD&D entities, including individuals, businesses, utilities and public and private research institutions. This program promotes greater natural gas reliability, lower costs and increases safety for Californians and is focused in these areas:

- Buildings End-Use Energy Efficiency.
- Industrial, Agriculture and Water Efficiency
- Renewable Energy and Advanced Generation
- Natural Gas Infrastructure Safety and Integrity.
- Energy-Related Environmental Research
- Natural Gas-Related Transportation.

Task D: Final Report – Seismic Response of Pipeline and Gas Storage Surface Infrastructure is an interim report for the Performance-Based Earthquake Engineering Assessment Tool for Natural Gas Storage and Pipeline Systems project (PIR-18-003) conducted by the University of California, Berkeley. The information from this project contributes to the Energy Research and Development Division's Natural Gas Research and Development Program.

For more information about the Energy Research and Development Division, please visit the CEC's research website (www.energy.ca.gov/research/) or contact the CEC at 916-327-1551.

ABSTRACT

This report is one of a series of reports documenting the methods and findings of a multi-year, multi-disciplinary project conducted by the Pacific Earthquake Engineering Research Center (PEER) with the Lawrence Berkeley National Laboratory (LBNL), and funded by the California Energy Commission (CEC). The overall project is titled "*Performance-based Earthquake Engineering Assessment Tool for Natural Gas Storage and Pipeline Systems*" henceforth referred to as the "*OpenSRA* Project."

The overall goal of the *OpenSRA* project is to create an open-source research-based seismic risk assessment tool for natural gas infrastructure that can be used by utility stakeholders to better understand state-wide risks, prioritize mitigation, plan new gas infrastructure, and help focus post-earthquake repair work.

The project team includes researchers from LBNL, UC Berkeley, UC San Diego, University of Nevada Reno, the NHERI SimCenter at UC Berkeley, and Slate Geotechnical Consultants and its subcontractors Lettis Consultants International (LCI) and Thomas O'Rourke. Focused research to advance the seismic risk assessment tool was conducted by Task Groups, each addressing a particular area of study and expertise, and collaborating with the other Task Groups.

This report is the product of Task Group D: Seismic response of pipeline and gas storage surface infrastructure. The scope of this report is to describe the approach used to analyze the surface infrastructure and present highlights of the key outcomes.

Keywords: gas piping, seismic fragility functions, surface piping, surface infrastructure, gas facilities

Please use the following citation for this report:

Pantoli, E., Hutchinson, T.C., Elfass, S.A., and McCallen, D.B. 2022. *Performance-Based Earthquake Engineering Assessment Tool for Natural Gas Storage and Pipeline Systems, Task D Final Report - Seismic Response of Pipeline and Gas Storage Surface Infrastructure*. California Energy Commission.

TABLE OF CONTENTS

Page

LIST OF FIGURES

Page

LIST OF TABLES

EXECUTIVE SUMMARY

Introduction

This report is one of a series of reports documenting the methods and findings of a multi-year, multi-disciplinary project conducted by the Pacific Earthquake Engineering Research Center (PEER) with the Lawrence Berkeley National Laboratory (LBNL), and funded by the California Energy Commission (CEC). The overall project is titled "*Performance-based Earthquake Engineering Assessment Tool for Natural Gas Storage and Pipeline Systems*" henceforth referred to as the "*OpenSRA* Project."

The overall goal of the *OpenSRA* project is to create an open-source research-based seismic risk assessment tool for natural gas infrastructure that can be used by utility stakeholders to better understand state-wide risks, prioritize mitigation, plan new gas infrastructure, and help focus post-earthquake repair work.

The project team includes researchers from LBNL, UC Berkeley, UC San Diego, University of Nevada Reno, the NHERI SimCenter at UC Berkeley, and Slate Geotechnical Consultants and its subcontractors Lettis Consultants International (LCI) and Thomas O'Rourke of Cornell University. Focused research to advance the seismic risk assessment tool was conducted by Task Groups, each addressing a particular area of study and expertise, and collaborating with the other Task Groups.

This report presents the work conducted by Task Group D: Seismic response of pipeline and gas storage surface infrastructure. The natural gas infrastructure in California comprises both underground and surface systems. The underground infrastructure includes hundreds of miles of pipelines and storage fields, where the gas is injected/withdrawn from underground reservoirs through casing and tubing systems. The surface infrastructure includes river crossings, service risers and gas meter units connected to consumers buildings as well as various facilities, such as storage field facilities, metering and pressure regulating stations, and compressor stations. Surface infrastructure generally contains similar components and subsystems such as tanks, pressure vessels, a network of steel pipelines on supports, tees, elbows, and bolted flange joints. However, the configuration and geometry will certainly vary depending on the type of surface infrastructure, rendering their analysis different from that undertaken to evaluate the performance of underground infrastructure.

Most of the systems of the surface natural gas infrastructure, as well as similar industrial systems and lifelines, have demonstrated good seismic performance during past earthquakes. However, some have repeatedly exhibited seismic vulnerability. For example, earthquake damage to industrial facilities including toppling of tall and heavy vessels or pieces of equipment, damage to pipe-to-vessels connections and damage to liquid-filled tanks are amongst the more common vulnerabilities observed. It is noted that many of these observations are not specific to California, since the State has not had a major earthquake in decades. Because of this, it is unknown whether some of the newer technologies used in California might have additional vulnerabilities.

To address the known and unknown seismic vulnerabilities of industrial systems, with the goal of improving their overall seismic performance, researchers have conducted shake table experiments on subsystems, pseudo-static tests on components, including pipe elbows and other connections, and complementary numerical analysis using refined finite element analysis software. While these efforts provide invaluable insight to understand the seismic behavior of the surface natural gas infrastructure in California, there are limitations. Importantly, most prior studies did not focus specifically on the natural gas infrastructure, but on similar types of industrial facilities. For example, they focused on liquid-filled rather than gas-filled piping subsystems and components; and they did not study the effect of very large internal pressure. In addition, prior studies have been performed mostly in Europe and Japan, where the design requirements as well as the materials and technology used are likely different from US practice. Notably lacking in prior investigations are consideration of 4 in Schedule 80 pipes and fittings, which are typically used in high-pressure facilities such as storage fields, and wellhead trees.

Task Purpose

Due to the complexity, extent, and variability of the surface natural gas infrastructure in California, as well as the limited detailed information on many of its systems, a detailed seismic analysis on all parts of this infrastructure is impractical. Early input from the project's Technical Advisory Committee (TAC) rendered a focus of the present effort towards studying the seismic behavior of high-pressure high-gas volume facilities, such as storage field facilities. Seismic damage to these facilities could lead to loss of lives, extensive pollution as well as disruption of natural gas service for millions of Californians. It is also worth noting that feedback from the TAC indicated that, to allow focus within the present study, this Task Group should not focus on the behavior of service risers and meter sets or other parts of the distribution system. Moreover, a survey of the natural gas pipelines crossing rivers in the State indicated that the vast majority do so underground, and hence it was decided not to focus on studying pipelines crossing rivers.

Each of the storage field facilities in California is unique and contains many subsystems with different features. For example, each includes horizontal and vertical pressure vessels of different heights, thickness and anchoring type; networks of steel pipelines with different diameters, schedules and support types; wellhead trees with different heights and masses connected to pipes with different geometries. Hence, with the guidance of the TAC, Task Group D provides two primary results, namely: 1) the fragility assessment of select key subsystems that were identified as either lacking prior studies (wellhead trees and connected piping) or demonstrating past vulnerability (tall and vertical pressure vessels and connected piping) and 2) a framework and supporting information to allow future researchers to extend the fragility assessment to components and subsystems of the surface natural gas infrastructure, considering varying features.

Project Approach

The results outlined above were approached through a combination of two experimental campaigns and complementary numerical analyses performed with two different finite element analysis platforms. Five different outcomes were achieved, as explained below.

- **Outcome #1:** Providing experimental data on the behavior of critical *components*. The components selected for testing were 4 in diameter Schedule 80 and 8 in diameter Schedule 40 straight tees and elbows. The specimens containing these components were gas pressurized and subjected to a displacement-controlled reversed cyclic testing protocol at the Powell Laboratories at the University of California (UC), San Diego. These specimens were provided and assembled by local manufacturers; hence their material property, technology, and geometry reflect California practice. From these tests, limit states and damage progression of these critical components were documented. In addition, displacements, forces, and strains were measured and utilized to calibrate and validate high-fidelity numerical models used to develop fragility curves for *OpenSRA*. Data obtained during the experimental campaign from analog sensors and digital cameras can be used by other researchers or as educational material.
- **Outcome #2:** Obtaining experimental data on the seismic behavior of *subsystems*. Because of the large variability of subsystems at critical facilities, a generic subsystem, which included select vulnerable components observed in the field, was designed and tested at full-scale on the pair of shake tables at the University of Nevada, Reno (UNR). The design of the setup was finalized with input from the TAC. Complementary to the UC San Diego component tests, the subsystem tested at UNR included 4 in diameter Schedule 80 pipes, 8 in diameter Schedule 40 pipes, elbows, tees, and in addition reducers, bolted flange joints and a model-scale vessel. It was constructed by local manufacturers who commonly construct such subsystems in practice. This subsystem was gas pressurized and subjected to both synchronous and asynchronous earthquake motions. In the latter case, a relative displacement was induced between the shake tables. Results from these tests could help utility companies screen out components with a low probably of seismic damage. In addition, the data from cameras and more than 150 analog sensor channels is available to researchers interested in validating numerical models of subsystems.
- **Outcome #3:** Obtaining calibrated nonlinear steel properties to be used within high-fidelity finite element analysis software. During earthquakes, critical components of the surface infrastructure such as steel elbows and tees are subjected to a cyclic loading, which could induce large plastic strains. Hence, to analyze the seismic behavior of these components it is essential to have a reliable nonlinear steel model, and a robust hardening model. The experimental results obtained from the component tests described in outcome #1 provided essential data to calibrate and validate important nonlinear properties of the steel typically used for tees and elbows in California. In this work, this effort was undertaken using 3D finite element models constructed in the high-fidelity Finite Element Analysis (FEA) platform Abaqus. These properties were then used to investigate the behavior under geometric, material, and load conditions beyond the scope of the test program (e.g. high internal pressure). Interested researchers can now use these material properties to reliably model the nonlinear cyclic behavior of different steel pipe components.
- **Outcome#4:** Developing a general procedure for the seismic analysis of surface subsystems and parametric models for two specific subsystems in a general-purpose

finite element software. The procedure developed can be used to generate seismic fragility curves for different subsystems with a generic or specific geometry. This procedure was demonstrated via application of two critical subsystems identified, namely: 1) wellhead trees and connected piping (WTP), and 2) vertical pressure vessels (VPV). The critical components of piping of the WTP subsystem were calibrated using the results from Outcome #3. In this work, this effort was undertaken using 2D finite element models constructed in the general-purpose finite element software OpenSees. Parametric models of these subsystems generated in OpenSees are available for future researchers.

- **Outcome #5:** Generating seismic fragility functions for select subsystems. For each of the subsystems analyzed, the most critical parameters were identified. The users of *OpenSRA* may assign values to these parameters or rely on built-in values, resulting in generation of fragility curves for a subsystem with either a specific or a generic geometry. In the latter, the uncertainty will inherently be larger.

  Fragility curves for the WTP subsystem were generated using three functions: one correlating the probability of failure to the damage measure (DM, strain in this case), the second providing the engineering demand parameter (EDP, peak rotations in this case) as a function of the DM, and the third correlating the EDP with some intensity measure (IM) of the input earthquake and selected key geometric parameters of the subsystem. The last two curves are generated through Abaqus and OpenSees models obtained in Outcome #3 and #4. Figure 1 presents a summary of the approach used to generate fragility curves for *OpenSRA* for the WTP subsystem. In the case of the VPV subsystem, fragility curves were generated comparing the demands obtained from OpenSees models and the capacities obtained from design calculations.

Figure 1: Overview of approach used to obtain fragility curves to be implemented in *OpenSRA* for surface subsystems

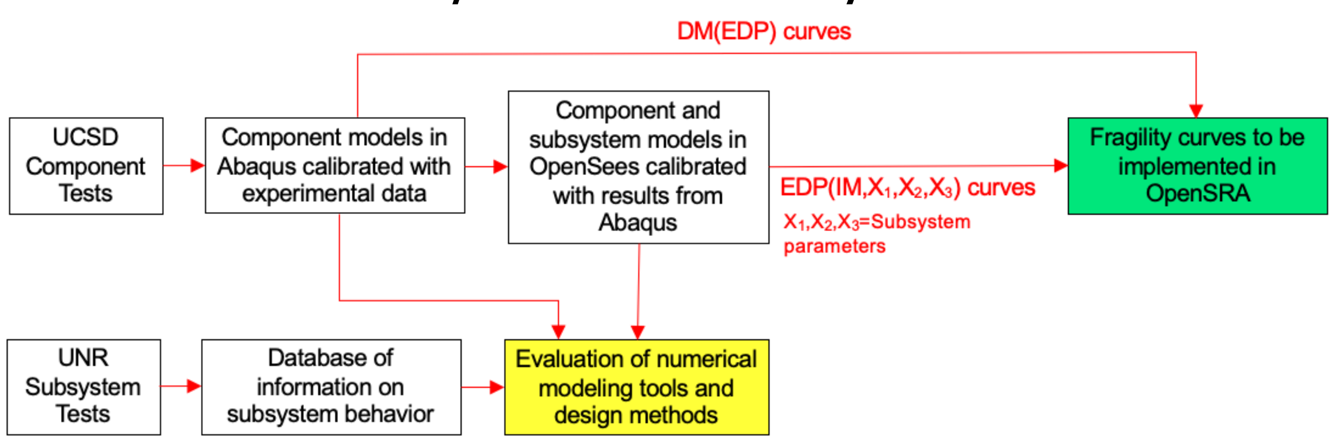

Project Results

The primary results for each outcome include the following:

- **Outcome #1.** All components tested at UC San Diego had a ductile failure with the exception of one. Ductile failures were characterized by the formation of a network of shallow cracks which, upon the application of continued displacement, developed into through-thickness cracks. Once through-thickness cracks developed, there was a complete and sudden loss of gas pressurization. All specimens which failed in a ductile manner demonstrated stable response to a joint rotation of at least ~10°. Rotations of more than 20° were measured for the 4 in diameter tee and 90° elbow tested. The locations of the cracks corresponded to the location of high strains identified by the pre-test numerical analyses conducted in Abaqus. The specimen which failed in a non-ductile fashion was an 8 in diameter Schedule 40 tee tested in-plane. In this case, a through-thickness crack formed suddenly in the body of the tee joint following attainment of a peak rotation of ~7°. While this rotation can still be considered relatively large, the observed non-ductile failure is reason for concern. In fact, not only did the ensuing through-thickness crack develop suddenly and with little warning, but it was also far from the location of high strains calculated by an Abaqus model.

- **Outcome #2.** The shake table tests confirmed that piping subsystems are generally not vulnerable to acceleration-induced damage. In fact, none of the components reached their yield limit state when the synchronous motions were applied. When asynchronous motions (i.e. relative displacement between the two shake tables) were applied, some of the critical components yielded, confirming that these subsystems can be sensitive to relative displacements. However, even at relatively large amplitudes of relative displacement between the shake tables, there was no visible damage or loss of pressure to the pipes or vessel. The final failure of this subsystem was characterized by a large region of spalling of concrete at one of the pipe run supports.
- **Outcome #3.** Task Group D was able to identify a set of optimal values of parameters needed to model the nonlinear hardening behavior of steel in Abaqus. Some of these parameters were obtained from the literature, while one was calibrated through the minimization of the error between the numerical and experimental results obtained from the component tests described in Outcome #1. Blind predictions using optimized material model parameters were able to predict both the global behavior of the components measured experimentally with minimal error, while also capturing local strains.
- **Outcome #4.** Natural frequencies and modes of the WTP and VPV subsystems obtained from OpenSees were compared with results from impact tests conducted at a gas storage facility and refined Abaqus models. In both cases, the OpenSees models were able to reasonably predict the dynamic characteristics of the subsystems.
- **Outcome #5.** The two subsystems under consideration are very different and thus their analysis varied.
  - WTP subsystem: Three different piping configurations were analyzed, and for each the critical component of the system was either the tee or the elbow in the pipes. The primary parameters identified for the different configurations include the height of the tree, the length of different pipe segments, and the weight of the valves in the pipe. The peak rotations of the critical components (either tees or elbows) of the pipes were defined as the EDP. The EDP(DM) curved was calculated using models of the component in Abaqus.

- VPV subsystem: For this subsystem, the following variables were considered: the height of the pressure vessel, its height-to-diameter ratio, the thickness of the vessel, and the flexibility of the base connection. The EDP used in this case was the ratio between the moment at the base of the vessel created by the earthquakes (demand) and the limiting moment capacity of the base connection. For example, for an assumed fixed connection, the moment associated with breakout of the concrete will occur at an early load stage. For the case of an assumed base connection designed with stretch length anchors, the strain in the anchors may lead to rotation of the top of the pressure vessel, which could limit functionality of attached piping.

It is noted that while the results in term of EDP(DM) curves are included in this report, the final fragility curves will be included in the System Wide Natural Gas Infrastructure Response and Fragility Model Report, forthcoming. Recommendations for future research are presented in the conclusion section of this report.

CHAPTER 1: Introduction

This report is one of a series of reports documenting the methods and findings of a multi-year, multi-disciplinary project conducted by the Pacific Earthquake Engineering Research Center (PEER) with the Lawrence Berkeley National Laboratory (LBNL), and funded by the California Energy Commission (CEC). The overall project is titled "*Performance-based Earthquake Engineering Assessment Tool for Natural Gas Storage and Pipeline Systems*" henceforth referred to as the "*OpenSRA* Project."

The overall goal of the *OpenSRA* project is to create an open-source research-based seismic risk assessment tool for natural gas infrastructure that can be used by utility stakeholders to better understand state-wide risks, prioritize mitigation, plan new gas infrastructure, and help focus post-earthquake repair work.

The probabilistic seismic risk tool developed in this project follows the widely-accepted risk methodology pioneered by Cornell (1968). A seismic source characterization is used to develop a suite of earthquake scenarios with associated rates of occurrence to represent the seismic hazard. Fault ruptures and the resulting ground deformation are generated for each earthquake scenario to represent the seismic loading, which includes a map of ground motion parameters. This scenario-based seismic parameter map is overlaid on the infrastructure system and the seismic loading combined with the capacities of the infrastructure to calculate the seismic performance of the natural gas system for the scenario. By repeating the process for all scenarios in the suite, the tool can evaluate the seismic risk to the system.

A user-driven research approach was used to develop *OpenSRA* to be used easily by regulators and utilities, and to include updated models and methods for the seismic demands and capacities that control the seismic risk for natural gas systems. The project includes several innovative approaches that improve the basic methodology and distinguish this project's approach from standard approaches currently used. Current risk studies developed by the utilities use risk scoring approaches that are highly subjective and qualitative. They do not properly incorporate the uncertainties in the seismic demand and in the fragility of the system and its components. Targeted research was conducted in this project to improve the characterization of uncertainty of key inputs to the seismic risk assessment tool. The seismic risk methodology employed in this project provides quantitative estimates of the probabilistic seismic risk. For risk-informed decision-making processes, the reliability of the risk estimates needs to be considered because this can be significant, particularly for large rare earthquakes.

The project team includes researchers from LBNL, UC Berkeley, UC San Diego, University of Nevada, Reno, the NHERI SimCenter at UC Berkeley, and Slate Geotechnical Consultants and its subcontractors Lettis Consultants International (LCI) and Thomas O'Rourke. Focused research to advance the seismic risk assessment tool was conducted by Task Groups, each addressing a particular area of study and expertise, and collaborating with the other Task Groups. The Task Groups are as follows:

- Task A: Fault Displacement
- Task B: Liquefaction-induced deformation and seismically induced slope displacement
- Task C: Performance of natural gas storage well casings and caprock
- Task D: Seismic response of pipeline and gas storage surface infrastructure
- Task E: Smart gas infrastructure sensing of wells and pipeline connections performance
- Task F: Synthesis of component fragilities into a system performance model

This report is the product of Task Group D: Seismic response of pipeline and gas storage surface infrastructure, and the scope of this report is to describe the approach used to analyze the surface infrastructure and present some of the key outcomes.

Description of Surface Infrastructure

California produces less than 10% of the natural gas consumed in the state, while most of the natural gas used in California is produced in the Southwest, Rocky Mountains Region and Western Canada. It enters California through interstate pipe networks from Arizona, Nevada and Oregon (EIA 2021). Natural gas coming from across state lines is moved interstate via transmission pipelines. These pipelines are generally referred to as California's "backbone" pipeline system (CPUC 2022). From these backbone pipelines, natural gas either enters local transmission and distribution pipelines, or is sent to natural gas storage fields, which are used to store gas and maintain an adequate supply throughout the year (CPUC 2022). In California there are 12 natural gas storage fields, which are able to store almost 400 billion cubic feet of natural gas (DoC 2022, EIA 2022). While some large noncore (i.e. large volume) customers obtain natural gas directly from the backbone or the transmission pipeline systems, core (i.e. residential and small commercial) customers take gas out of the distribution system (CPUC 2022). Figure 2a presents a general schematic of this process.

For the most part, natural gas moves in underground pipelines. However, at certain locations it is necessary for natural gas processing, transmission and/or distribution elements of the infrastructure to be installed above ground. In California, this occurs for example at the following locations:

1. Storage field facilities. As mentioned above, natural gas from states outside of California may be temporarily stored to balance supply and demand. This occurs in natural gas storage fields, where natural gas is injected/withdrawn into/from underground reservoirs through wellheads. A photograph of section of a storage field is presented in Figure 2b.
2. Meter and pressure regulating (M&R) stations. These are facilities that regulate gas pressure and/or measure the gas flow for example for accounting purposes (EPA 1996). Figure 3 provides select photographs of M&R stations.

Figure 2: Natural Gas Infrastructure

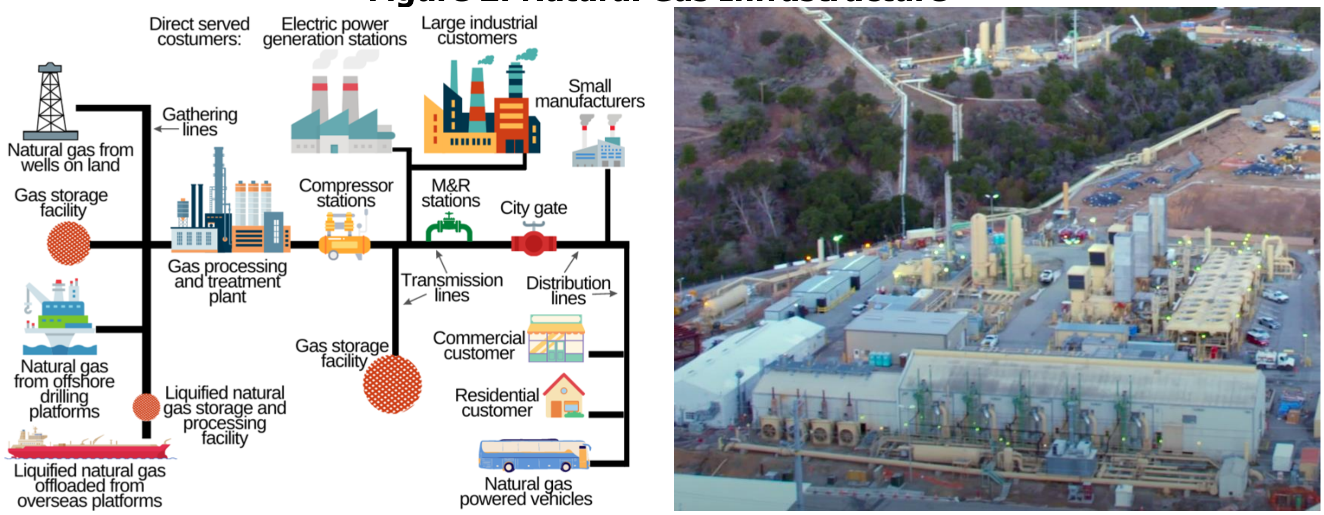

(a) (b)

(a) Schematic of the natural gas infrastructure (modified after US DoT 2022), (b) Photograph of a section of the Aliso Canyon Gas Storage Field (SoCalGas 2016a)

Figure 3: Examples of M&R stations

(a) (b)

(a) For transmission lines (Rongere and Eimon, 2019), (b) or distribution lines (Rongere and Eimon, 2019)

3. Compressor stations. In these facilities, natural gas is compressed to maintain the desired pressure. Compressor stations are situated 50-100 miles apart along natural gas pipelines (EIA 2007).
4. City gates. These are M&R stations where natural gas is delivered from transmission pipelines to the high-pressure lines of the local distribution company (EPA 2003).
5. River crossings. While generally natural gas pipelines cross a river via underground pipelines, in some cases the pipelines need to be brought above ground.
6. Gas service risers / gas meters sets. In residential or commercial units, service risers are the vertical pipes moving natural gas from underground service laterals to the gas meters, which measure the gas flow and connect to the building inlet, which is called "houseline" in case of residential units. Examples of different configurations of gas risers and meters sets are shown in Figure 4.

Figure 4: Examples of service riser and gas meter sets

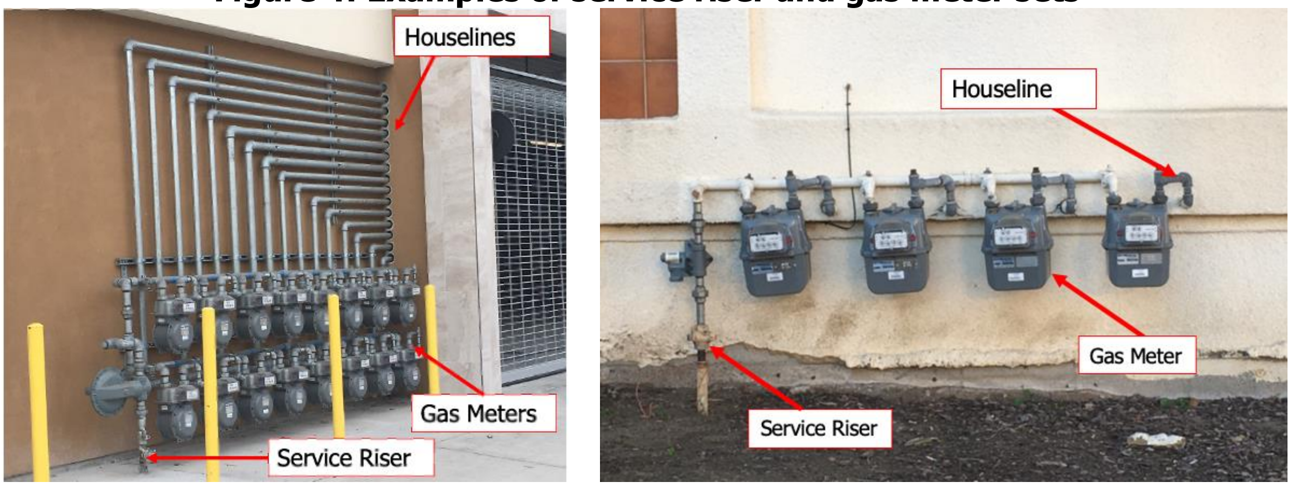

(a) **(b)**

(a) For large residential unit, (b) For small residential unit

Surface Natural Gas Facilities: Infrastructure Generalized

Surface natural gas facilities in California include storage field facilities as well as M&R stations, compressor stations and city gates, as noted above. In each surface natural gas facility, the following generalized infrastructure can be identified, as shown in Figure 5a:

- Systems: part of the facility that can perform a specific function.
- Subsystems: part of a system that can be analyzed as a unit from a dynamic standpoint but it cannot function as a unit. Examples include pipe racks and pipes; tanks and connected pipes.
- Components: individual parts of a subsystem. Examples include pressure vessels, straight pipes, elbows, tees, reducers, and bolted flange joints.

Certain components and subsystems are specific to specific facility types. For example, wellheads are specific to storage fields. However, generally surface facilities contain similar components, such as:

- Tanks and pressure vessels. The difference between the two is that pressure vessels are designed to operate at a pressure above 15 psi (OSHA 2022). Facilities can contain tanks filled with water or other liquid at ambient pressure as well as pressure vessels containing natural gas at high pressure. While pressure vessels can be used simply to store gas, those in natural gas facilities are generally used as filters, scrubbers or to perform other functions.
- Pieces of equipment. This include both heavy pieces of equipment such as compressor and lighter pieces of equipment such as electric cabinets.
- Networks of pipes. In surface facilities pipelines transition from below ground, run across the facility on supports and connect to tanks, vessels or pieces of equipment.

Figure 5b provides examples of typical surface components of required at storage fields, notably, tall and vertical pressure vessels, heavy equipment, pipes with intermediate along length supports and wellhead trees. The latter is the surface portion of wellheads.

Figure 5: Example of natural gas storage fields in California

(a) (b)

(a) Playa del Rey storage field (Witt 2018), (b) Honor Rancho storage field (SoCalGas 2016b)

While it is accurate to observe that each facility contains similar components and subsystems, it is essential to note that each facility has a unique geometry and configuration. Differences amongst facilities include not only the type of systems and subsystems at the facility, but also a vast number of details such has the height and diameter of vessels and tanks, the diameter and thickness of the pipes used, the type of pipe supports, and the type of anchoring used for tanks, pressure vessels and equipment.

Above-to-below ground transitions

In many cases, an underground pipe or other component, such as a wellhead, must transition from below to above ground. While below ground, it is surrounded by the soil present on site. This could be a compacted fill or a native in-situ soil (e.g. Figure 6). In some cases, however, the pipe transitioning below ground may require encasement in a drainage material or in concrete, as shown in Figure 3 and Figure 4a.

Figure 6: Pipe transitioning from above to below ground

(SoCalGas 2017)

Materials

Underground gas transmission pipelines must travel long distances, thus are made of steel, while underground gas distribution pipelines may have a blend of long and short travel paths, thus can be made of either steel, cast iron or plastic. Cast iron was used for urban utilities for most of the 20th century due to its resistance to corrosion. However, it was largely by steel in the 1950s. In the past 30 years, plastic pipelines emerged as predominant where the gas system operates at low pressures (AGA 2022).

It is unclear if the trend in the use of cast iron and plastic for underground distribution pipelines affected the surface system. However, Task Group D confirmed that steel is the material of choice for the transmission pipelines and their surface infrastructure.

Damage During Past Earthquakes

The natural gas surface infrastructure is generally very robust and has performed reasonably well during past earthquakes. This was recognized in the 1990s by the Federal Emergency Management Agency (FEMA) which, in reference to surface facilities supporting the gas and liquid fuel infrastructure, noted that "modern facilities designed and constructed in accordance with modern United States seismic practice, with particular attention given to adequate anchorage of equipment, can be expected to sustain no significant loss of operating function when subjected to high-level resonant ground motion" (Yokel and Mathey 1992).

Certain components of the infrastructure have demonstrated vulnerability to seismic damage. In particular, observations from past earthquakes indicate damage to natural gas surface infrastructure or similar industrial facilities and lifelines may include:

- Failure of anchorage at the base of tanks, pressure vessels and equipment. This can lead to movement or complete toppling of these important components of the gas infrastructure. Particularly sensitive are tall and heavy components such as vertical pressure vessels (Lund et al. 1995, see example in Figure 7a) and large pieces of equipment (Jaimes and Candia 2018, see example in Figure 7b).
- Failure of pipes at their connection with vessels or tanks. This occurs due to excessive relative displacement created by the movement of the equipment and/or component. Figure 7c shows an example of such a failure (Eshghi and Razzaghi 2004).
- Damage to liquid-filled tanks. This damage is extensively reported during past earthquakes, and can be in the form of sliding of the tank, failure of the pipes connected to the tank and "elephant foot" deformation at the base of the tank (Lund et al. 1995; Suzuki, 2008). Figure 8a provides an example of a tank which failed during the 1994 Northridge earthquake in California.
- Damage to a pipe connected to a structure which is moving and deforming during an earthquake (e.g. a pipe rack, a bridge, a platform) (Eidinger 2021). An example of a damage to a sewer pipe connected to a bridge is shown in Figure 8b. In some case the supporting structure might also be damaged, consequently damaging the pipes, as shown in Figure 8c (Suzuki 2008).

- Leaks in the service risers and meter sets. The California Seismic Safety Commission (CSSC 2002) reports that after the 1987 Whittier, California earthquake almost 2000 repairs were performed by SoCalGas, and of these 20% was in the meter set assembly and 26% in the house lines. in the 1989 Loma Prieta (California) earthquake there were around 600 leaks reported in the distribution system, of which 20-30% where in the riser pipe/meter set (Eidinger 2021).

Figure 7: Examples of seismic damage to vessels, equipment and pipes

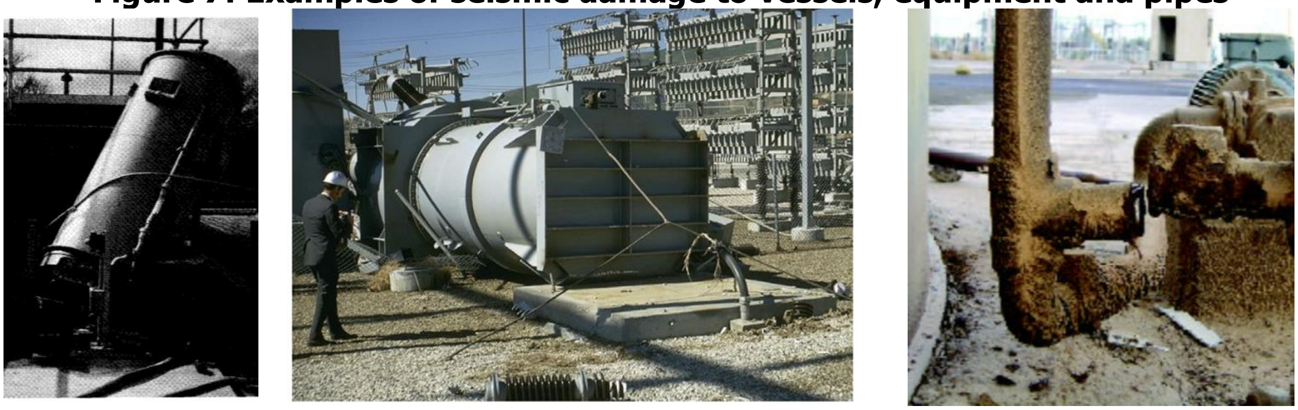

(a) (b) (c)

(a) Toppled air scrubber during the 1994 Northridge, California earthquake (Lund et al. 1995), (b) Collapsed anchored electrical equipment during the 1971 San Fernando, California earthquake (James and Candia 2018), (c) Damage to a pipe connection after the 2003 Bam, Iran earthquake (Eshghi and Razzaghi 2004)

Figure 8: Examples of seismic damage to tanks and pipes

(a) (b) (c)

(a) Collapsed tank after the 1994 Northridge, California earthquake (Lund et al. 1995), (b) Damage to a sewer pipe connected to a bridge during the 2010 Christchurch earthquake (Eidinger and Tang 2012), (c) Damage to a pipe rack during a recent earthquake in Japan (Suzuki 2008)

Infrastructure at the storage fields and supporting processing plants have also demonstrated vulnerability during past earthquakes. For example, damage specific to storage fields facilities in California was reported after the 1994 Northridge earthquake (Lund et al. 1995). Notably, the Aliso Canyon Storage Field damage observed included:

- Deformation of pipe supports.

- Displacement of injection/withdrawal pipelines (without rupture of the pipelines, except for a leaking flange close to an area of slope movement).
- Damage to a fan unit used to cool gas.
- Damage to three water tanks, including damage to the inlet/outlet pipes.
- Failure of pipelines transporting water within the facility.
- Damage to six oil storage tanks.

During the same earthquake, the Honor Rancho Storage Field, another large storage field in Southern California, reported damage to a water tank, gas piping and an electrical transformer, together with disruption of a brine filtration equipment (Lund et al. 1995). It is noted that additional details specific to these facilities are not publicly available.

Past Research

Research specific to the seismic behavior of the surface components of the natural gas infrastructure is limited. However, general research on steel pipes, which are widely utilized within a variety of industrial facilities can be extended to understand the behavior of the natural gas surface infrastructure. An overview of this research is presented in this section.

Research on Components

Past research on the critical components of industrial systems have been both analytical and experimental in nature. One component extensively studied is steel elbows, as they serve an essential service of facilitating a pipelines transition in direction. Experimental campaigns on elbows included monotonic tests in the in-plane and out-of-plane directions (e.g. Yoshizaku et al. 2000, see Figure 9a, Karamanos et al. 2003, Karamanos et al. 2006), in-plane cyclic tests (e.g. Varelis et al. 2013, see Figure 9b) and shake table tests (Nakamura and Kasahara 2017, see Figure 9c), to name select investigations. A summary of past experimental studies on elbows is presented by Karamanos (2016).

Figure 9: Examples of past tests on steel elbows

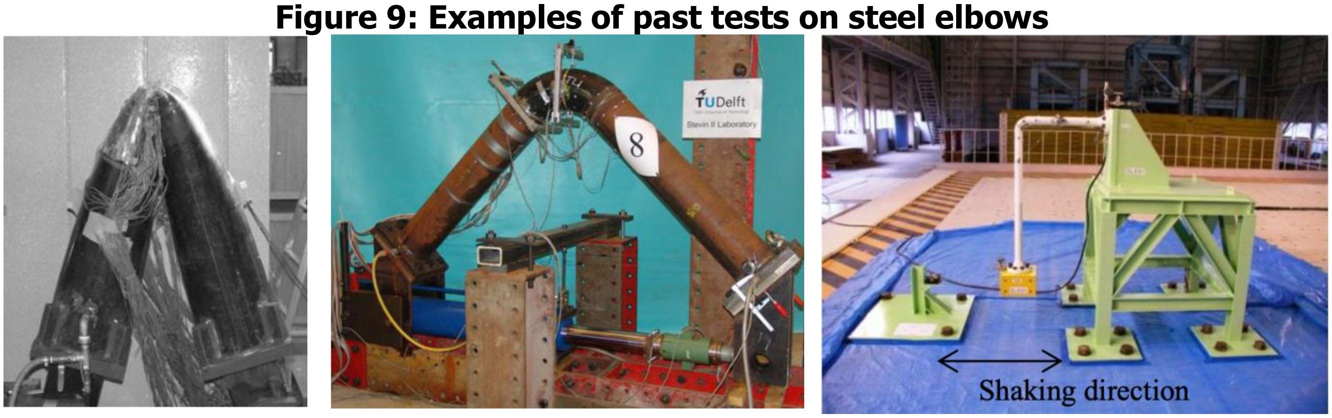

(a) (b) (c)

Performed by (a) Yoshizaki et al. 2000, (b) Varelis et al. 2013, (c) Nakamura and Kasahara 2017

Transitions in directionality and size of pipelines is also readily facilitated using tees. Research on the behavior of steel tees however is more limited, though select investigations are available. Relevant studies included monotonic and cyclic tests of tee with loads imposed in the out-of-plane and in-plane directions (Papatheocharis et al. 2013 see Figure 10a, DiFilippo et al. in 2019 Figure 10b), shake table tests (Watakabe et al. 2014 Figure 10c) and numerical investigations on the failure modes of different types of tees (Nakamura 2019). Other critical components considered by groups of researchers include bolted flange joints (e.g. La Salandra et al. 2016) and nozzles (e.g. Wieschollek et al. 2013).

Studies on the seismic behavior of liquid-filled tanks have been performed for decades, particularly to understand the effect of liquid sloshing inside the tanks (e.g. Clough 1977, Chen et al. 1996, O'Rourke and So 2000, Moslemi and Kianoush 2012, D'amico and Buratti 2019). More limited are studies specific to pressure vessels (Di Carluccio et al. 2008, Wieschollek, Diamanti et al. 2013, Cademartori et al. 2019).

Figure 10: Examples of past tests on tees

(a) **(b)** **(c)**

Tests performed by (a) Papatheocharis et al. (2013), (b) Di Filippo et al. 2019, (c) Watakabe et al. 2014

Research on Subsystems

Several experimental, hybrid and numerical studies on subsystems have been performed in the past. Amongst notable test programs, include shake table tests on subsystems performed in 2013 by Nakamura and in 2021 by Butenweg et al. While the former included shake table tests on a network of pipes connected to tanks, see Figure 11a, the latter focused on piping and vessels supported by a multistory frame as seen from Figure 11b.

Figure 11: Shake table tests on subsystems

(a) **(b)**

Tests performed by (a) Nakamura 2013, (b) Butenweg et al. 2021

In 2015, Bursi et al. performed an evaluation of a full-scale petrochemical piping systems, and as a part of this study they conducted a hybrid simulation on a subset of the piping network, see Figure 12. Hybrid tests were also performed by DiFilippo et al. 2019 within the goal of studying the coupled behavior of tanks and connected pipes. Numerical studies on the interaction between tanks or vessels and pipes were also performed by Abbiati et al. (2016) and Korndorfer et al. (2017).

Figure 12: Study performed by Bursi et al. (2015)

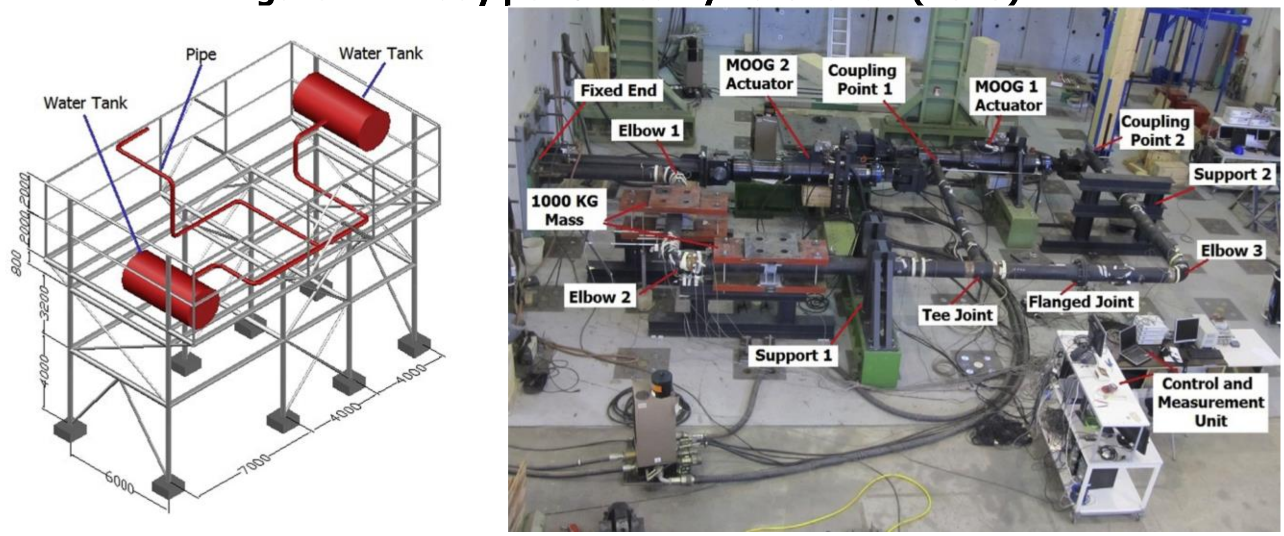

(a) **(b)**

(a) Rendering of the subsystem under consideration (all units in mm), (b) Experimental set-up

Limitations

While past research on components and subsystems including steel pipes and industrial facilities is rich and relevant, there are several limitations to the application of these results to the natural gas infrastructure in California. These include:

- Most of this research is not specific to the natural gas infrastructure. While natural gas facilities are similar to other industrial facilities, there are differences in some of the components and subsystems that are not addressed by past studies. For example, there are no studies on the wellhead tree assembly typically used in natural gas storage fields.
- Most of this past research was performed in European countries and Japan, and thus the design selection may adopt materials, technologies, and codes specific to those Countries. In some cases, these could be different than those used in California.
- There is a large variability of geometry and behavior within the natural gas infrastructure, and tests were performed only on a subset of geometries and loading conditions. For example, past research focused on 8 in and 6 in diameter Schedule 40 pipes while studies on the small diameter Schedule 80 pipes typically used in high-pressure natural gas facilities fie is more limited, as are limited the number of studies considering the effect of very large internal pressures on pipe component behavior.

Differences between underground and surface infrastructure

The underground portions of the natural gas infrastructure include most notably the pipelines transporting natural gas to users and the underground components of storage fields (wells, caprocks, reservoirs). These systems are clearly different from those above the ground surface in so much as they are encapsulated by surrounding soil and the ensuing ground conditions that manifest in the event of an earthquake.

Table 1 summarizes the main differences between the surface and underground portions of the gas infrastructure, with particular focus on the attributes anticipated to be most influential to their seismic behavior. The differences in the types of components, location distribution, and boundary conditions lead to very different behavior during earthquakes. Namely, the surface infrastructure comprises a set of subsystems anchored at discrete support location that can oscillate, while the underground components are surrounded by soil and consequently, their dynamic movement is constrained by the surrounding soil. However, since pipelines span continuously throughout California, they are sensitive to damage created by permanent ground deformation. These dramatically different boundary conditions lead to variations in failure modes when comparing underground and surface infrastructure.

Although not noted in Table 1, another relevant difference in these two parts of the gas infrastructure is the effect of corrosion. Because the underground components are continuously surrounded by soil and are more difficult to inspect and replace, they may naturally be more exposed to saturation and thus vulnerable to corrosion damage. In contrast, surface components are readily visible and thus may be regularly inspected, and if necessary, replaced upon observation of significant corrosion damage. It is worth noting however that in the present study the effects of corrosion are not considered for the natural gas surface infrastructure.

Table 1: Summary of key differences between surface and underground gas infrastructure

System attribute	Surface infrastructure	Underground infrastructure
General type of components	Created by many subsystems moving independently. The components are heterogeneous	Contain one primary component: a straight (or curved) pipe or tubing interconnected by joints or elbows. The system is homogeneous
Location distribution	Installed at discrete locations throughout the State	Transmission and distribution pipelines run continuously throughout the State. Wellhead tubing spans for miles underground
Boundary conditions	Discrete support locations (e.g. a base support)	Continuous confinement by soil

System attribute	Surface infrastructure	Underground infrastructure
Response sensitivity	Subsystems are sensitive to ground accelerations. However, seismic accelerations of connected components can create a relative displacement between them, which could drive damage formation	Mostly sensitive to ground displacements (permanent fault deformation, landslides etc.)
Nature of loading (deemed most detrimental to failure)	Cyclic	Monotonic
Typical failure modes	Failure of connections between components, permanent deformation of components, failure of anchors	Compression buckling of straight pipes, tensile failure of welds, failure of caprock

CHAPTER 2:
Project Approach

As noted, the surface infrastructure is comprised of many different subsystems and components (storage field facilities, M&R stations, service risers, to name a few), each having a large variability in terms of type of subsystems and geometry of components. Consequently, it was not possible to perform a seismic fragility analysis on each of these parts within the time frame of the present project. Thus, it was decided to focus on developing a framework for generalization of seismic fragility functions for the surface infrastructure, and through feedback received by the TAC, identified the highest priority surface infrastructure components to utilize this approach and provide seismic fragility data for implementation within *OpenSRA*.

The TAC identified as a main priority the seismic analysis of storage field facilities, due in large part to the catastrophic consequences of seismic damage to these facilities. Namely, utility companies were particularly interested in analyzing the seismic behavior of wellhead trees, in particular due to the implementation of more modern wellheads, which tended to be taller and heavier in their basic configuration. The development of fragility curves for tall vertical pressure vessels with adjoining piping containing natural gas are also prevalent at storage field facilities and thus deemed to be of high priority, since these vessels and in particular their connected piping elements are prone to seismic damage. The analysis of non-critical equipment and tanks or vessels not containing natural gas was considered a lower priority. Lower priorities identified by the team of experts also included M&R stations and service riser/meter sets. The decision relative to M&R stations was dictated by their robustness observed in past earthquakes, the large variability in their geometry and configuration, and the lack of detailed information available. The decision not to prioritize service riser/meter sets was dictated by the less serious consequences of a leak in a low-pressure small-flow service riser versus a leak in a high-pressure large-flow facility. Based on an initial survey of the small amount of available information it was revealed that the vast majority of river crossing occur underground. As such, pipe river-crossings were set to a lower priority.

Based on this feedback the present analysis focused on two subsystems typical of storage facilities: wellhead tree and the piping connected to it (WTP) and vertical pressure vessels (VPV). The geometry of these subsystems can have a large variability both within the same storage facility and from facility to facility. This variability can include the height of the vessel or wellhead tree, their mass stiffness and boundary conditions; the thickness and length of pipes forming the subsystem, and the presence of components such as elbows, tees, bolted flange joints, and reducers. In addition to the complexity created by the large number of variables, there was another severe limitation in the analysis of these subsystems: the limited well-documented information regarding their typical geometry and configuration. The primary information available to describe the features of such subsystems were derived from photographic evidence publicly available on utility websites, information obtained during a site visit to a gas storage field in California, and select drawings and details provided by utility companies.

The present effort also provides information and guidelines that allow future researchers to readily expand the results to multiple subsystems with different geometries. To achieve this goal, the approach herein includes the following outcomes:

1. Experimental data on the behavior of critical components.
2. Experimental data for the seismic behavior of subsystems.
3. Calibrated nonlinear material properties to be used within FEA software such as Abaqus. These properties can then be utilized by future users to obtain the behavior of new components.
4. A general procedure for the seismic analysis of complex nonlinear subsystem as well as numerical models for the seismic analysis of the WTP and VPV subsystems.
5. Fragility curves for these same subsystems.

Each of these outcomes will be further described in the following sections.

Outcome #1: Experimental Data on Critical Components

The natural gas surface infrastructure contains many important components, including straight pipes, elbows, tees, bolted flange joints, reducers, pressure vessels, tanks to name a few. Among these, it was decided to focus component tests on elbows and tees. This decision was driven by the fact that these components may behave nonlinearly during a strong earthquake and could also be a failure point. In addition, while tests on elbows and tees have been performed in the past, prior tests focused on components more readily utilized in the distribution system (e.g. Schedule 40 components), whereas the focus herein was on components typical of high-pressure facilities, such as 4 in diameter Schedule 80 pipes. It is noted that such components are pervasively utilized throughout high-pressure facilities, yet data regarding their cyclic behavior are lacking in the literature.

Table 2 presents the test matrix for the component tests performed at the Powell laboratories at the University of California, San Diego. Tests were performed 4 in diameter Schedule 80 and 8 in diameter Schedule 40 components. Since these components behave differently depending on the direction of loading, select components were tested both in the in-plane and out-of-plane direction.

Table 2: Test matrix of component specimens

Component type	Diameter (Schedule)	Direction of loading	Shortname
Tee	4 in (80)	In-plane	4T-IP
	4 in (80)	Out-of-plane	4T-OP
	8 in (40)	In-plane	8T-IP
	8 in (40)	Out-of-plane	8T-OP
90° elbow	4 in (80)	In-plane	4E-90

Component type	Diameter (Schedule)	Direction of loading	Shortname
45° elbow	4 in (80)	In-plane	4E-45

The specific tests goals were the following:

- Provide a database of information on critical components specific to the material and technologies used in California. This included data from an array of analog sensors as well as from cameras monitoring the tests.
- Understand the damage development and limit states of the components. This included not only understanding crack formation, but also tracking the deformation at which the component develops different limit states.
- Obtain the global behavior of the components, namely in terms on moment and rotation. The experimental moment-rotation curve obtained is deemed essential to proceed with a numerical analysis of the components, and is thus used to achieve outcomes #3 to #5.
- Measure local behavior of the components, in particular strain. Strain measurements were used to validate numerical models of the components for outcome #3.

Description of the Specimens

To recreate field conditions, each specimen was created by welding the critical component under consideration to segments of straight pipes. The length of the straight pipes was three to five times the specimen's diameter, similar to what was done by previous researchers (e.g. Di Filippo et al. 2019). The ends of the straight pipes not connected to the critical component was welded to thick steel plates connecting the specimen to the test frame and actuator. Stiffeners were added at the end of pipe far from the critical component to reduce the probability of failure at these locations. Three olets were inserted in each specimen to allow for the pressurization and pressure monitoring of the specimens. A photograph the specimen 4T-OP is presented in Figure 13a. Additional details regarding the individual test specimens and results may be found in Pantoli et al. (2022).

The specimens were constructed and donated by local manufacturers, who procured the material locally and welded the components according to standards common in practice. The mill certificates provided by the manufacturers revealed that the material used were A106 Gr.B for the 4 in diameter components, A53B for the 4 in diameter straight pipe, CSA Z245.11 (equivalent to API 5L) Gr. 241 for the 8 in diameter tee and API 5L X42 for the 8 in diameter straight pipe. Table 3 shows the yield strength (f_y), tensile strength (f_u), tensile strain (ε_u) obtained from the mill certificates as well as the yield strain (ε_y) calculated from f_y and assuming an elastic modulus E of 29000 ksi.

Table 3: Properties of the components tested

Component	f_y (ksi)	f_u (ksi)	ε_y (%)	ε_u (%)
4 in tee	42.0	72.6	0.14	42.0
8 in tee	47.1	66.8	0.16	30.7
4 in 90° elbow	37.8	61.6	0.13	44.0
4 in 45° elbow	38.6	61.9	0.13	44.0

Pre-test Simulations in Abaqus

Pre-test simulations using the high-fidelity FEA software Abaqus (Smith 2009) were performed for each specimen to support the development of the load protocol and instrumentation plans. Figure 13b shows an example of the meshed model of a specimen in Abaqus. While elbows were drawn within Abaqus using the sweep method, tees had a very complex curvature and thus 3D models of these components were imported to Abaqus using manufacturer supplied models (McMaster Carr 2022). The olets, end plates and stiffeners were not modeled in Abaqus, but the boundary conditions created by the end plates and stiffeners were considered by applying appropriate restraints. The elastic material properties selected were those typical of steel (Young Modulus=29000ksi and Poisson ratio=0.3). Simplified nonlinear steel properties were used during this phase of modeling. Specifically, the yield strength, ultimate strength and ultimate strain assigned to the model were obtained from the mill certificates. The specimens were modeled using solid elements, in part because of the low diameter-to-thickness ratio of some of the specimens, and in part because the parts imported courtesy of manufacturer supplied geometric models were optimally imported as solid elements. The type of finite element used was C3D8 (8-node linear brick). Reduced integration was used in the segments of straight pipes, but could not be used in the critical components.

Figure 13: Specimen 4T-OP

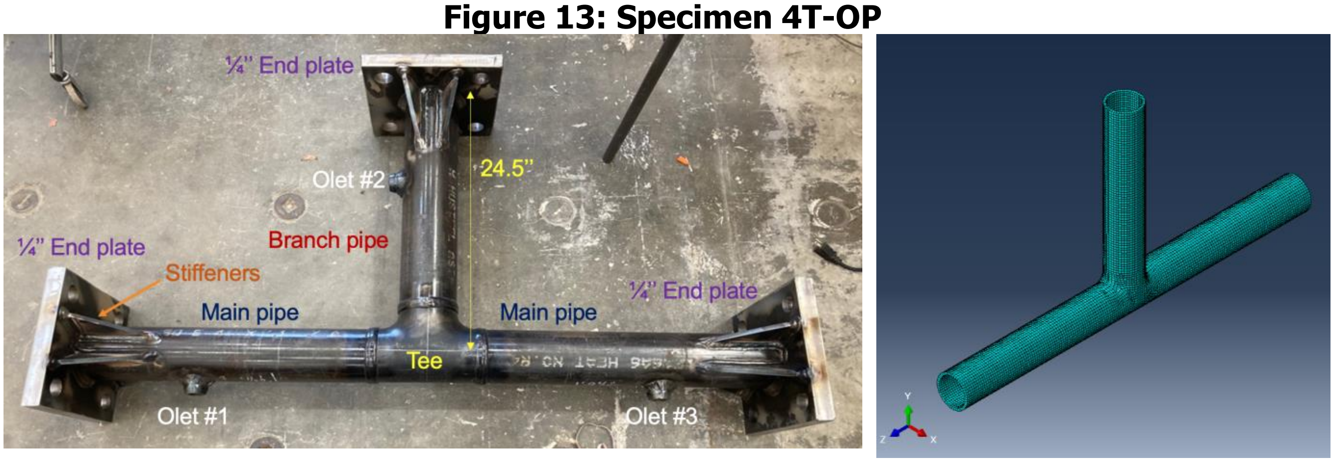

(a) **(b)**

(a) Photograph, (b) Modeled and meshed in Abaqus

Description of the Test Protocol

Quasi-static, reversed cyclic, displacement-controlled loading was imposed on each specimen following the cyclic load protocol recommended by FEMA-461 (FEMA 2007). This protocol involves imposition of two full cycles per amplitude target, with displacement amplitudes increased 40% in each subsequent cycle grouping. The main parameters of this protocol are the initial displacement Δ_0, the target displacement Δ_m and the number of cycle sets. The target displacement Δ_m was selected based on pre-test simulation as the displacement resulting in a 20% reduction in the peak force during monotonic loading (Krawinkler et al. 2001). The selection of Δ_0 was based on the minimum of 0.15% of a key length recommended by FEMA-461. This load protocol contained at least six cycle groups in the elastic range, as recommended by FEMA-461. Based on these criteria, tests 4T-IP and 4T-OP had a Δ_0 of 0.03 in, a Δ_m of 9.15 in and 18 cycle sets. Tests 8T-IP and 8T-OP had the same Δ_0 of 0.036 in, however 8T-IP has a Δ_m of 10.97 in (18 cycle sets) and 8T-OP has a Δ_m of 5.6 in (16 cycle sets). Displacements were applied using a double-acting 50-kip hydraulic actuator with a stroke of +/- 24 in. During testing, the specimens were internally pressurized at a constant pressure between 25 and 30 psi. Tests were performed until a through crack developed and internal pressure decreased to zero.

Test Setups

The test setup for the tee specimens involved in-plane and out-of-plane loading, while the two elbow specimens were tested in an in-plane loading configuration. As feasible, like loading configurations will be described in pairs in the following sections.

In-Plane Tee Specimens (4T-IP and 8T-IP)

Figure 14 shows the test setup for the 8 in diameter tee specimens tested in-plane (8T-IP). In this setup, the ends of the main pipes were bolted to reaction columns, while the end of the branch pipe was loaded with the actuator through a corbel. When the load was applied, the head of the actuator and the corbel slid on a steel block which was covered in Teflon to reduce friction.

Figure 14: Specimen 8T-IP

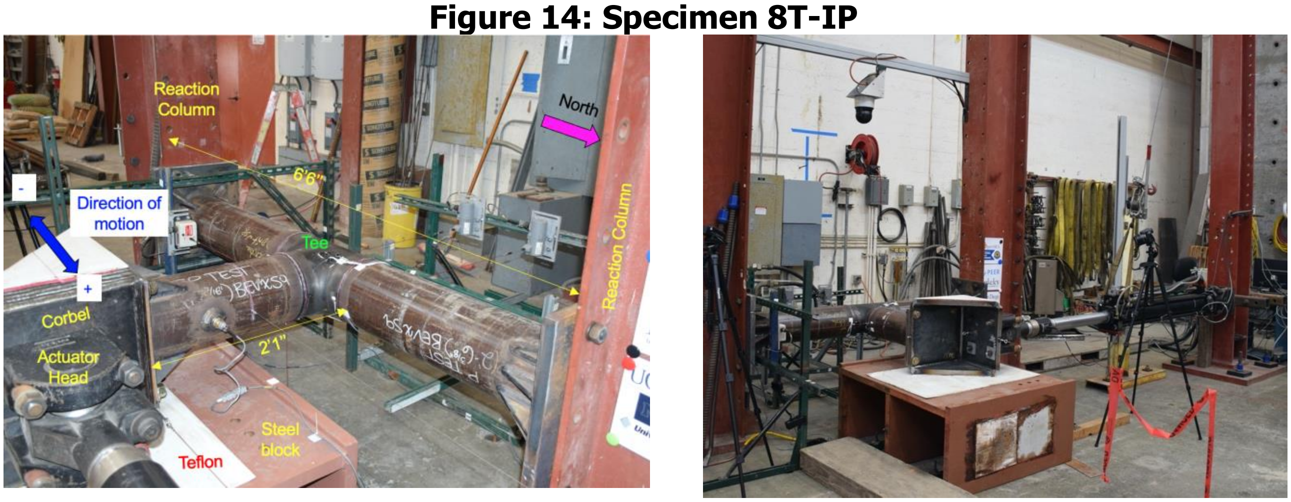

(a) **(b)**

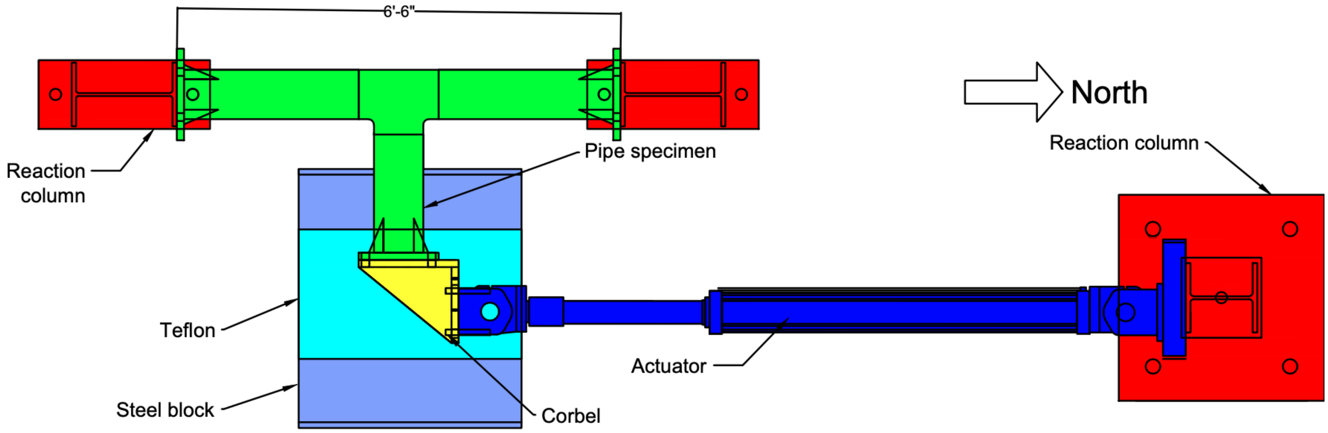

(c)

(a), (b) Photographs, (c) Plan view

Out-of-Plane Tee Specimens (4T-OP and 8T-OP)

Figure 15 shows an example of the test setup for the 4 in diameter tee specimen tested out-of-plane (4T-OP). The setup was similar to that one used for in-plane tests, with the difference that the specimen was rotated 90° and welded at its top to a reaction frame and at its bottom to a steel plate post-tensioned to the strong floor of the laboratory.

Figure 15: Specimen 4T-OP

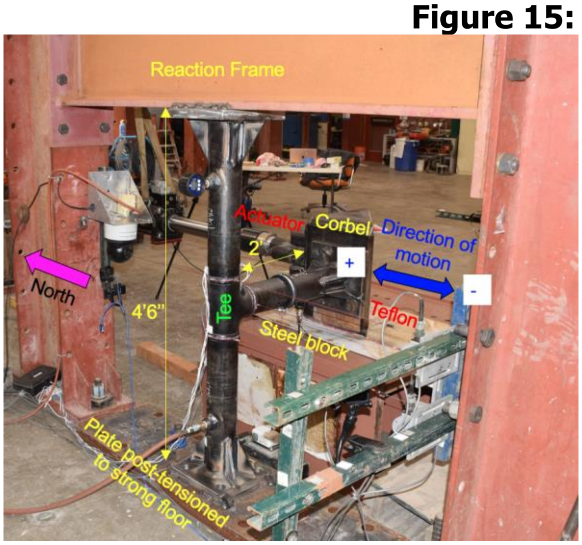

(a)

(b)

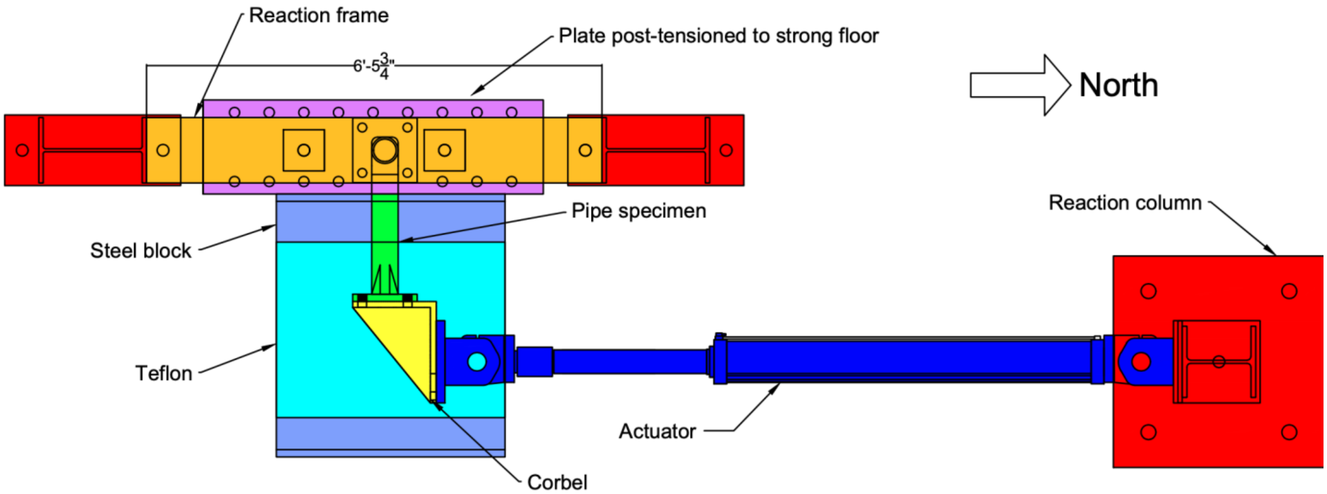

(c)

(a), (b) Photographs, (c) Plan view

In-Plane Elbow Specimens (4E-90 and 4E-45)

Figure 16 shows the test setup for the 90° elbow specimen tested in-plane (4E-90). The specimen was held in between hinges allowing the rotation of the straight pipes. While the southern hinge was bolted to a reaction column, the northern hinge was connected to the actuator through the corbel. The bottom of the corbel was connected to a railing system designed to ensure that the movement remained in the plane of the specimen and that out-of-plane movement was avoided. This was made of two rectangular sliders connected to the corbel and moving around steel rods. These steel rods were then fixed to a hollow structural steel (HSS) beam which was post-tensioned to the strong floor of the laboratory. It is noted that at the time of preparation of this report, two additional elbow specimens are planned for testing, each of diameter 8 in.

Figure 16: Specimen 4E-90

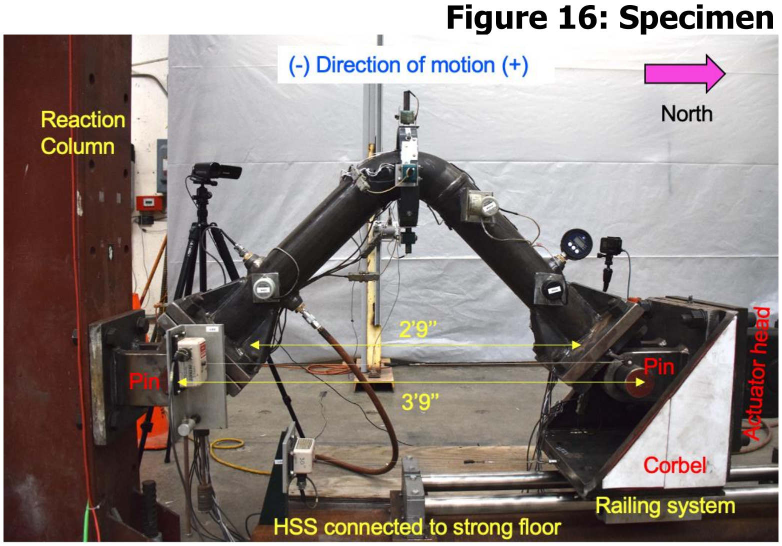

(a)

(b)

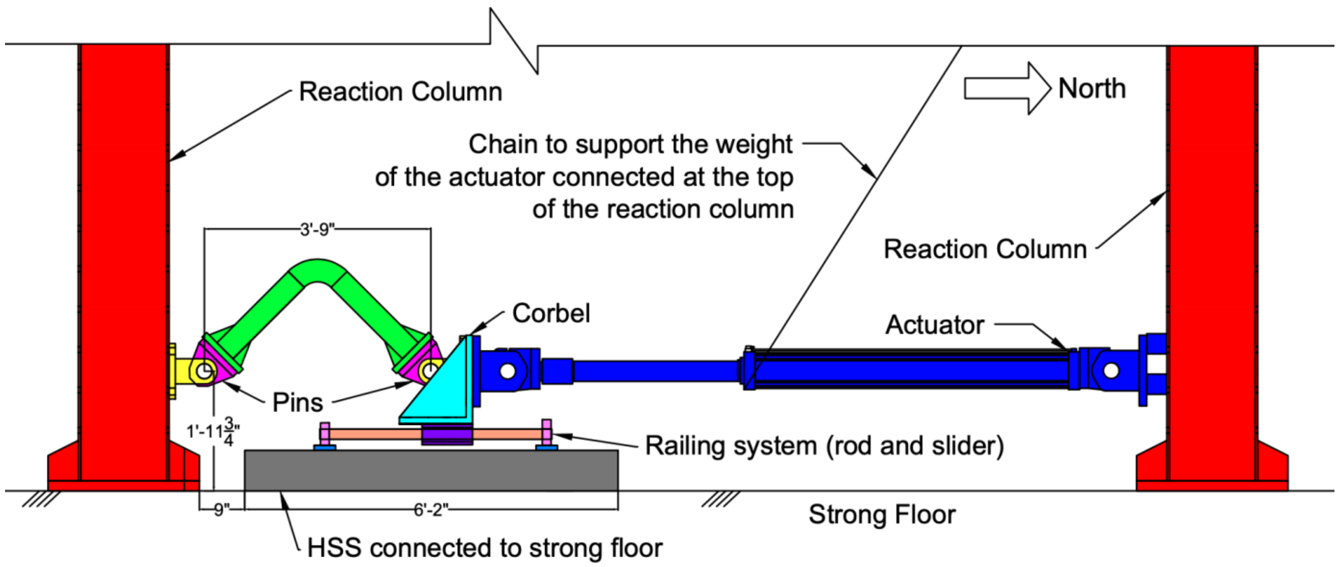

(c)

(a), (b) Photographs, (c) Plan view

Instrumentation

The specimens were instrumented with displacement potentiometers and uni-axial and rosette strain gauges, in addition to the internal measurements obtained with the hydraulic actuator (load cell and displacement transducer). In total, between 15 and 35 analog sensor channels were distributed on each specimen. In addition, an array of digital high-resolution video cameras surrounding the specimen was used to capture physical damage during the experiment. Sample instrumentation plans and camera views for specimen 4T-IP are presented in Figure 17. In addition, test 8T-OP was instrumented with fiber optics installed by the project team from the University of California, Berkeley (Wang et al. 2022).

Figure 17: Sample of Instrumentation (Specimen 4T-IP)

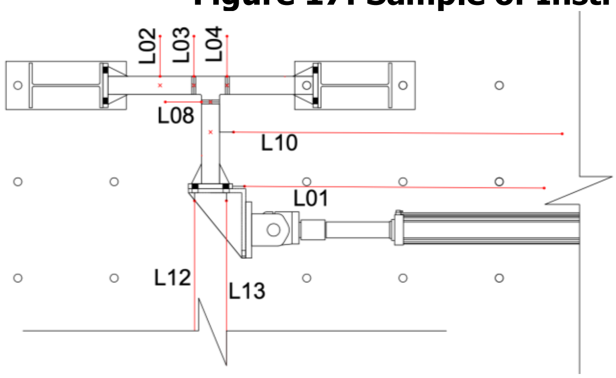

(a)

(b)

(c)

(d)

(a) Instrumentation plan for displacement potentiometers, (b) Instrumentation plan for uniaxial strain gauges, (c) View from the upper south-east camera, (d) View from the lower south-east camera. Note that L = linear displacement transducer and SG = strain gauge.

Outcome #2: Experimental Data Relative to Subsystems

A dynamic test series was conducted on a generic (full-scale) surface infrastructure subsystem at the Earthquake Engineering Laboratory at the University of Nevada Reno (UNR) using two biaxial shake tables. These shake tables not only can move together and simulate earthquake accelerations but can also move independently thus simulating relative displacements. As discussed in the introduction, surface natural gas infrastructure components are vulnerable to damage created by relative displacements, and thus the ability to simulate these relative displacements was essential to complement experimental findings from the component tests conducted at UC San Diego.

The large variability in configuration and geometry of storage facilities led the team to design a generic subsystem representing typical field conditions while also containing a wide variety of common components, including straight pipes, elbows, tees, reducers, bolted flange joints, concrete pipe supports and a model-scale vessel. The final design of this subsystem was based on an extensive literature review as well as several rounds of feedback obtained by utility company stakeholders.

The specific objectives of the subsystem level test program were the following:

1. Assess the response of a representative subsystem when subjected to different levels of earthquake ground motions including new data on significant relative support motions.
2. Improve understanding of the resilience, evolution of damage and potential failures in natural gas subsystems.
3. Support experimental validation of the first OpenSees (Mazzoni et al. 2006) model of the piping subsystem.
4. Provide a new and unique dataset of high-quality data which will be an important asset for future validation and calibration of numerical models of piping systems in support of numerically-based fragility function generation. Given the myriad of configurations of surface piping systems, the ability to reliably model system response will be an important tool in future risk assessments.

Description of the Subsystem

Figure 18 shows a rendering of the subsystem tested at UNR while Figure 19 shows a photograph of this subsystem and its relevant components. This subsystem contained the following components: one simulated 5 ft tall vertical tank/vessel, 8 in diameter Schedule 40 pipes, 4 in diameter Schedule 80 pipes, four 8 in diameter 90° elbows, one 8 in straight tee, five 4 in diameter 90° elbows, three 4 in tees, three reducers, and five pipe supports made of a concrete base and steel rings holding the pipes in place. Roughly half of these components were installed in each of the two shake tables.

Figure 18: Rendering of the subsystem experiment

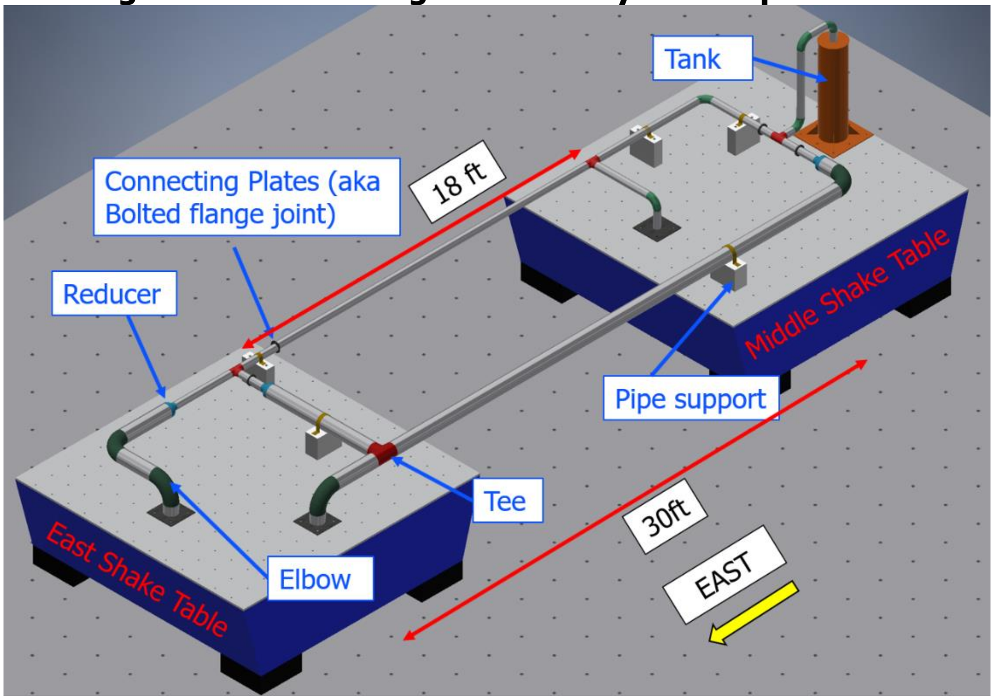

Figure 19: Photograph of the subsystem tested at UNR

(a)

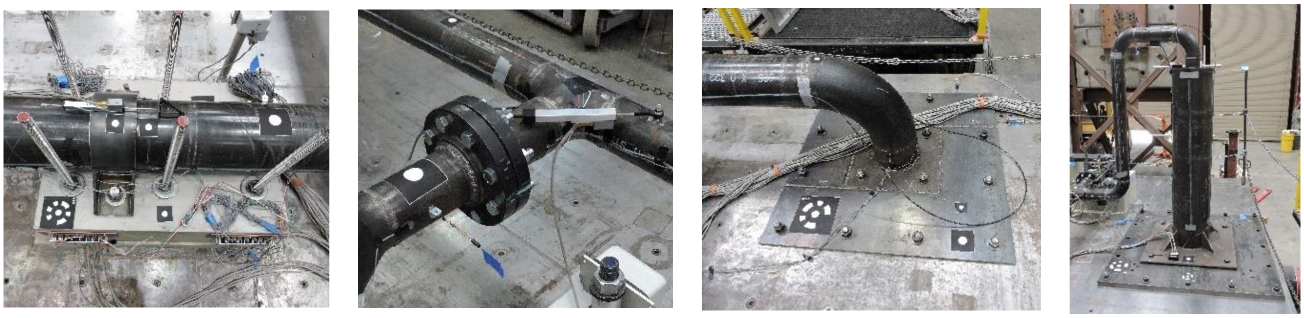

(b) (c) (d) (e)

(a) Assembled subsystem on the UNR shake tables, (b) Pipe support, (c) Connecting plates, (d) Elbow , (e) Vertical tank.

RHP Mechanical Systems, Inc., an experienced local piping fabricator, was employed to fabricate the subsystem specimen. Welding of the components was performed by certified welders and in accordance with current codes and regulations.

To allow early detection of any through crack, the subsystem was divided into four separate pressurization zones. Each zone was sealed, its components were welded together, and it was pressurized at ~15 psi before and during testing. All zones were fitted with connecting plates, which are structurally similar to bolted flange joints, but their function was to seal the ends of each zone. These plates were installed to facilitate the assembly of the subsystem.

Pre-Test Simulations in OpenSees

As seen for the component tests, also for the subsystem test a nonlinear numerical model was developed before the test to gain insights on the expected behavior of the subsystem. This model was developed using the open-source software OpenSees and is shown in Figure 20. In this model, all pipes were simulated using beam elements with fiber sections. The nonlinearity of the pipe was represented by nonlinear material properties within the fiber discretization of the section. The model was validated by comparing one simulated fundamental natural frequency of the subsystem with closed-form analytical solutions of the 4 in diameter straight pipe crossing the two tables. Once validated, the model was subjected to time-shifted ground motions designed specially to create a relative displacement between the tables to study their effect on the performance of the subsystem. This exercise was crucial in selecting the appropriate ground motions, pipe support locations, and the type and locations of instrumentation necessary to fully measure system response. It was also effective for assessing the anticipated reaction forces at the points of connection between the subsystem and the shake table and prevent any damage to the shake tables themselves.

Figure 20: Plan view of pre-test model in OpenSees

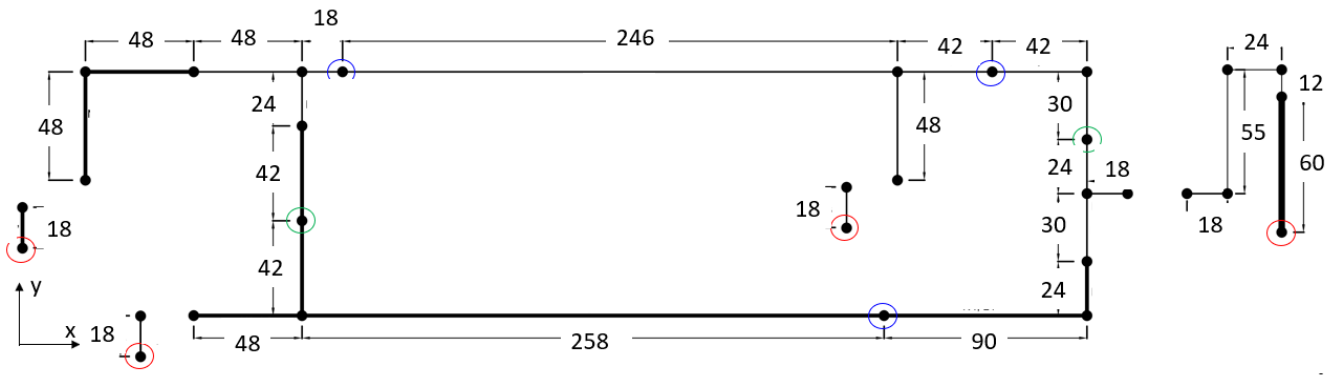

All dimensions in inches. Red circles denote fixed supports in all degrees of freedom, green circles denote restrained supports in X and Z directions, blue circles denote restrained supports in Y and Z directions.

Instrumentation

A total of 169 data channels were used to data from 145 sensors. Table 4 presents the type, quantity and purpose of the sensors used and

Figure 21 shows samples of the sensors deployed. The subsystem was also fitted with fiber optic sensors installed by the UC Berkeley team members to capture pipe strains, and visual targets for digital image correlation (DIC) installed by UNR faculty. Furthermore, two digital high-resolution video cameras were strategically placed around the specimen to capture the overall response of the subsystem and have a record of any physical damage that occurred. The views from both cameras are presented in Figure 22. In addition to video recording, still photographs were taken at every stage to properly document the experiment.

Table 4: Instrumentation table

Type	Quantity	Purpose
Foil strain gauges	102	Measure strains at different locations of critical components
String potentiometers	19	Measure pipe and tank deflection
LVDT (displacement transducers)	26	Measure joint rotations and pipe displacement at pipe support
Accelerometers	6	Measure pipe accelerations
Pressure transducers	4	Measure pipe air pressure
Accelerometers	6	Measure pipe accelerations

Figure 21: Example of instrumentation used in the subsystem experiment

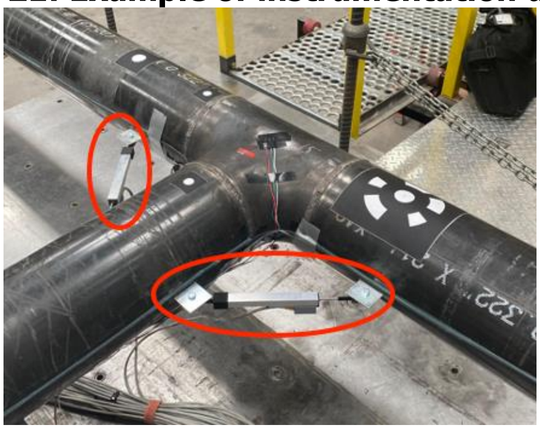

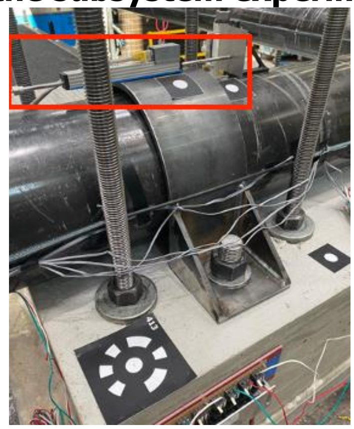

(a) (b)

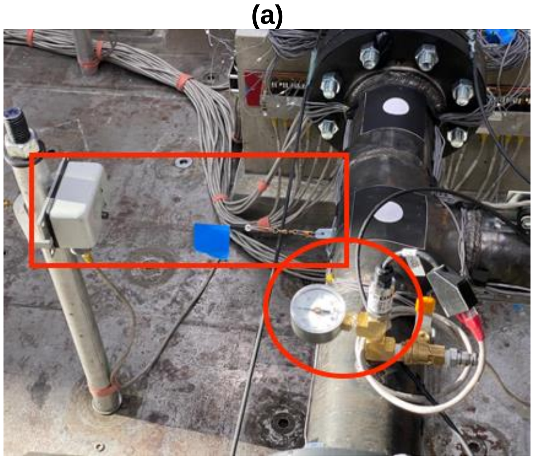

(c) (d)

(a) Rotation sensors, (b) Sensors to measure pipe displacement relative to support, (c) Pipe displacement and pressure sensors, (d) Strain gauges to measure strain in the piping components

Figure 22: Views from two high-resolution cameras

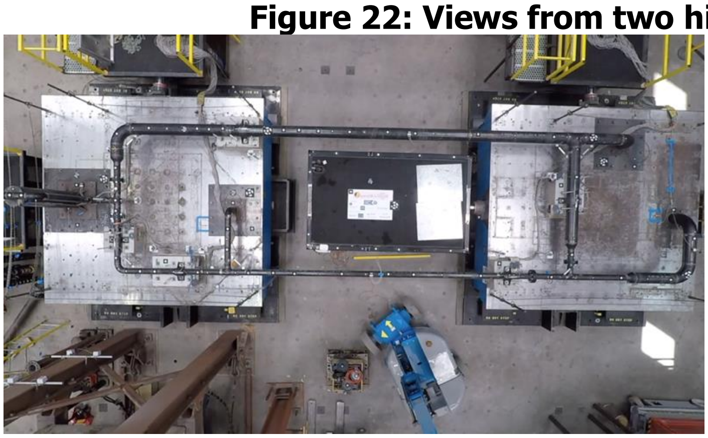

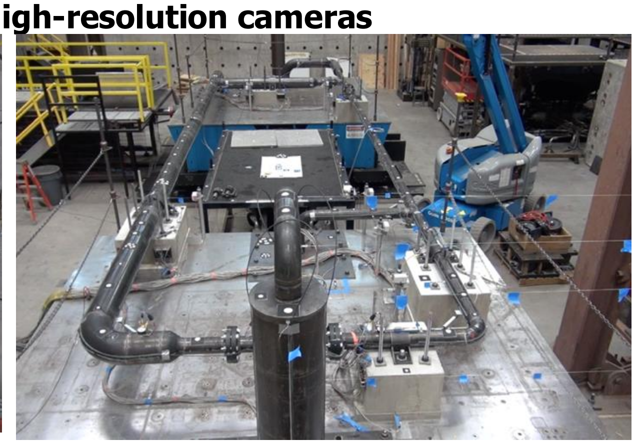

(a) (b)

(a) Top view, (b) Side view

Test Protocol

Results from the OpenSees model were instrumental in selecting the ground motions to which the subsystem was subjected. The model indicated no damage should occur if the subsystem was subjected to uniform earthquake accelerations, however, significant deformation and yielding could occur if the subsystem was subjected to large relative displacement. Thus, the subsystem was subjected to three types of motions designed to assess its performance as well as to check its resilience. These motions included:

1) Broad-band white noise excitation for system identification. These motions were executed at different times to evaluate any changes in the dynamic characteristics of the subsystem.
2) Synchronous motions comprising uniaxial and biaxial ground motions of the 1940 El Centro earthquake record with increasing amplitude of up to 200%.
3) Asynchronous (time shifted) motions which subjected the two tables and the subsystem to a relative displacement from 5 in to 17 in. Figure 23 presents an example of asynchronous time motion.

The complete loading protocol is presented in Table 5. Information on the test setup, instrumentation and loading protocol are provided by Elfass et al. (2022).

Figure 23: Time history of the asynchronous motions

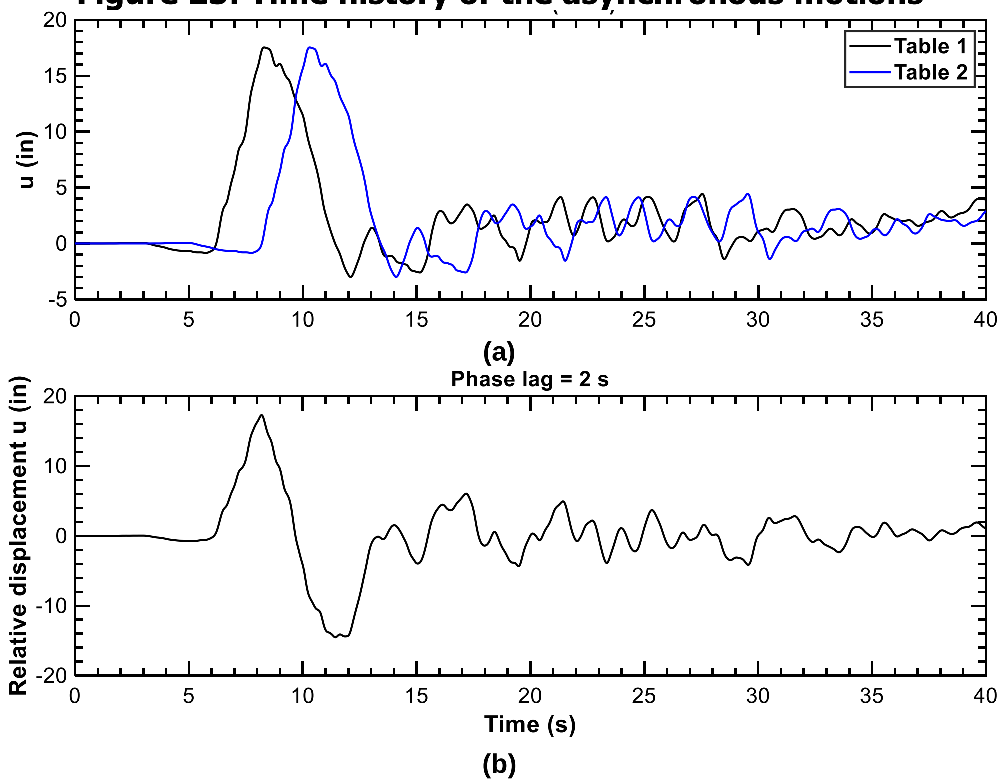

(a) Displacement time history for each shake table, (b) Time history of the resulting relative displacement between shake tables

Table 5: Load test protocol

Day	Description	Magnitude
Day 1	White noise – Long (0.5 to 30 Hz)	0.05 g RMS
	White noise – Lat (0.5 to 30 Hz)	0.05 g RMS
	Synchronous, El-Centro - Long (270)	50% (0.105 g)
	Synchronous, El-Centro - Lat (180)	50% (0.14 g)
	Synchronous, El-Centro - Biaxial	50%
	Synchronous, El-Centro - Long (270)	100% (0.211 g)
	Synchronous, El-Centro - Lat (180)	100% (0.281 g)
	Synchronous, El-Centro - Long (270)	200% (0.422 g)
	Synchronous, El-Centro - Lat (180)	200% (0.562 g)
	Synchronous, El-Centro - Biaxial	200%
	White noise – Long (0.5 to 50 Hz)	0.05g RMS
	White noise – Lat (0.5 to 50 Hz)	0.05g RMS
	Asynchronous motions (Lat)	Δ = 1 in
	Asynchronous motions (Lat)	Δ = 2 in
Day 2	White noise – Long (0.5 to 50 Hz)	0.05 g RMS
	White noise – Lat (0.5 to 50 Hz)	0.05 g RMS
	Asynchronous motions (Lat)	Δ = 5 in
	Asynchronous motions (Lat)	Δ = 8 in
	Asynchronous motions (Lat)	Δ = 12 in
	Asynchronous motions (Lat)	Δ = 17 in
	White noise – Long (0.5 to 50 Hz)	0.05 g RMS
	White noise – Lat (0.5 to 50 Hz)	0.05 g RMS
	Asynchronous motions (Lat)	Two cycles, Δ = 17 in
	White noise – Long (0.5 to 50 Hz)	0.05 g RMS
	White noise – Lat (0.5 to 50 Hz)	0.05 g RMS

g is the acceleration of gravity; RMS is root mean square; Δ refers to the relative displacement between the shake tables

Outcome #3: Calibrated Nonlinear Steel Properties

Creating a robust and reliable nonlinear material model for steel is required for the reasonable prediction of the behavior of a steel component subjected to the large cyclic deformations that can be caused by earthquakes. To support this need, the aforementioned component experimental data was utilized in iterative form to calibrate the nonlinear material properties for the steel used for tees and elbows. Namely, starting from the Abaqus models of the specimens developed for the pre-test simulations (shown for example in Figure 13b), key nonlinear parameters of the generic steel material model were systematically modified to optimize the comparison amongst the numerical and experimental results. The nonlinear parameters requiring calibration where the cyclic hardening parameters of steel, as explained in the following sections.

Once the nonlinear material properties are calibrated and validated, they could easily be adopted to model other components made of the same type of steel.

Nonlinear Material Properties: Cyclic Hardening

The behavior of steel under monotonic and cyclic loading is different. Notably, the cyclic behavior of steel is characterized by "cyclic hardening". "Hardening models" are well documented in the literature to reproduce this complex behavior (e.g. see a summary in Ryu et al. 2018), and some of the most representative hardening models are also implemented within FEA software packages, including Abaqus. Models commonly used are the isotropic, kinematic and combined hardening models. These models are parametric, meaning that the user need only input material properties specific to the material under consideration.

For this study, the combined hardening model in Abaqus was adopted allowing both isotropic and kinematic hardening of the material. This model involves a minimum of five parameters, namely:

- Q, b= material parameters for isotropic hardening.
- C, γ= material parameters for kinematic hardening.
- σ_0 =initial yield stress.

The calibration of these parameters and the validation of the model are shown in the Results chapter.

Extension of the Results to Components beyond the Experimental Program

After obtaining the calibrated and validated nonlinear steel properties, it was possible to extend their use to obtain cyclic response predictions of components beyond that tested during the component experimental program, i.e. specifically considering other loading cases and boundary conditions. To do this, models of specimens were created in Abaqus similar to those tested and applied a similar load protocol based on the rules proposed by FEMA-461 was imposed on each model. Namely, this protocol had a Δ_0 of 0.03 in, and the amplitude of each cycle increased by 40% up to a displacement of 9.15 in.

Outcome #4: Seismic Analysis of Nonlinear Subsystems

Procedure

Task Group D developed a procedure for the seismic analysis of nonlinear natural gas subsystems that can be used to generate fragility curves for *OpenSRA*. This procedure uses the opensource software OpenSees, however it could be used also with another software capable of performing dynamic nonlinear earthquake analysis. In this procedure, the nonlinearities and failure points of the subsystem are concentrated at the location of critical components, while the remainder of the model subsystem remains linear. The procedure adopts the following steps:

1. Identify the critical components and their engineering demand parameter (EDP). The critical components are those with nonlinear behavior and where failure occurs.
2. Obtain the nonlinear behavior of the critical components.
3. Create a model of the critical components in OpenSees. Critical components are modeled in OpenSees using a simplified lumped phenomenological representation offered by nonlinear zero-length springs, while the other sections of the subsystem are modeled with linear elements. The material and parameters of these springs depends on the type of components and needs to be calculated by the researchers.
4. Create a model of the subsystem in OpenSees. In this model, all the components of this system except the critical components are modeled as linear elements.
5. Validate the model.
6. Run earthquake motion simulations on this model.

The following sections will present example of the key steps of these procedure for the WTP and VPV subsystems, starting from the description of the subsystem and model (point #4) followed by a description of the critical components (point #2). Validation of the OpenSees model is presented in the results section.

Numerical Models of Subsystems and Critical Components in OpenSees

The geometry of these subsystems is based on photographic evidence found on public resources, design calculations, manufacturer catalogues of valves and other components, site visits to a gas storage facility, and personal communication with experts at utility companies.

WTP Subsystem

In storage facilities, the natural gas is injected and/or withdrawn from underground storage through a wellbore and a system of tubing and casings which facilitate the flow of the gas to/from the surface (U.S. DoT 2018). At the surface, the tubing/casing assembly terminates with a wellhead tree which is then connected to a network of pipes (or laterals) where the gas can flow, as shown in Figure 24a. The seismic response of these components will largely be defined by the behavior of the transitional joints (elbows and tees), therefore understanding both the elbow and tee response is essential.

The wellhead trees observed at storage facilities in California include the upper section of the tubing/casing assembly, the casing head, the casing spool, gate valves, and a cross converting the flow from vertical to horizontal. The branches of the tree are also valves connected to the cross and the laterals. Generally, a portion of the tree is below the ground level inside the "wellhead cellar".

The wellhead tree was modeled in OpenSees as a cantilever beam with two branches, as shown in Figure 24b. Both tree and branches are modeled as linear elements. The area, mass and stiffness of the wellhead tree and branches were calculated using the average dimensions of the different components found in manufacturer catalogues.

Figure 24: Wellhead tree

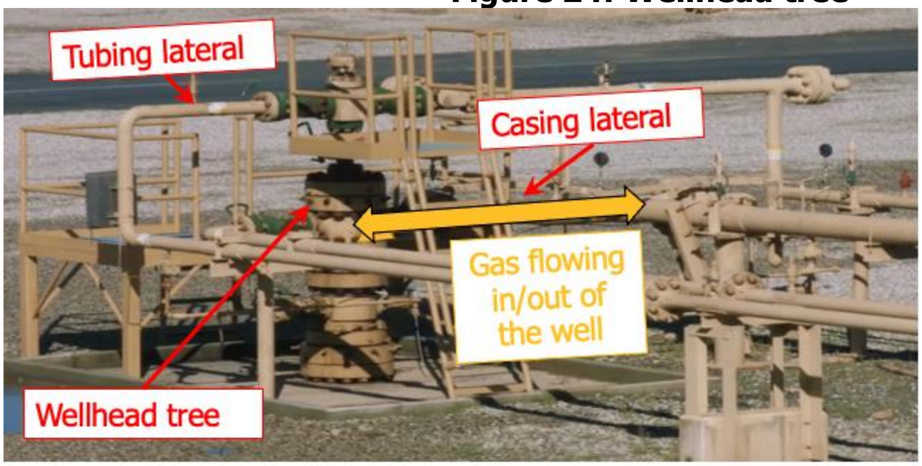

(a)

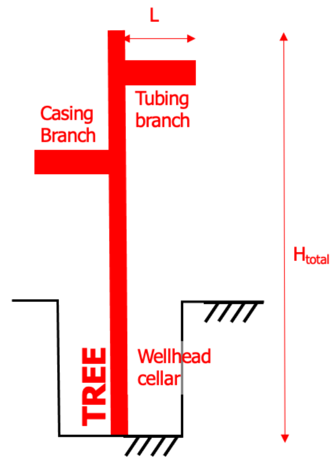

(b)

(a) Photograph of a wellhead tree and connected piping (edited from SoCalGas 2016b), (b) Schematic of a wellhead tree showing relevant nomenclature

Depending on the type of wellhead, there are either one or two pipes at the top. When two pipes are present, the top pipe is connected to the wellhead tubing, while the lower pipe is connected to the wellhead casing, and hence they are referred herein as "casing lateral" and "tubing lateral" (Figure 24). Based on available evidence, 4 in diameter Schedule 80 pipes is the most common for this type of application, and hence it was used in the present analysis.

In the OpenSees model of the WTP subsystem, only one lateral at a time is considered. Based on available evidence, three geometries of laterals are common in storge facilities in California, and they implemented within the OpenSees model. The main difference between the models is the number of pipe segments contained in the lateral, as such the various configurations are denoted as P2, P3 or P4, see Figure 25. For each configuration, the joints can be either tees or elbows. In the end, a total of six possible scenarios can be selected by the users of *OpenSRA*. Pipe segments are modeled as linear elements in OpenSees, with nonlinearities concentrated at the joints where critical components, either tees or elbows, are located. If valves are installed on the pipes, they are modeled as lumped masses.

The validation of the OpenSees model of the WTP subsystem was performed by comparing the experimental and numerical natural frequencies of a wellhead tree and piping subsystem at a natural gas storage facility in California. The experimental natural frequencies were obtained by performing low amplitude impact tests at various directions to excite the important modes of the subsystem.

Figure 25: Summary of configuration of laterals

Configuration	Sample Photograph	Key features
P2	 SoCalGas 2017b	Lateral extends to the top of the wellhead tree, changes direction and then runs along pipe supports
P3	 SoCalGas 2016b	The lateral starts close to the top of the wellhead, runs vertically down and then runs along supports
P4	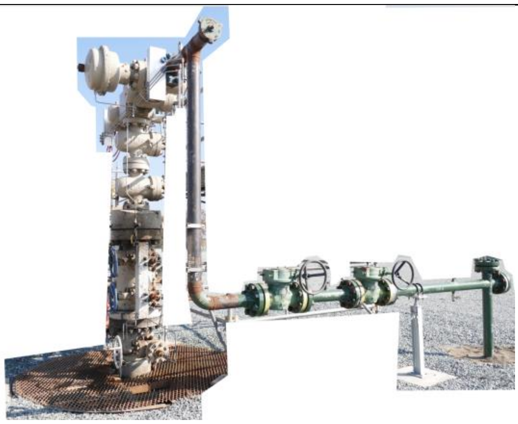	Pipe starts at the top of the tree, runs vertically down, then runs horizontally and runs vertically into the ground

VPV Subsystem

The vertical pressure vessels observed at gas storage facilities comprise a tall cylindrical vessel with hemispherical or elliptical heads supported by a skirt. The skirt is then connected to the concrete base with anchors. These vessels are connected to a pipe at their bottom right above the skirt, and to another pipe either going vertically upward on top of the vessel or laterally close to the head of the vessel (Figure 26a). Tall pressure vessels are particularly vulnerable to seismic motions, with their behavior often dictated by the base condition and its ensuing flexibility. Hence, the critical component of this subsystem is deemed to be its base. The optimal EDP for these analyses is the ratio between the moment demand at the base imposed by an earthquake (M_d) and the moment capacity at which a limit state is achieved (M_c). For the VPV subsystem under consideration, when the base connection is fixed, the M_c is the moment associated with concrete breakout of the anchorage, as this will occur at an early load stage. Alternatively, when the base connection is designed with anchors that are intended to stretch, the moment associated with expected limit states is evaluated to identify the controlling minimum. For example, the strain beyond yield in the anchors will lead to plastic rotation of the top of the pressure vessel, which could limit functionality of attached piping, particularly for piping attached at the top of the VPV. Pressure vessels were modeled in OpenSees as cantilever beams. The areas and moments of inertia assigned to the beam varied, for the lower most portions properties were defined based on the skirt at the base, while the cylindrical portion of the pressure vessel extended for the remainder of the height (Figure 26b). In a first phase of analysis, the inlet and outlet pipes were also modeled. However, the model revealed that the presence of these pipes has very little influence on the dynamic characteristics of the subsystem, and hence these pipes were removed in subsequent phases of the analysis.

Validation of the OpenSees model was performed by comparing the natural frequencies and modes predicted with those predicted using a high-fidelity 3D Abaqus model for a sample VPV subsystem with the pipes connected to it (Figure 26c).

Figure 26: Vertical pressure vessels

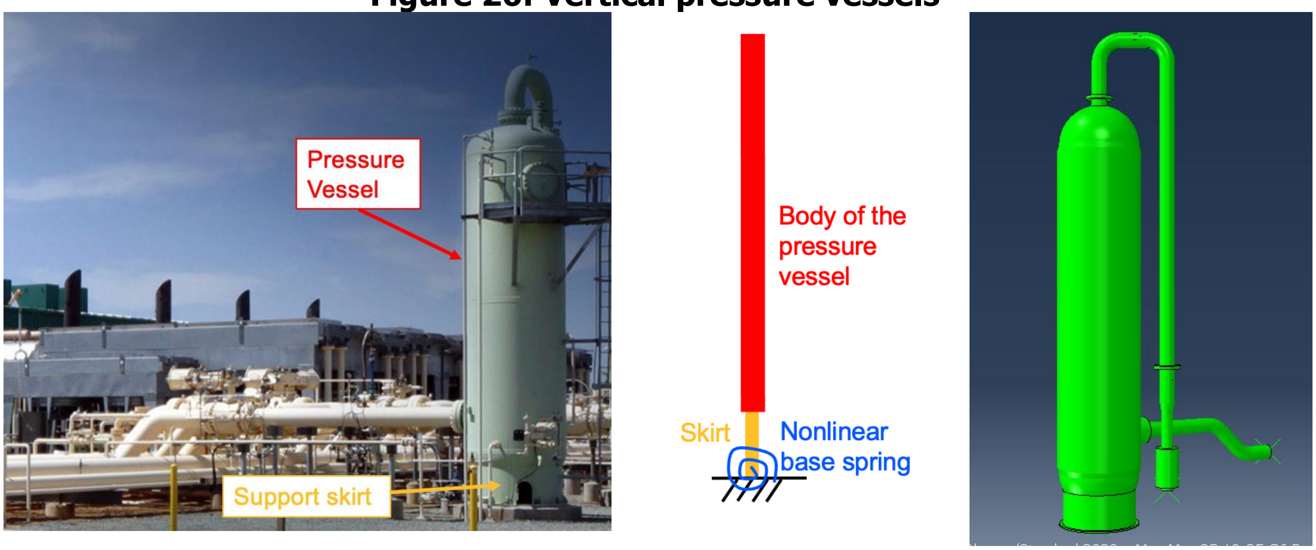

(a) **(b)** **(c)**

(a) Photograph (RockPoint Gas Storage 2021), (b) Schematic of the OpenSees Model, (c) Abaqus model

Numerical Models of Critical Components in OpenSees

WTP subsystem: Tees and Elbows

The critical components selected for the WTP subsystem were in-plane and out-of-plane tees and in-plane elbows with 4 in diameter Schedule 80 pipe. These types of pipes were selected as they were identified from on available evidence and discussion with utility companies as being typical of gas storage facilities. The nonlinear material model utilized within OpenSees to capture the local behavior at each tee-joint and elbow is the generalized *Steel4* material model, see Figure 27. *Steel4* is characterized by an approximately bilinear response, with a smooth transition between initial (elastic) behavior and hardening-large strain behavior. Kinematic hardening is available within *Steel4* and was deemed reasonable based on observations from the component experiments. This model requires the assignment of the following parameters:

- f_y: yield strength
- E_0: initial stiffness
- b_k: hardening ratio
- R_0, r_1, r_2: parameters controlling the exponential transition from linear elastic to hardening asymptote.

The nonlinear stress-strain behavior (or moment-rotation, as in this case) of *Steel4* can be either symmetric or asymmetric. When the material is asymmetric the four parameters b_k, R_0, r_1 and r_2 need to be specified for both directions of loading (the second direction is indicated with a superscript "c" in Figure 27), while f_y and E_0 remain the same. Hence, springs defined with the properties of the *Steel4* material have six parameters if they are symmetric and ten parameters if they are asymmetric.

Figure 27: Stress-strain behavior of Steel4 in OpenSees

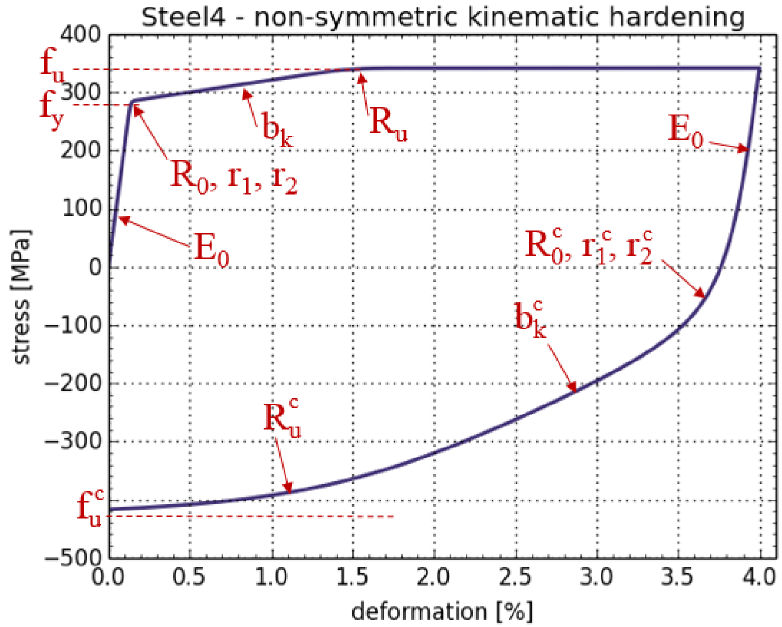

(Zsarnoczay 2015)

The procedure used to calibrate the parameters of the nonlinear springs in OpenSees involved the following:

- A numerical model of the critical component and sections of straight pipes is created in Abaqus. This model uses the calibrated material properties obtained in outcome #3 and the field boundary conditions. The Abaqus model of the tee rotating in-plane is shown in Figure 28a. Because Abaqus models with calibrated material properties showed to be able to reproduce actual behavior of the components very precisely, the behavior of this specimen in Abaqus is considered to be the real behavior.

- An OpenSees model of the same geometry and boundary conditions is created, as shown in Figure 28b. In this model, all the plasticity of the tee is concentrated in a nonlinear spring made of Steel4 material (point B in the Figure 28b), while the other elements are linear.
- The two models are subjected to the same displacement-controlled cyclic analysis with a load protocol following the FEMA-461 recommendations and similar to that used for the component tests.
- The forces necessary to obtain this displacement in the Abaqus and OpenSees are compared, and the parameters of the *Steel4* spring in OpenSees varied to minimize the difference between the two for the displacement producing a strain from 1% to 6%.

This same procedure can be used to extend the results to a wider range of component types/details and loading conditions.

Figure 28: Component models for the tee rotating in-plane

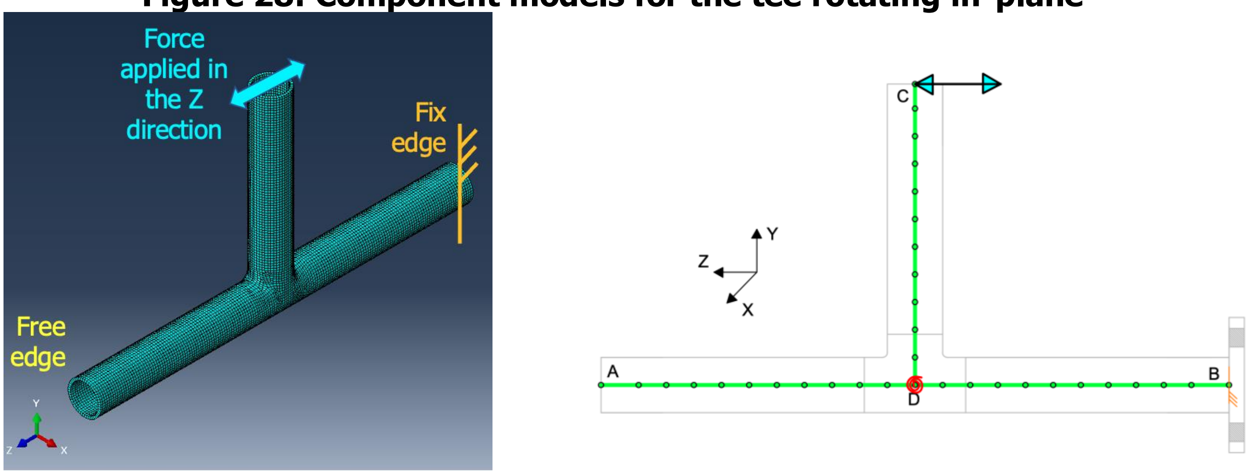

(a) **(b)**

(a) Abaqus model, (b) OpenSees model

Pressure Vessels: Base Connection

For the pressure vessels, the critical component considered was the base of the pressure vessel. Two types of base connections were considered. The first represents the configuration of older pressure vessels, in which the base anchors are embedded in a concrete footing and thus designed as a fully fixed connection. In this case, no elongation of the anchor will occur, and minimal base rotation is anticipated, consequently the base of these pressure vessels is considered fixed. The second configuration is typical of newer pressure vessels. In this case, the anchors have a designed free stretch length of at least eight times the diameter of the anchor, as recommended by ACI 318-19 (2019). This allows the base to rotate, hence a nonlinear spring is incorporated in the model at the base of the vessel, as shown in Figure 26b. The behavior of this spring was assumed to be elastoplastic with nominal strain hardening of mild steel (e.g. common anchorage material of grade A36 steel is utilized in practice). The yield moment and rotation were obtained from the geometry and material properties of the pressure vessel and anchors.

Outcome #5: Fragility Curves for Selected Subsystem Geometry

WTP Subsystem

Seismic fragility curves were obtained for the selected common geometries of the subsystems under consideration. These curves were developed using the following three functions:

1. The probability of attaining the damage state of leakage or rupture based on the damage measure (DM), which in this case is uniaxial strain.
2. The DM as a function of the engineering demand parameter (EDP).
3. The EDP as a function of the intensity measure of the earthquake (IM) and the key parameters (X_1,X_2,X_3 etc.) of the subsystem. It is noted that the users of *OpenSRA* may explicitly define the subsystem parameters, or leave them blank. In the former, the user can find the fragility function of a specific subsystem with an assigned geometry, while in the later the fragility function adopted is a generic function for the subsystem and all parameters within an assigned range. In the former case, the uncertainly of the function will be larger.

Details regarding the development and features of the first function is presented in Hutabarat et al. (2022). Additional information regarding the second and third functions are presented in this section.

Development of the DM(EDP) Function

DM(EDP) curves for the WTP subsystem were developed for each of the critical components under consideration for the cases of no internal pressure and large internal pressure (1500 psi). These curves were obtained as follows:

- Abaqus FE models of these components were subjected to the FEMA-461 cyclic protocol adopted in the experimental component campaign and subsequently in the calibration of the FE models.
- Maximum and minimum principal stresses in the tees and elbows were extracted and correlated to the applied rotation.
- To obtain a monotonic strain-rotation (i.e. DM(EDP)) curve, the strain response at each first rotation cycle, at each of the positive and negative rotations, within a group like amplitude cycles is selected.
- At this instance in the response history, the absolute value of uniaxial strain was considered for all components. For components behaving asymmetrically, the rotation was preserved as either positive or negative.
- The curves were only fit to the data points only up to a strain of 6%, which slightly larger than the range of strain associated with 50% probability of failure (2-4% strain, see the System Wide Natural Gas Infrastructure Response and Fragility Report).

The DM(EDP) curves for the VPV subsystem were calculated from geometric configurations based on the strain in the anchors at the base of the pressure vessels.

Development of the EDP(IM,X_1,X_2,X_3) Function

To develop the EDP(IM,X_1,X_2,X_3) function for each of the subsystems, the following steps were adopted:

- Among all parameters of the subsystems, the key parameters X_1,X_2,X_3 etc. were selected based on the following criteria:
  - They have a significant variation.
  - They are those most likely to affect the overall seismic behavior of the system.
  - The *OpenSRA* analyst may easily obtain them, when analysis of a subsystem with a specific geometry is desirable.
- Each key parameter was assigned a distribution function based on available evidence and/or feedback from PG&E.
- Latin hypercube sampling was used to select N combinations of the key parameters to be assigned to the subsystem. It is noted that other parameters are considered fixed and cannot be modified by *OpenSRA* users.
- N subsystem models with the combination of parameters noted above were created and each of them was subjected to a suite of earthquakes scaled to different intensity levels these will be published in the System Wide Natural Gas Infrastructure Fragility Model Report later this year. This allowed definition of the EDP for each combination of parameters, earthquake, and scaling factor.
- Numerical simulation results were then analyzed using the statistical software JMP (Sall et al. 2017) to obtain the optimal function correlating the EDP, IMs and the parameters X_1,X_2,X_3 etc.

Description of the WTP Subsystem Configurations

Table 6 presents a summary of the six configurations of the WTP subsystem, which the *OpenSRA* analyst may select. The distributions of the three key parameters were lognormal with an assigned average (μ) and standard deviation (σ), as presented in the fourth column of Table 6. For each configuration, earthquakes are independently imposed in both directions, and for each case the EDP is the peak rotation θ at a single or multiple joints. This is coded automatically in *OpenSRA* and need not be defined explicitly the user.

Table 6: Configurations of WTP subsystem, variables considered and EDP

Conf.	Comp.	Schematic and name	Variables	Dir.*	EDP
P2	Elbow	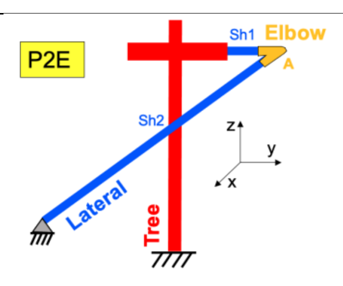	X_1) Tree Height H_t (μ=9 feet, σ= 3 feet) X_2) Length of pipe Sh1 L_{p1} (μ=5 feet, σ= 3 feet)	X	θ_A (in-plane)
				Y	θ_A (in-plane)

<table>
<tr><th>Conf.</th><th>Comp.</th><th>Schematic and name</th><th>Variables</th><th>Dir.*</th><th>EDP</th></tr>
<tr><td rowspan="2"></td><td rowspan="2">Tee</td><td rowspan="2">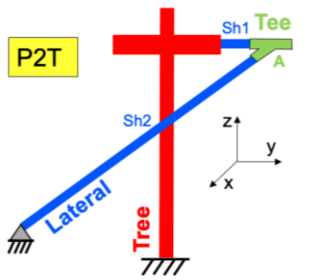</td><td rowspan="2">X3) Length of pipe Sh2 L_{p2} (μ=10 feet, σ= 6 feet)</td><td>X</td><td>θ_A (in-plane)</td></tr>
<tr><td>Y</td><td>θ_A (in-plane)</td></tr>
<tr><td rowspan="4">P3</td><td rowspan="2">Elbow</td><td rowspan="2">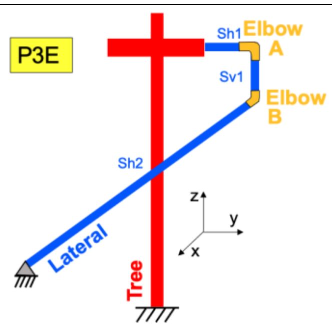</td><td rowspan="4">X1) Tree Height H_t (μ=9 feet, σ= 3 feet)
X2) Length of pipe Sh1 L_{p1} (μ=5 feet, σ= 3 feet)
X3) Length of pipe Sh2 L_{p2} (μ=10 feet, σ= 6 feet)</td><td>X</td><td>θ_B (in-plane)</td></tr>
<tr><td>Y</td><td>θ_A (in-plane)</td></tr>
<tr><td rowspan="2">Tee</td><td rowspan="2">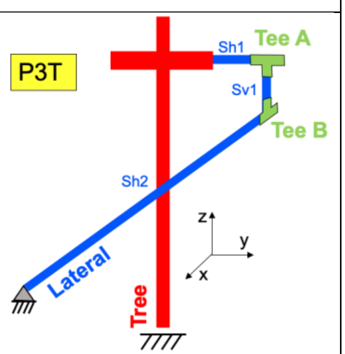</td><td>X</td><td>θ_A (out-of-plane)
θ_B (in-plane)</td></tr>
<tr><td>Y</td><td>θ_A (in-plane)</td></tr>
<tr><td rowspan="3">P4</td><td rowspan="2">Elbow</td><td rowspan="2">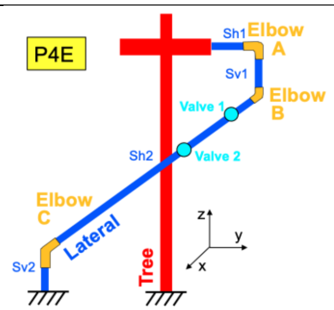</td><td rowspan="3">X1) Tree Height H_t (μ=9 feet, σ= 3 feet)
X2) Length of pipe Sh2 L_p (μ=16 feet, σ= 6 feet)
X3) Weight of valves W_v (μ=350 lb, σ= 150 lb)</td><td>X</td><td>θ_B (in-plane)
θ_C (in-plane)</td></tr>
<tr><td>Y</td><td>θ_A (in-plane)</td></tr>
<tr><td>Tee</td><td></td><td>X</td><td>θ_A (out-of-plane)
θ_B (in-plane)
θ_C (in-plane)</td></tr>
</table>

Conf.	Comp.	Schematic and name	Variables	Dir.*	EDP
		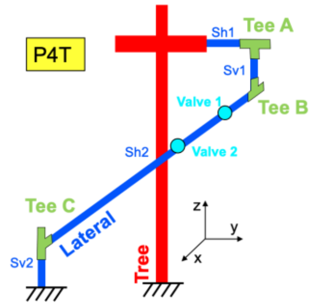		Y	θ_A (in-plane) θ_C (out-of-plane)

***Dir. = direction of the input excitation**

VPV Subsystem

The VPV subsystem used for this phase of the analysis included the pressure vessel body and skirt either fixed at the base or connected through a nonlinear spring representing the behavior of the stretch anchors, as explained in the previous sections. The four independent key parameters X_1-X_4 were the following:

1. Total height of the pressure vessel.
2. Height to diameter ratio of the pressure vessel. The combination of these first two parameters defines the diameter of the pressure vessel.
3. Pressure vessel design pressure. Using the internal pressure and diameter of the vessel it was possible to estimate the thickness of the pressure vessel.
4. The diameter of the anchors.

As seen for the WTP subsystem, the user of *OpenSRA* can input these parameters, to obtain a fragility curve for a specific VPV configuration or a generic fragility curve, respectively. To calculate the generic fragility curve, each of these parameters was assigned a distribution and N combinations of these parameters were selected using Latin hypercube sampling. Subsequently:

- A model of each configuration was created in OpenSees and subject to the same set of ground motions used for the WTP subsystem. The demand moments at the base of the vessels M_d were extracted from OpenSees.
- The moment capacity was either of the limiting moment (M_c) defined based on the connection being fixed or designed with stretch length anchors.
- The moment ratio (M_d/M_c) was obtained for each earthquake and each configuration. A moment ratio larger than unity indicates that failure is anticipated. This was associated with a probability distribution function to obtain the fragility function for the VPV subsystem.

CHAPTER 3: Project Results

Outcome #1: Experimental Data on Critical Components

This section presents the main limit states observed during testing in relation to the moment-rotation curves. It is noted that all moment-rotation curves are plotted at the same scale to facilitate comparisons.

The progression of damage was the same for all the specimens except 8T-IP, and included the following limit states:

1. First ovalization. This limit state identifies the moment when a visible deformation of the component could be observed for the first time.
2. First crack. This limit states indicate the appearance of a shallow crack at locations of high strains. It is noted that these specimens were characterized by the appearance of a network of cracks, instead of a single crack. The location of these cracks corresponded to the location of high strains predicted by the Abaqus models.
3. Through crack. Sudden loss of internal pressure happened when the continuous displacement applied to the specimen lead one or more shallow cracks to become through cracks. This is considered the "failure" of the specimen.

Components failing in this way are deemed "ductile", since they show warning signs before failure happens. In the case of these specimens, the warning signs were in the form of shallow cracks.

The only specimen that had a "brittle" failure far from the location of high strains predicted by Abaqus was 8T-IP. More information about this is provided in the corresponding section. The nomenclature used to describe the location of damage in the next sections is presented in Figure 29.

Figure 29: Relevant nomenclature for critical components

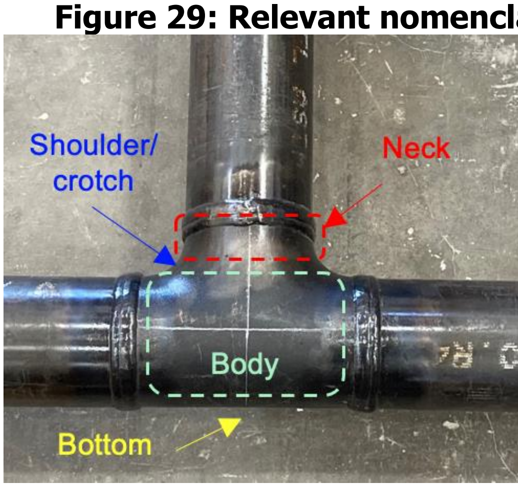

(a)

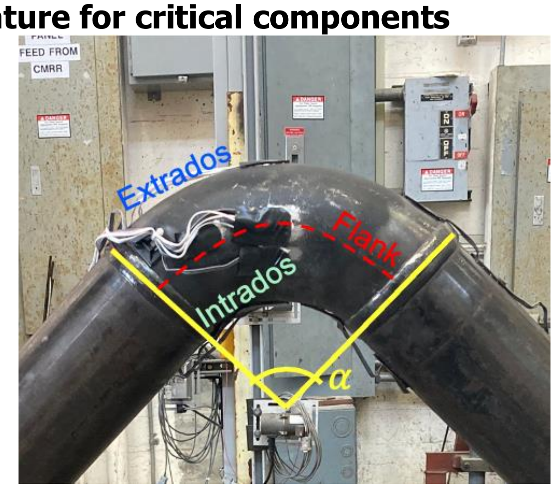

(b)

(a) Tees; (b) Elbows

In-Plane Tee Specimens (4T-IP and 8T-IP)

Figure 30a presents select results for specimen 4T-IP. Cracks started developing in the shoulder of the tee a rotation of 17° and failure happened at 24°. A photograph of the failed tee is shown in Figure 31a.The maximum moment developed was ~350 kip-in in the northward direction and ~250 kip-in in the southward direction.

Specimen 8T-IP had a very different failure mode than specimen 4T-IP and all other specimens. In fact, this failed when a through crack formed suddenly in the body of the tee, see Figure 31b. This is different than the failure of other specimens not only because the body of the tee is not the location of high strains predicted by Abaqus, but also because there were no visible shallow cracks before the through crack developed. Figure 30b shows that the through crack developed when the specimen was being loaded in the South direction at very small rotation. The maximum rotation reached by the specimen before failing was 7°, while the maximum moments were ~900 kip-in in the northward direction and ~800 kip-in in the southward direction. These moments are much larger than those developed for specimen 4T-IP because of the larger diameter of the specimen.

Figure 30: Moment-rotation for tee specimens tested in-plane

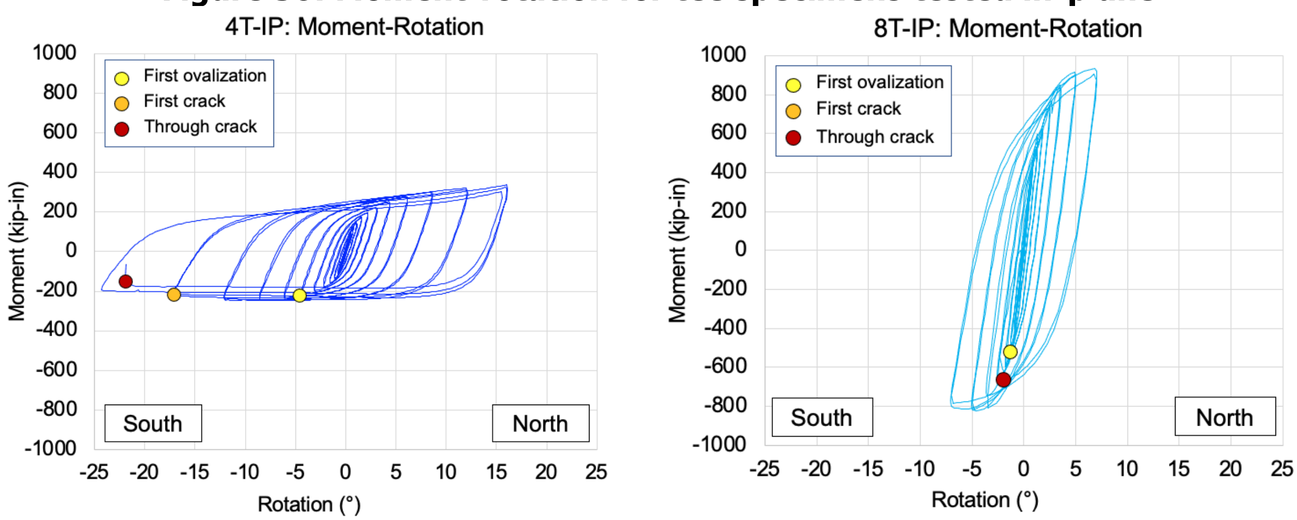

(a) Specimen 4T-IP; (b) Specimen 8T-IP

Figure 31: Through crack for tee specimens tested in-plane

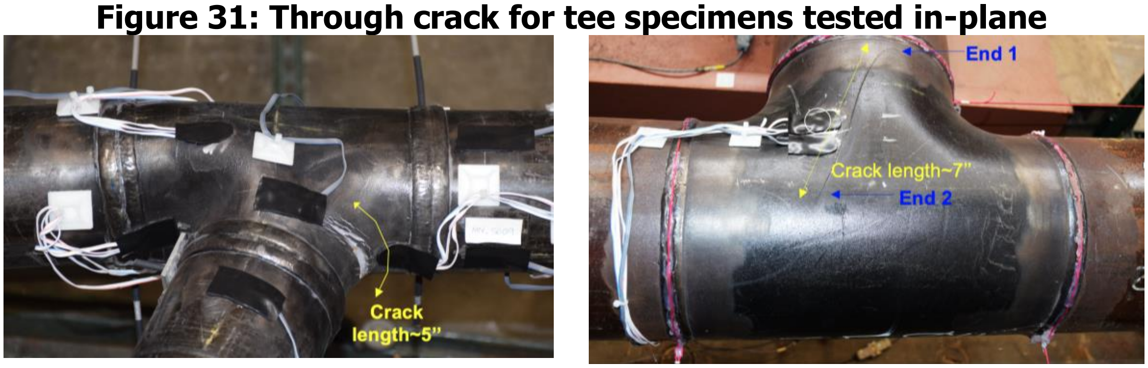

(a) (b)

(a) Specimen 4T-IP; (b) Specimen 8T-IP

Out-of-Plane Tee Specimens (4T-OP and 8T-OP)

Figure 32 shows the moment-rotation curves and relevant limit states for the tee tested out-of-plane. As expected, specimen 4T-OP fails at a larger rotation (~24°) than specimen 8T-OP (~10°) due to its smaller diameter-to-thickness ratio. However, specimen 8T-OP is able to develop larger moments than specimen 4T-OP (900 kip-in versus 200 kip-in) because of its larger diameter. A comparison of the results from tests in the out-of-plane direction in Figure 32 with those in the in-plane direction in Figure 30 shows that the tees are stronger when deforming in-plane. Figure 33 shows the through cracks for both specimens. These cracks occurred in the body of the tee close to the neck as predicted by the Abaqus models.

Figure 32: Moment-rotation for tee specimens tested out-of-plane

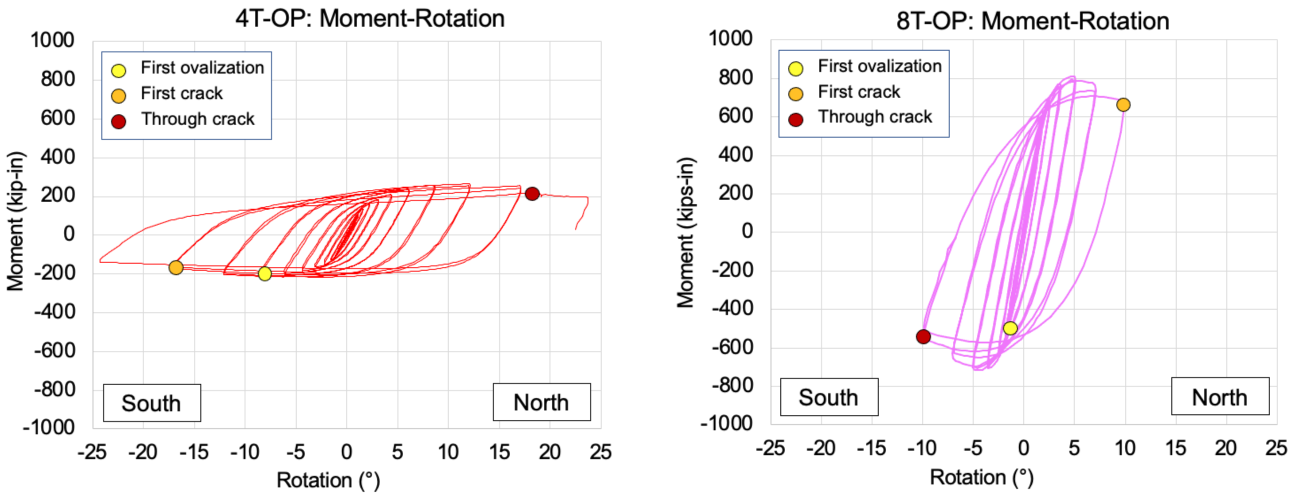

(a) **(b)**

(a) Specimen 4T-OP; (b) Specimen 8T-OP

Figure 33: Through crack for out-of-plane tee specimens

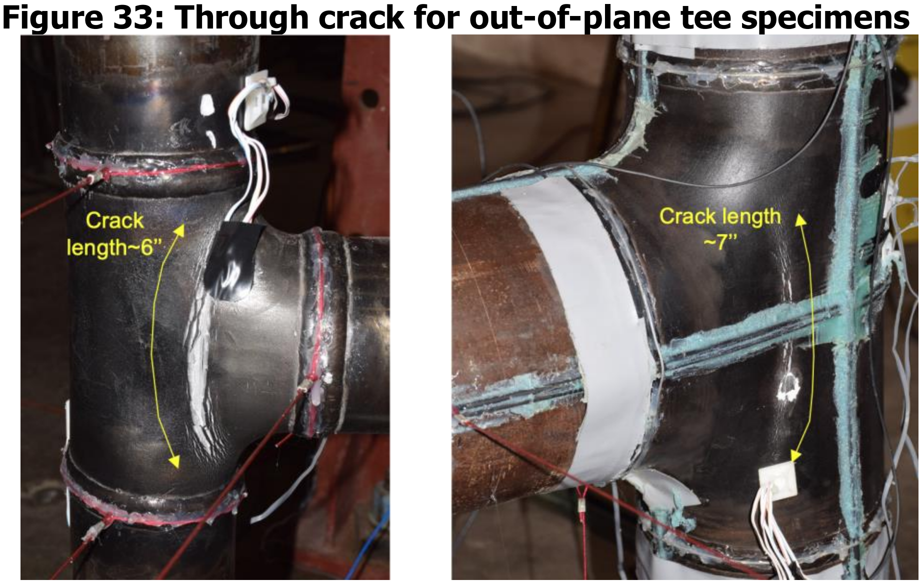

(a) **(b)**

(a) Specimen 4T-OP; (b) Specimen 8T-OP

Elbow Specimens (4E-90 and 4E-45)

Figure 34 shows the moment rotation for elbows tested in-plane. Both elbows became stiffer during opening and softer during closing, as predicted by the Abaqus models. This happens because elbows become taller when they open and squatter when they close. Both specimens showed good ductility, but specimen 4E-90 failed at the larger rotation of ~22° compared to ~10° of specimen 4E-45. The failure mode was similar for both specimens and consisted of through cracks at the center intrados of the elbows, as shown in Figure 35.

Figure 34: Moment-rotation for elbows tested in-plane

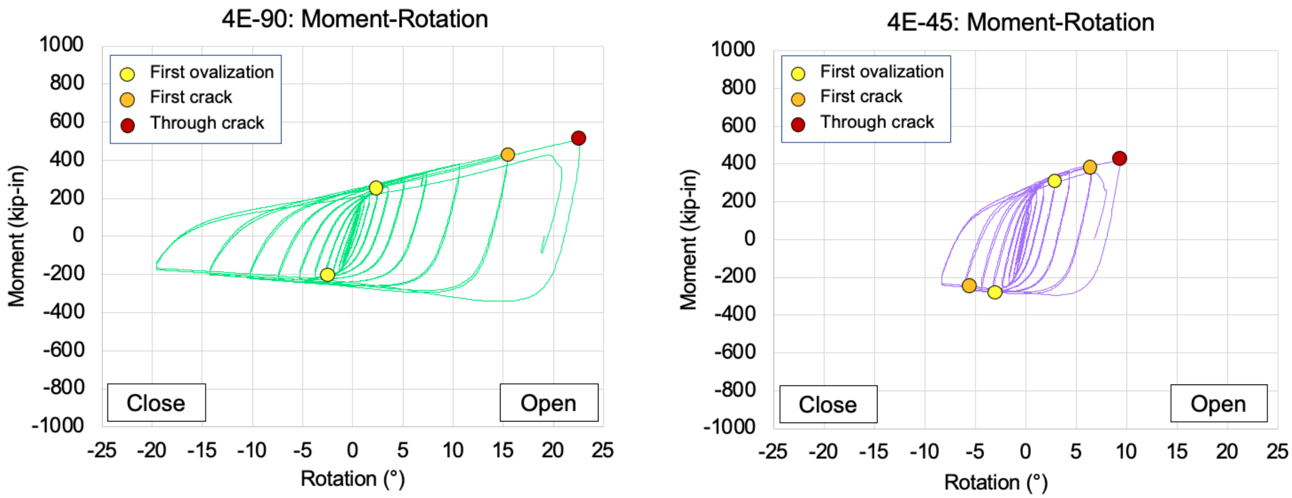

(a) (b)

(a) 90° elbow; (b) 45° elbow

Figure 35: Through cracks for elbows tested in-plane

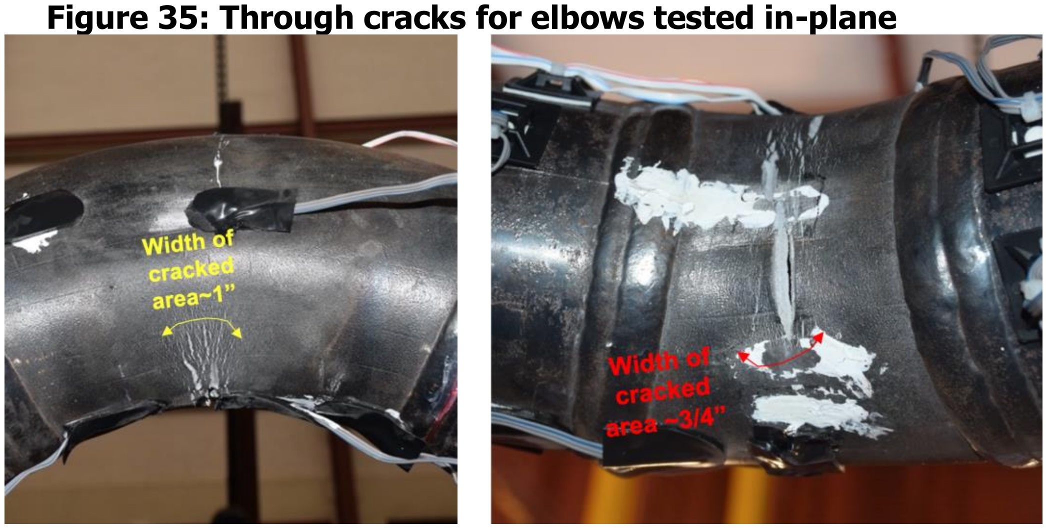

(a) (b)

(a) 90° elbow; (b) 45° elbow

Outcome #2: Experimental Data Relative to Subsystems

Synchronous Earthquake Motions

No yield, damage, or loss of pressure was observed in the subsystem under synchronous motions. Analysis of the subsystem response under the broad-band white noise excitations before and after the different levels of shaking concluded that there was no change in the dynamic properties of the subsystem, just means that the subsystem did not undergo any plastic deformation.

Asynchronous Motions Producing Relative Displacements

The subsystem did not experience any yield, damage, or loss of pressure when subjected to a relative displacement of up to 8 in between the tables. At larger relative displacements, data from strain gages indicated a clear progression of nonlinear behavior, with yielding at larger number of locations as the relative displacement increased. Figure 36 present the progression of this yielding behavior corresponding to a relative displacement of 17 in. The red dot denotes where yielding occurred and the number represents the ratio between the maximum strain measured at that location at the yield strain, assuming a yield stress of steel equal to 65 ksi. A value of 1.4 means that this location experienced strain 1.4 times the yield strain of steel. Higher values indicate higher strain and thus more yield.

Significantly, it was also noted that the subsystem did not experience any leaks or loss of pressure despite the extreme deformation the system experienced at 17 inches of relative displacement, which is equivalent to 7.8% rotation relative to the span of the 4 in pipeline (17 in/216 in) and 6.7% rotation relative to the span of the 8 in pipeline (17 in/252 in). Figure 37 provides pictures of pipe deformations at 17 in showing the rotation experienced by both pipelines. However, at such rotation, damage was observed to the concrete pedestal at one pipe support, as shown in Figure 38.

Figure 36: Observed yielding at two cycles of 17 in of shake table relative displacement

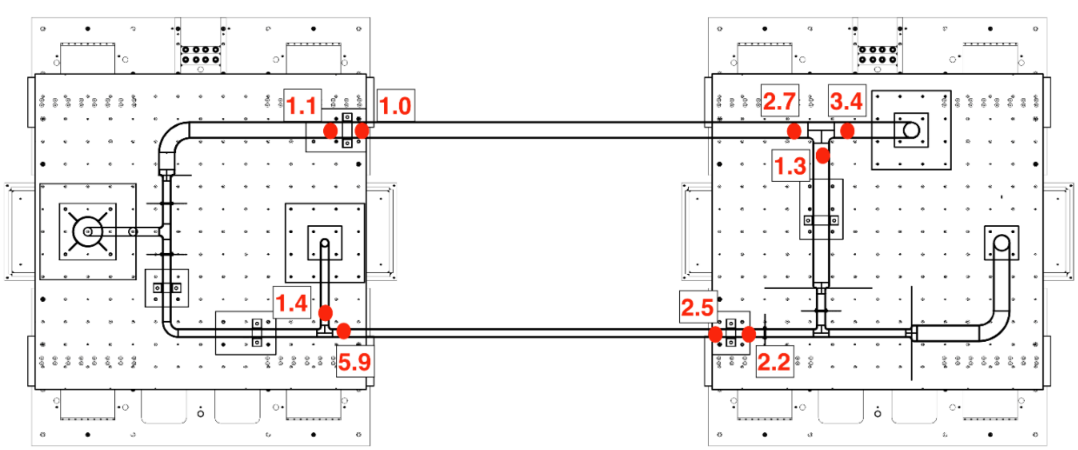

Figure 37: Piping deformation at 17 in of relative shake table displacement

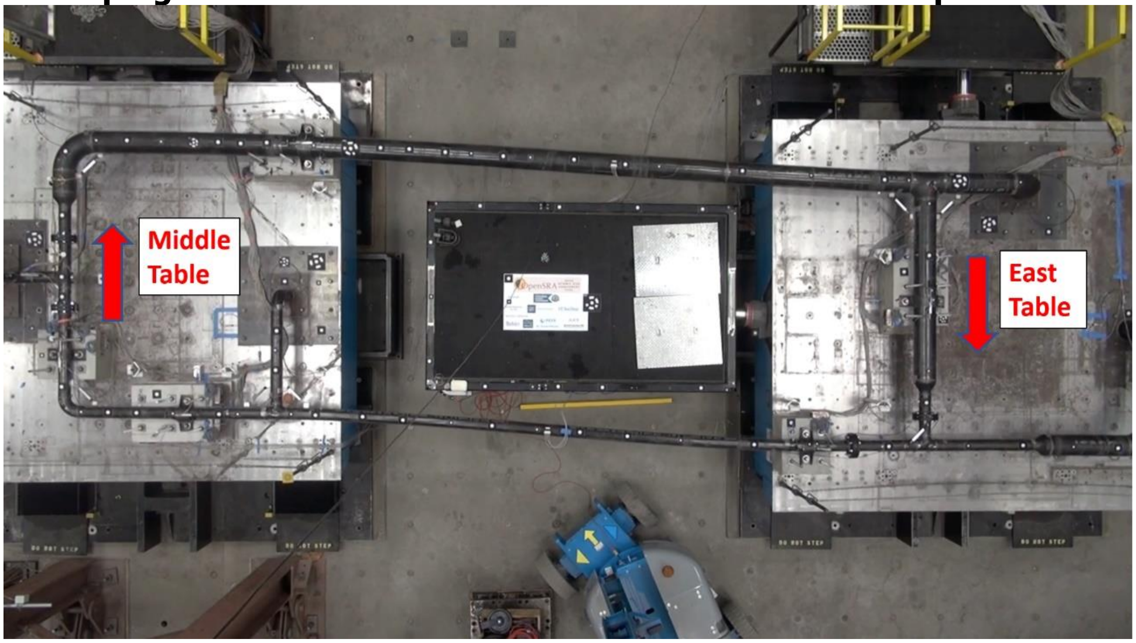

(a)

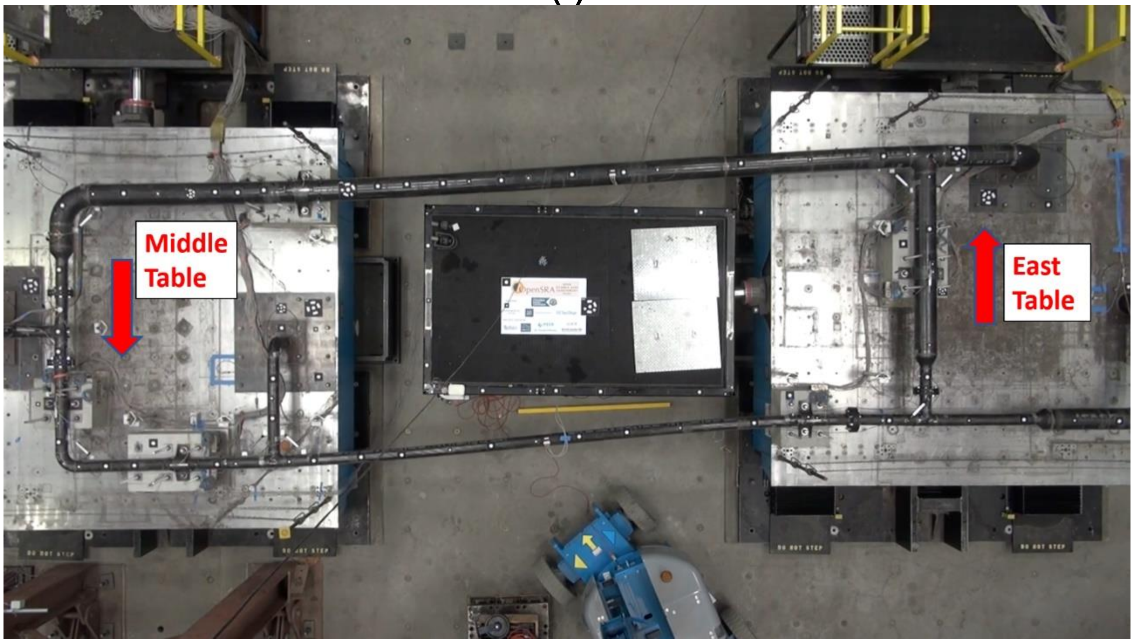

(b)

(a) North table moving east, (b) North table moving west

Figure 38: Damage at a pipe support after the final motion

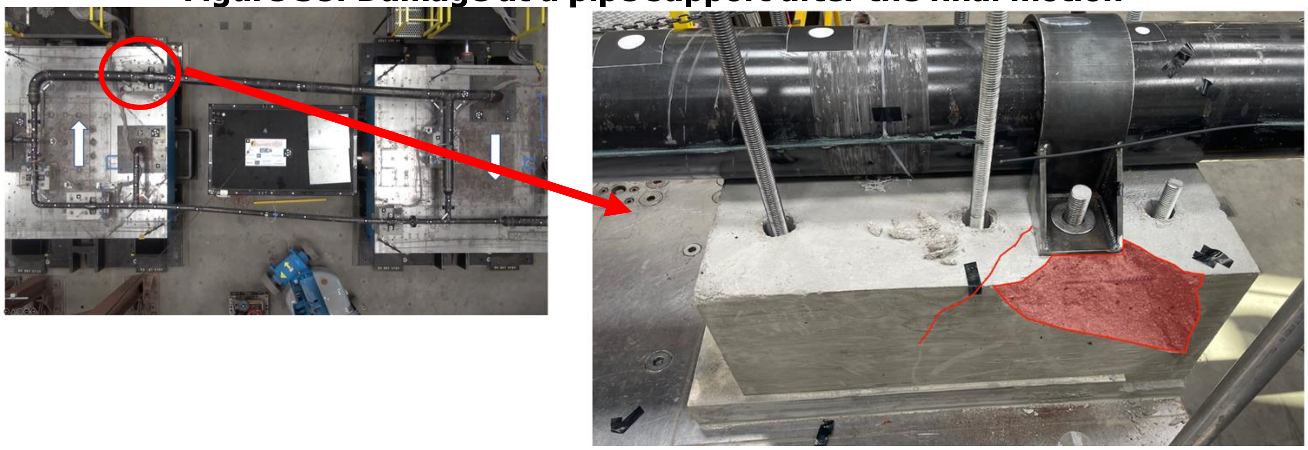

Implementation into *OpenSRA*

There are a very broad set of different configurations of actual natural gas surface piping systems. To help ensure the most effective long-term application of *OpenSRA*, users will need to generate configuration-specific fragility functions based on accurate nonlinear numerical models of key specific configurations, it will simply be impractical to experimentally test all configurations for fragility characterization. The UNR dataset for the extreme response of a representative above ground piping system undergoing large relative displacements will provide a key benchmark problem for testing and validation of various numerical models which end-users will be using for representation of the nonlinear response of piping systems. The UNR test included a suite of increasing amplitude experiments that track the initiation and evolution of system yielding. Given the myriad of configurations of surface piping systems, the ability to reliably model system response will be an essential tool for future risk assessments and for the broadest application of *OpenSRA*.

Outcome #3: Calibration of the Material Properties for Abaqus

Calibration of Cyclic Hardening Parameters

As explained in Chapter 2, the optimal values of the cyclic hardening parameters were obtained by minimizing the error between the experimental results from component tests and the corresponding Abaqus numerical predictions for all specimens tested.

Calibration efforts were initiated by implementing hardening parameters obtained by past researchers, namely those provided in Table 7. Since the values of Q, b, C, and γ obtained by Zakavi et al. (2017) provided a very good comparison with experimental results, it was decided to adopt these values directly. However, the value of σ_0 used in this study did not provide an optimal match, hence a calibration was performed specifically on this parameter. The optimal value of σ_0 was obtained for each specimen by minimizing the error between the time history of the force measured experimentally and obtained numerically. This optimal value of σ_0 was then compared to the value of σ_y from the mill certificates for each specimen, and they were found to be very close, with a difference of plus or minus 20%. In this way, it was possible to find the optimal values for the five material parameters needed in the combined hardening model. Comparison of experimental results and numerical predictions for specimens 8T-OP and 4E-90 in terms of moment-rotation and time-history of force are shown in Figure 39 and

Figure 40.

Table 7: Values of cyclic hardening parameters obtained by past researchers

Reference	Component/ Material	σ_0 (ksi)	Q (ksi)	b	C (ksi)	γ
Chatziioannou et al. 2021	8 in diameter/Sch.40 elbow; API 5L X52	45.7	-7.2	80	C_1=6526 C_2=1667 C_3=870 C_4=391	$\gamma_1 = 650$ $\gamma_2 = 200$ $\gamma_3 = 190$ $\gamma_4 = 15$
Payne (2000)	Steel beams, A36	51	20	10	500	50
Zakavi et al. (2017)	Elbows, A106B	47.6	19.7	4.76	400	17.66

Figure 39: Comparison of numerical and experimental moment-rotation curves

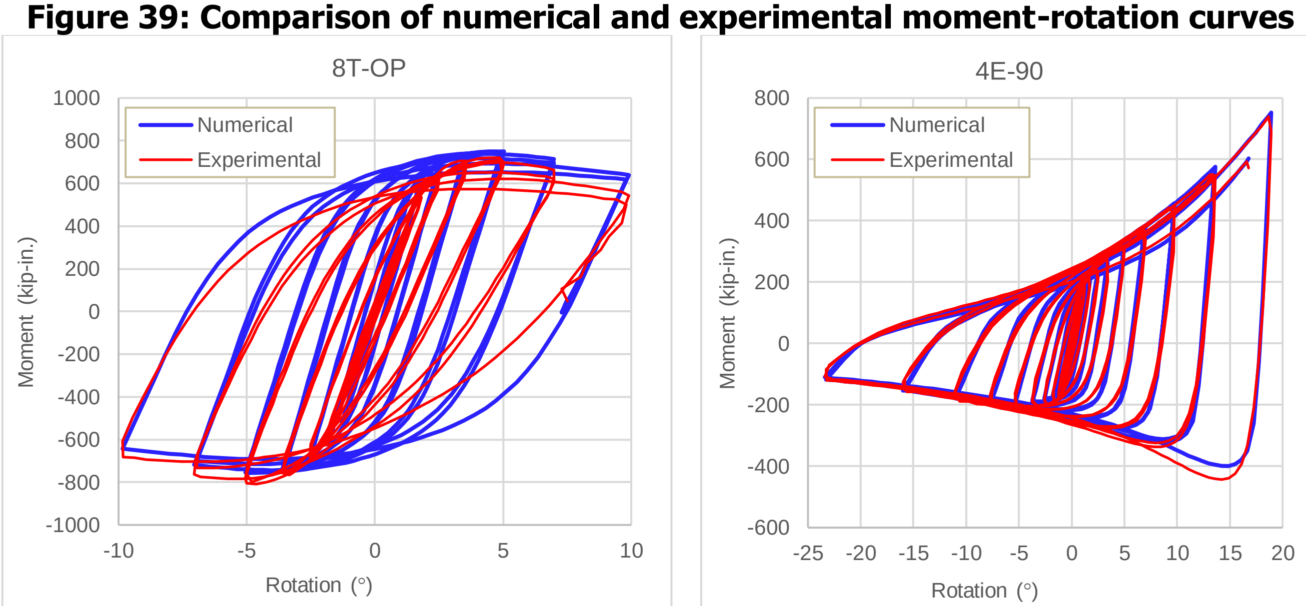

(a) **(b)**

(a) Specimen 8T-IP, (b) Specimen 4E-90

Figure 40: Comparison of numerical and experimental time history of moment

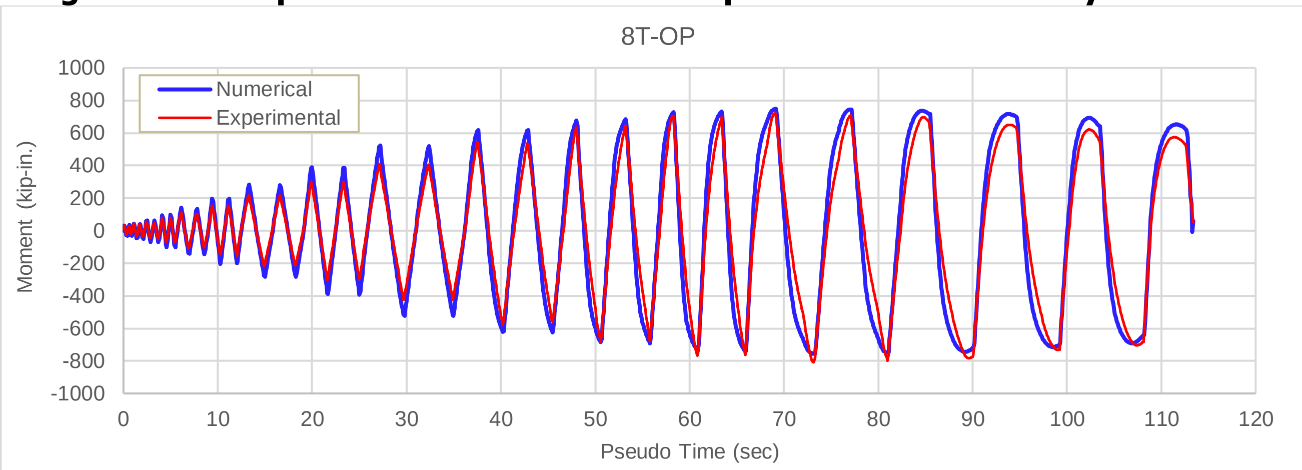

(a)

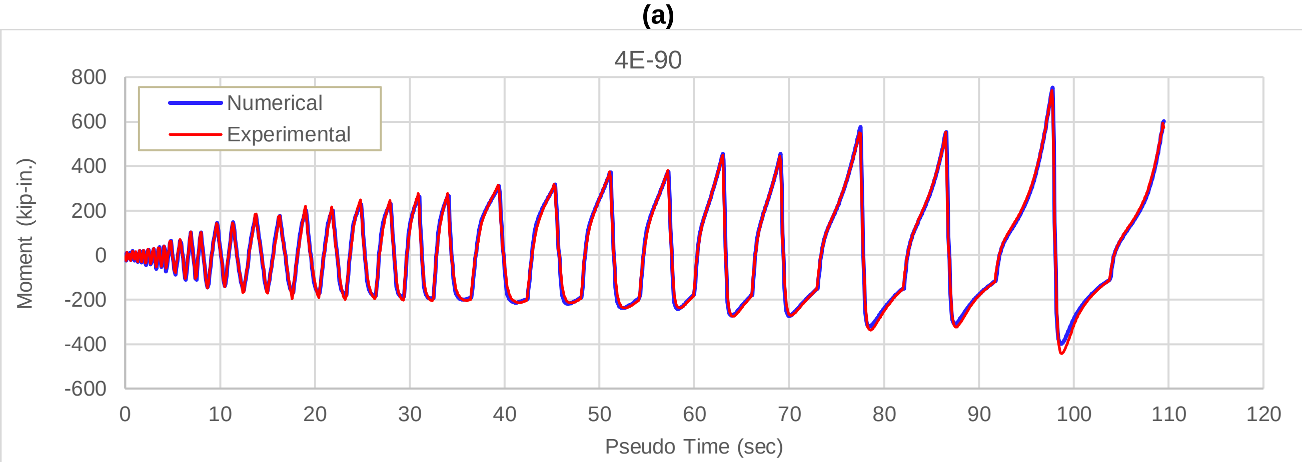

(b)

(a) Specimen 8T-IP, (b) Specimen 4E-90

Validation of Strains

While calibration of the model was performed on the global results of each test (e.g. moment, force and rotation), it was also important to ensure that the numerical model could reliably predict local results, especially in terms of strain. This was particularly relevant since strain is the damage measure utilized for the calculation of fragility curves. Namely, it was crucial for the numerical model to be able to reliably predict strains in the strain range of interest, which was in this case between 1% and 6%.

Strain measure experimentally by uniaxial and rosette strain gauges was compared to the one obtained numerically at the same location. Results were compared in terms of time history and peak strains at each cycle. Sample results for specimen 8T-OP from Pantoli et al. 2022 are presented in this section. Figure 41 shows the location of uniaxial and rosette strain gauges in this specimen. Figure 42 shows sample comparisons in terms of time history. These comparisons are generally good, with the model able to predict the general trend of the strains and predicting the value of strain reasonably. Figure 43a shows that the peak numerical and experimental strain track quite well, while Figure 43b shows that the larger errors in predictions happen at very small and very large strains, while the model can predict the peaks quite well in the range of strain of interest.

Figure 41: Uniaxial (SG) and rosette (R) strain gauges installed in specimen 8T-OP

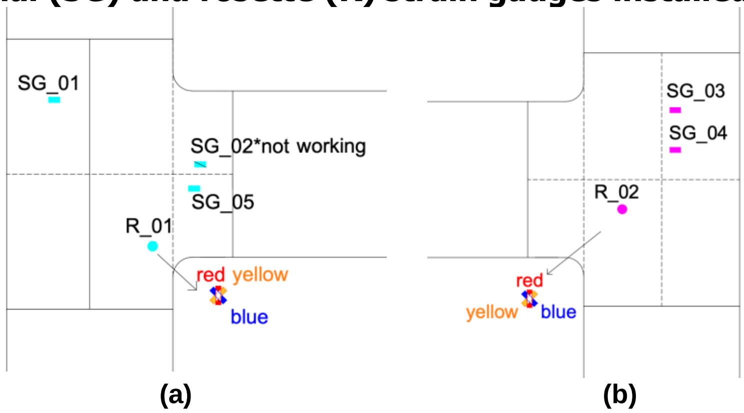

(a) South side, (b) North side

Figure 42: Comparison of time-history of strain for specimen 8T-OP

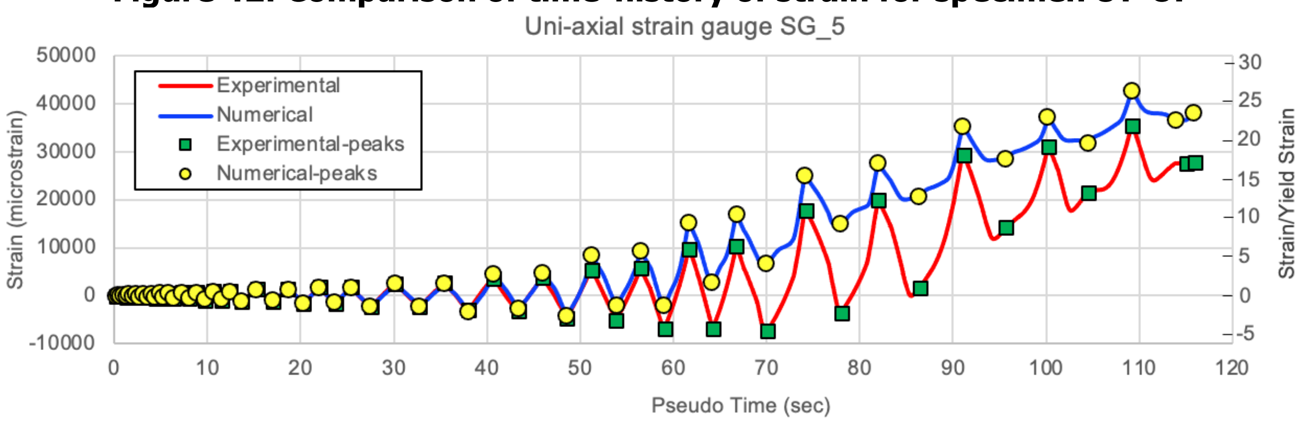

(a)

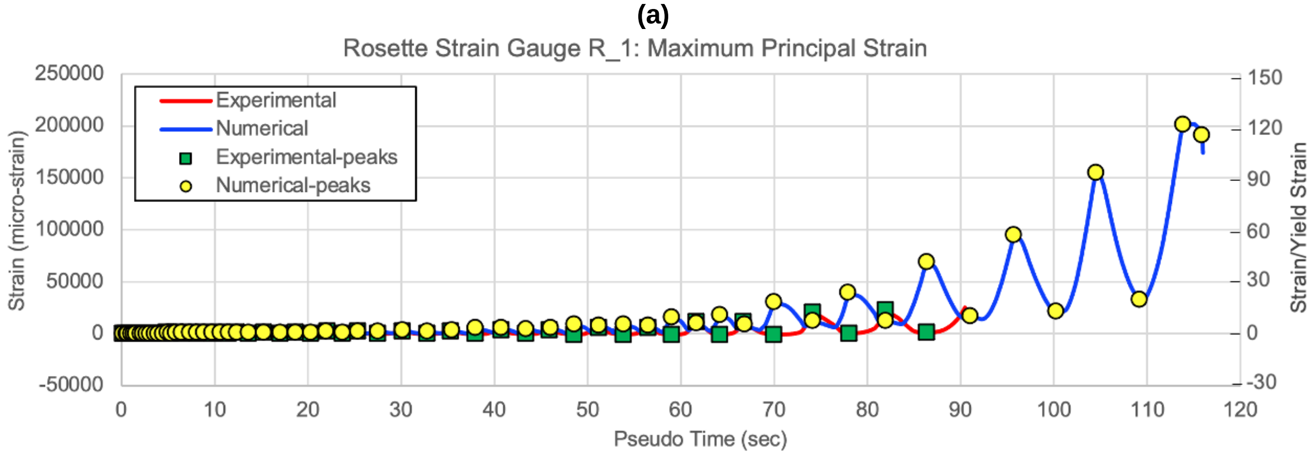

(b)

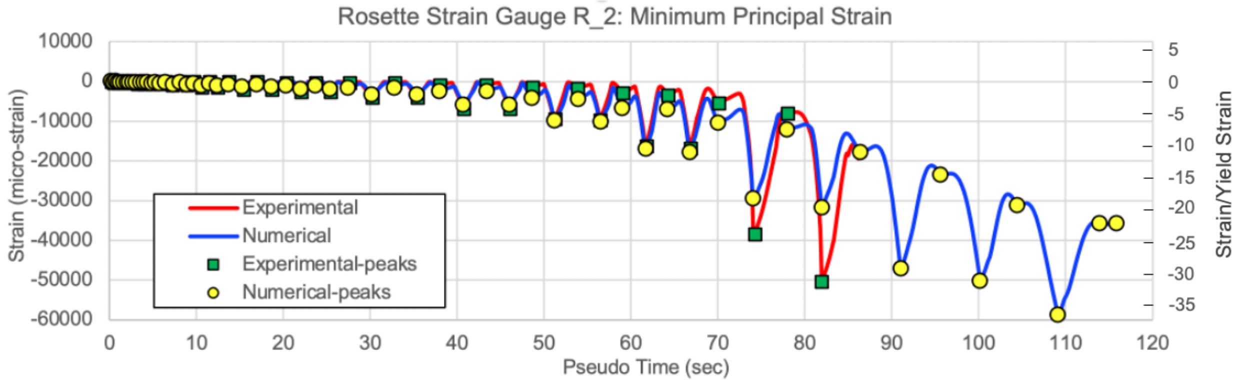

(c)

(a) Sensor SG_5; (b) Maximum principal strains for Sensor R_1; (c) Minimum principal strains for Sensor R_2

Figure 43: Experimental and numerical strain comparison

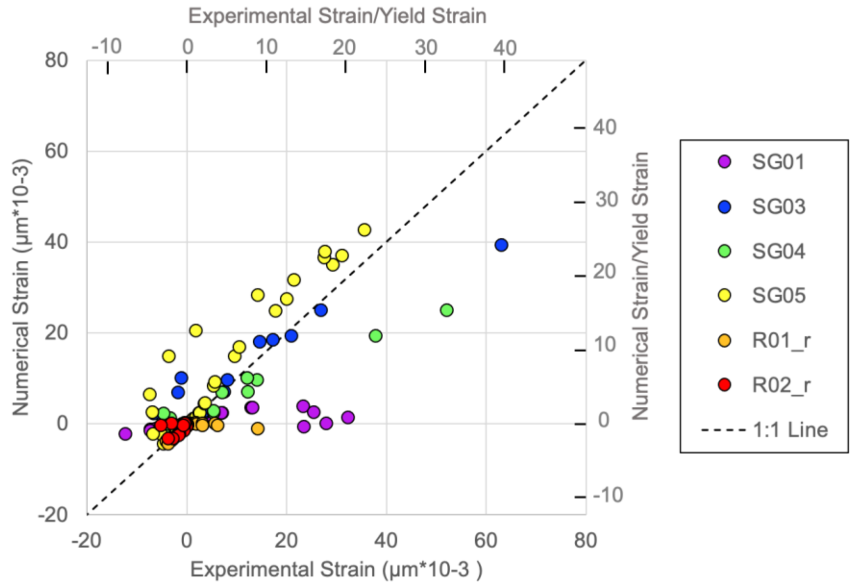

(a)

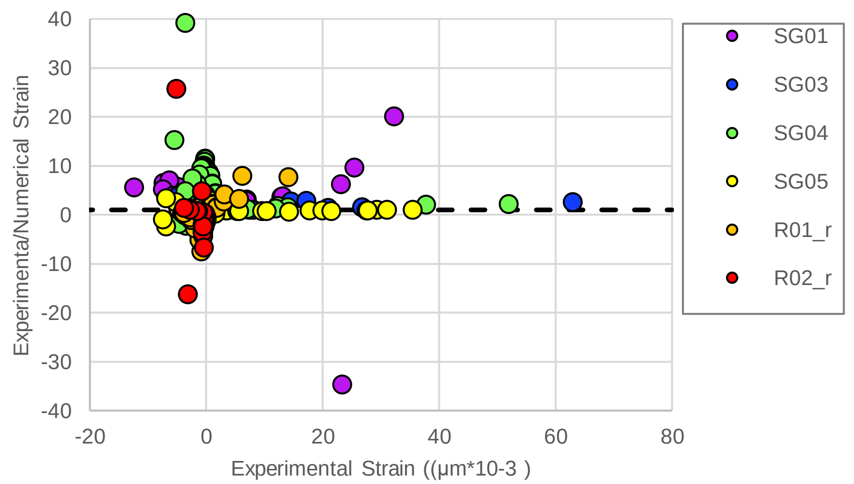

(b)

(a) Numerical strain vs. experimental strain, (b) Experimental/Numerical strain vs. experimental strain

Yield Strength

To find an appropriate average value of the parameter σ_0, mill certificates from a variety of pipes used by manufacturers of gas piping systems were obtained to develop a statistical distribution and guide in the selection of σ_0. The mill certificates obtained by the manufacturers were relative to ASTM 53B and API X42 pipes, which are common types of steel for pipes and pipe fittings used in natural gas facilities. The cumulative distribution of the values of σ_y for the data obtained is shown in Figure 44. The normal distribution had a mean of 52.3 ksi and standard deviation of 8.1 ksi. Hence, a σ_0 of 52.3 ksi was adopted to extend the results in Abaqus. Assuming an elastic modulus E of 29000 ksi, the corresponding ε_y is 0.18%.

Figure 44: Cumulative distribution of σ_y

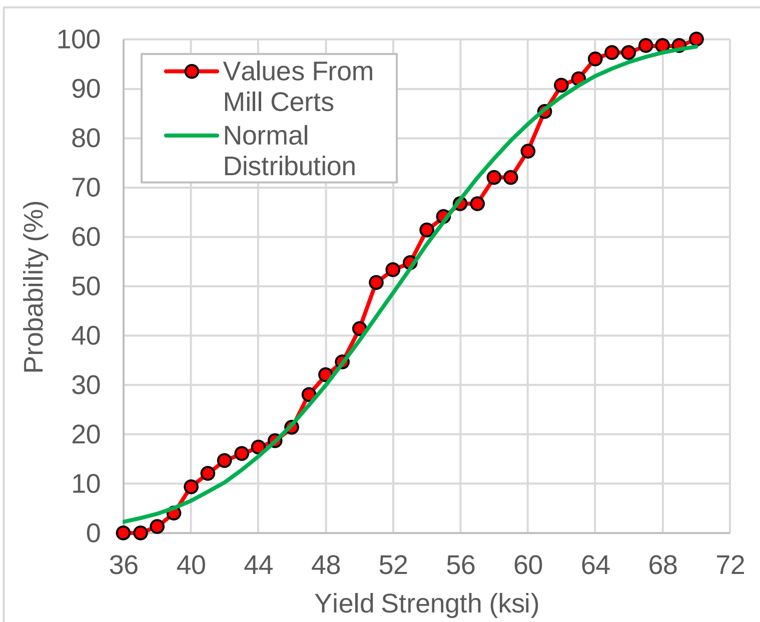

Extension of the Results using Abaqus

For 4 in diameter Schedule 80 pipe, the Abaqus model with the new material properties was analyzed considering the components and loading conditions shown in Table 8. Results from these models lead to the following conclusions:

- The moment-rotation curves of these components obtained at no pressure and 1500 psi pressure were similar, as shown in Figure 45a. This is attributed to the small diameter-thickness ratio of this particular type of pipe. However, the relationship between strain and rotation was impacted at the varied internal pressures as shown in Figure 45b.
- When an elbow was loaded out-of-plane, plasticity concentrated at the base of the specimen instead of in the elbow itself. For this reason, elbow deforming out-of-plane are not considered critical nonlinear components and thus modeled as springs in the OpenSees model.

Table 8: Component and load conditions modeled in Abaqus for 4 in Schedule 80 pipes

Component	Boundary Condition	Direction of Loading	Internal pressure
Tee	Reflecting those observed in the field for piping connected to wellhead trees, as shown in Figure 28	In-plane	0 psi
			1500 psi
		Out-of-plane	0 psi
			1500 psi
90° elbow	Pin-pin	In-plane	0 psi
			1500 psi
	Fix at the base with load applied at the other edge	Out-of-plane	0 psi
			1500 psi

Figure 45: Comparison of results at high and no pressure for 4T-IP

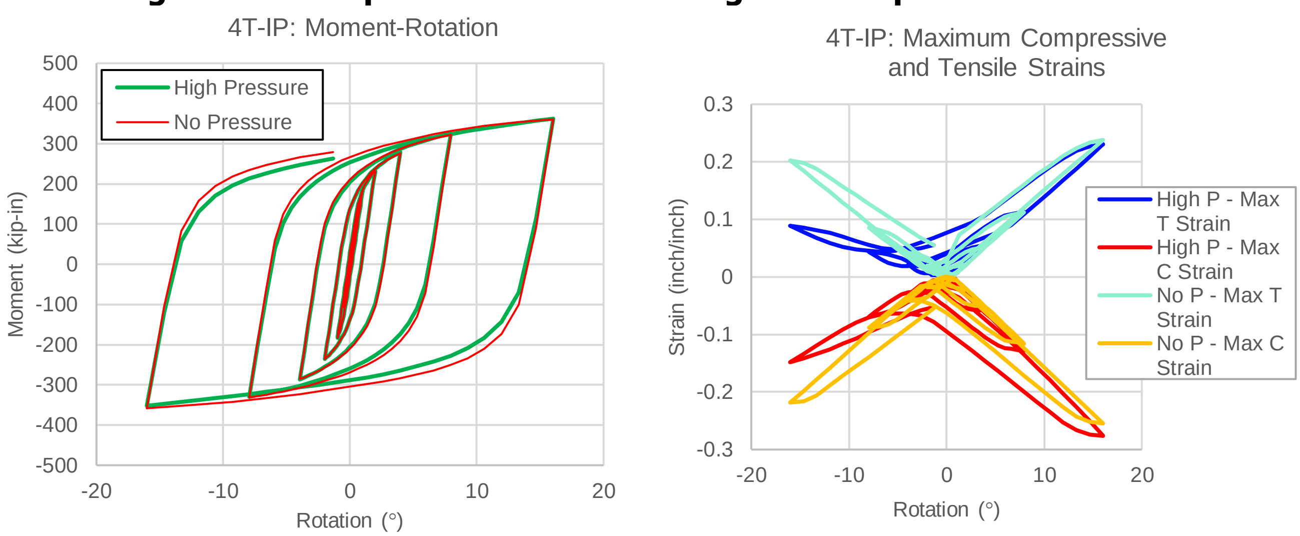

(a) **(b)**

(a) Moment-rotation curve, (b) Strain vs. rotation (Note: P=pressure; T=tensile; C=compressive)

Outcome #4: Seismic Analysis of Nonlinear Subsystems

Validation of the WTP Subsystem

Impact tests on two WTPs at a natural gas storage field in California were performed. This section focuses on presenting the results for the WTP whose configuration is shown in Figure 46. Impact tests on this WTP were performed at two locations and directions: the tree was hit in the X direction at different heights, and the pipe was hit in the Y direction. Table 9 shows the experimental natural frequencies measured in the X and Y directions, while Figure 47 presents corresponding numerical modes and frequencies.

Figure 46: WTP on which impact tests were performed

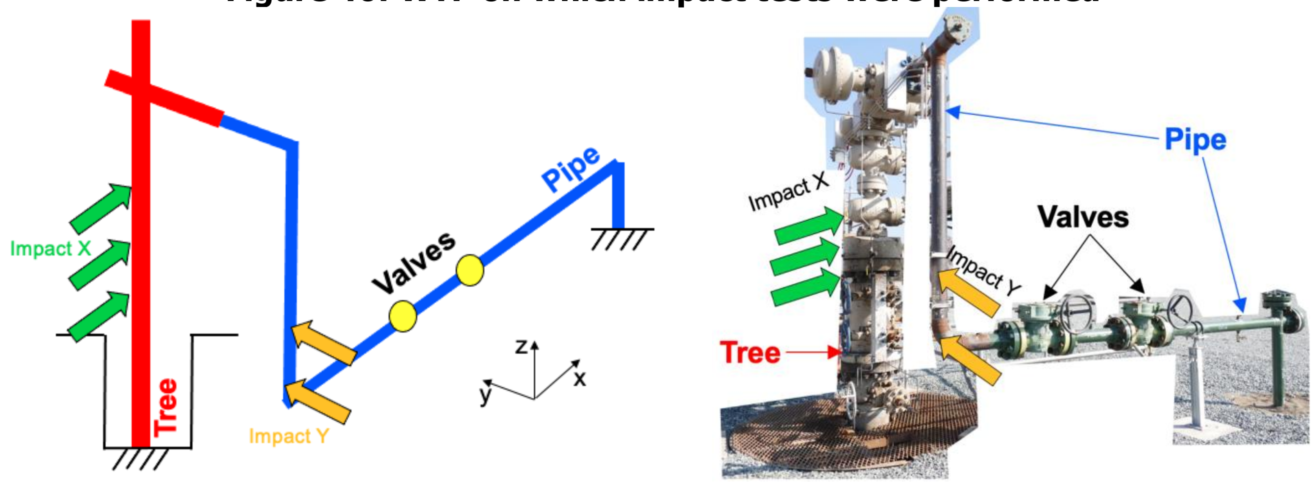

(a) (b)

(a) Schematic, (b) Photograph

Table 9: Natural frequencies measured on the WTP tested at a gas storage facility

Impact Location, Direction	Natural Frequency (Hz)		
Pipe, Y direction	5.8	22.4	62.7
Tree, X direction	19.8	37.5	N/A

Figure 47: Natural modes of a wellhead at a gas storage facility predicted by OpenSees

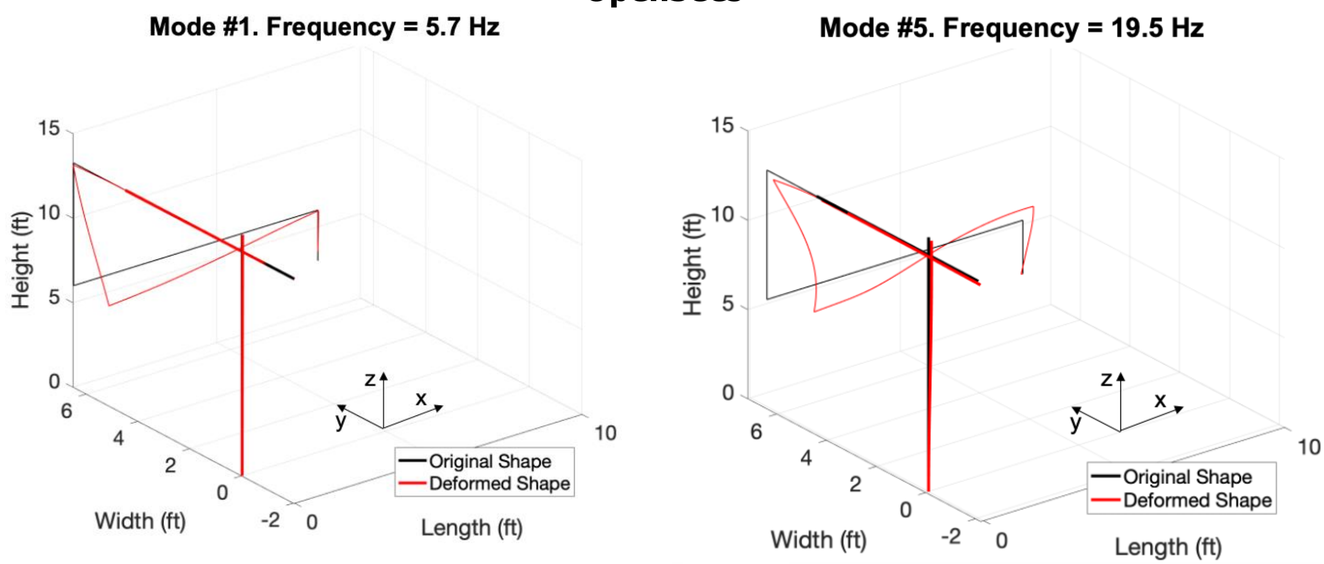

(a) (b)

(a) First mode, (b) Fifth mode

The first fundamental experimental frequency in the Y direction was identified as 5.8 Hz. The OpenSees model predicts a mode at 5.7 Hz whose shape is characterized mainly by a movement of the pipe in the Y direction. The first experimental frequency in the X direction was at 19.8 Hz. At a very similar frequency (19.5 Hz), the OpenSees model predicts a natural mode involving mainly the movement of the pipe in the X direction. It is noted that that this model is the fifth one predicted by the OpenSees model, meaning that the impact tests were not able to activate some of the modes of the system.

Validation of the VPV Subsystem

For the validation of this subsystem, a sample VPV geometry was selected based on representative information of a pressure vessel provided by a gas company in California. This sample VPV was modeled with a high-fidelity 3D FE model using Abaqus and complimentary but simplified linear version utilizing 1D finite elements within OpenSees. Both models included a representation of the skirt, pipes, bolted flange joints and valves and both models were fixed at the base of the skirt. In the OpenSees model, the pressure vessel was represented by a cantilever beam, and pipes with linear beam elements. Bolted flange joints and valves were considered as lumped masses. The first four natural modes and frequencies predicted by the two models are presented in

Table 10, while

Figure 48 and (a) From OpenSees, (b) from Abaqus

Figure 49 compare the natural mode shapes of the first and third mode, respectively. These results show that:

- The movement of the pressure vessel itself is not affected by the movement of the pipes. In fact, the local mode of the long vertical segment of the pipe seem not to affect the movement of the pressure vessel.
- The inlet pipe connected to the bottom of the pressure vessels has minimal movement in these lower frequency modes.
- The simplified Opensees model can capture the behavior of this subsystem predicted by the more refined Abaqus model.

Table 10: Comparison of natural frequency of the sample pressure vessel from Abaqus and Opensees

Mode #	Description of the Mode	Natural frequency in Abaqus (Hz)	Natural frequency in Opensees (Hz)	Difference (%)
1	Lateral translation of the vessel and vertical segment of the pipe	7.8	7.8	0
2	Lateral translation of the vessel and vertical segment of the pipe	8.5	8.6	1.2
3	Lateral translation of the vertical segment of the pipe	11.6	11.8	1.7

Mode #	Description of the Mode	Natural frequency in Abaqus (Hz)	Natural frequency in Opensees (Hz)	Difference (%)
4	Lateral translation of the vertical segment of the pipe	12.8	14.6	14.0

Figure 48: First mode of the sample pressure vessel and connected piping subsystem

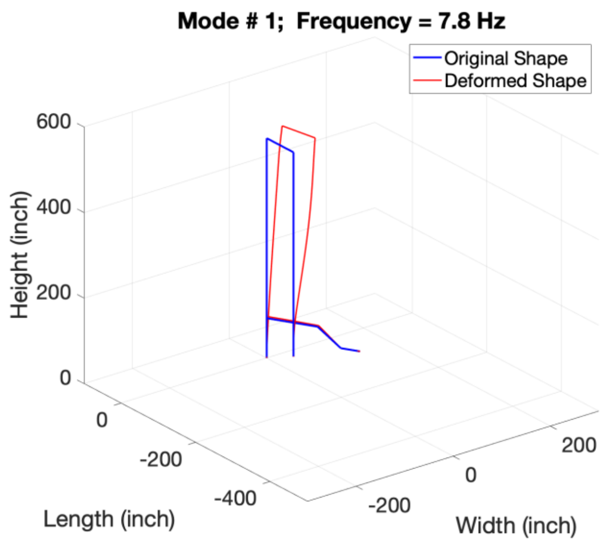

(a)

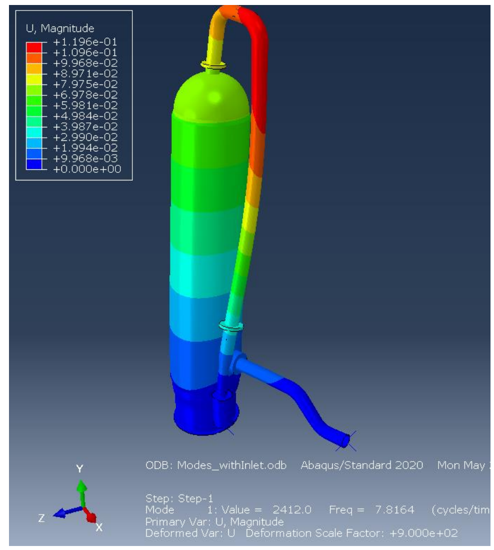

(b)

(a) From OpenSees, (b) from Abaqus

Figure 49: Third mode of the sample pressure vessel and connected piping subsystem

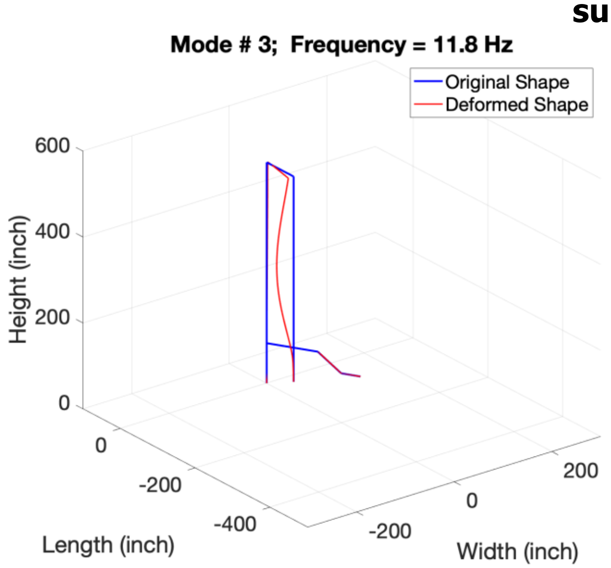

(a)

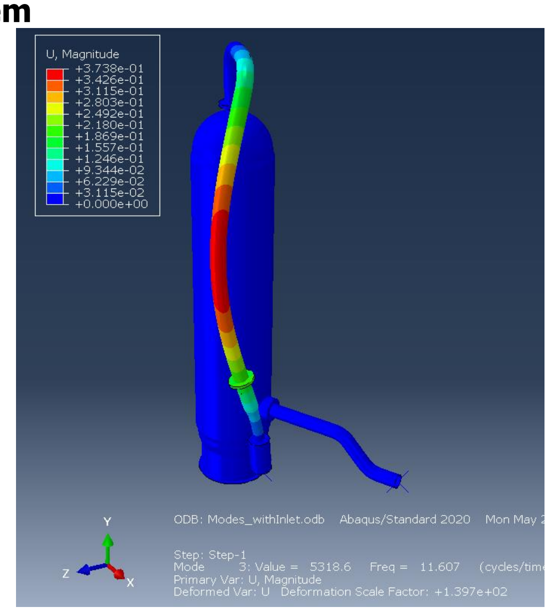

(b)

(a) From OpenSees, (b) from Abaqus

Outcome #5: Fragility Curves for Selected Subsystem Geometry

The final fragility functions developed for outcome #5 will be presented in the System Wide Natural Gas Infrastructure Response and Fragility Report. The present report includes the DM(EDP) curves developed for the WTP subsystems to offer an example of the procedure and outcome.

WTP Subsystem - DM(EDP) Functions

A sample of the DM(EDP) curves developed for 4T-IP at no pressure and high pressure are presented in blue and orange in Where ε is the strain, θ is the rotation, NP stands for No Pressure and HP for High Pressure. A comparison of the two plots in Figure 50 allow to understand the consequence of pressurization on the strain developed in the components. Namely, they show that when the component is pressurized, a smaller rotation is needed to achieve the same level of strain.

Figure 50. These polynomial curves were obtained interpolating the relevant points, as explained in the approach section:

$$\varepsilon_{4T-IP,NP,\theta-} = -0.0011 - 0.0092\theta - 0.0002\theta^2$$

$$\varepsilon_{4T-IP,NP,\theta+} = -0.0003 + 0.0037\theta + 0.0041\theta^2$$

$$\varepsilon_{4T-IP,HP,\theta-} = -0.0006 - 0.0061\theta + 0.0028\theta^2$$

$$\varepsilon_{4T-IP,HP,\theta+} = +0.00004 + 0.0021\theta + 0.0121\theta^2$$

Where ε is the strain, θ is the rotation, NP stands for No Pressure and HP for High Pressure. A comparison of the two plots in Figure 50 allow to understand the consequence of pressurization on the strain developed in the components. Namely, they show that when the component is pressurized, a smaller rotation is needed to achieve the same level of strain.

Figure 50: DM(EDP) curves for 4T-IP

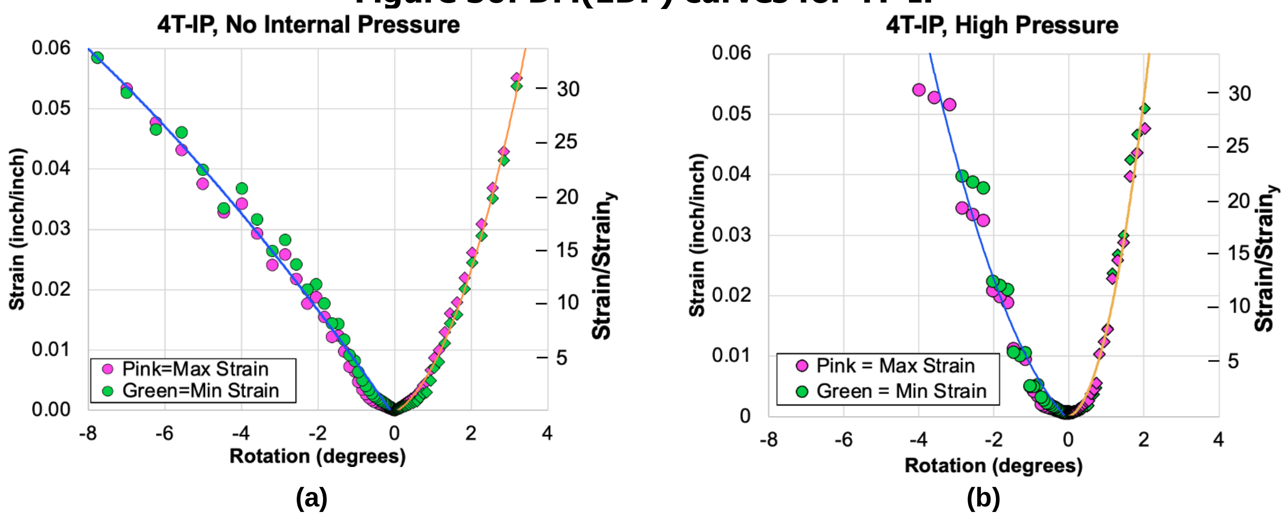

(a) No internal pressure, (b) High internal pressure

CHAPTER 4: Conclusions/Recommendations

Task Group D performed experimental campaigns and numerical analyses on select key components and subsystems of the natural gas infrastructure. These were identified in collaboration with a Technical Advisory Committee (TAC), which included members of the California Energy Commission and stakeholders from SoCalGas and PG&E. Fragility curves to be implemented in *OpenSRA* were subsequently generated utilizing both high fidelity and simplified parametric finite element models of components and subsystems developed Abaqus and OpenSees, respectively. These will be published in the System Wide Natural Gas Infrastructure Response and Fragility Model Report, later this year. These models were calibrated and validated using laboratory experimental programs at UC San Diego and complementary field tests performed at a gas storage facility in California.

The key conclusions of this study include most notably the following:

- Tees and elbows generally exhibit ductile behavior and fail at relatively large rotations. However, during the experiments performed at UC San Diego, one of the components observed a nominally abrupt failure at a much lower rotation capacity than all other specimens. This type of failure may have catastrophic consequences because it does not present ample warning and it is not as easily predicted using commercial finite element analysis software.
- Piping subsystems are not particularly acceleration sensitive, but rather are sensitive to damage induced by relative displacement. Any subsystem containing components that can have a relative displacement from each should be carefully evaluated. This may occur for example in the case of pipes connected to the ground and to an elevated platform, or when pipes are supported by a flexible pipe rack.
- The subsystems created by the wellhead tree and the piping connected are resilient to seismic damage. However, certain configurations and geometries could be more vulnerable to seismic damage.
- Tanks and pressure vessels can be sensitive to ground acceleration, since large forces at the base may be observed.
- High fidelity finite element models created in Abaqus using the calibrated nonlinear steel properties back estimated from experiments conducted in this project observed reliable and accurate prediction of the cyclic behavior of steel components, notably steel tee and elbow joints.

While the present task contributes to advancing the state of knowledge and practice of the seismic analysis of surface gas infrastructure, a number of recommendations for future researchers are evident. Most notably:

- Utility of the unique database of dynamic shake table test results obtained during the subsystem tests performed at UNR. These tests offer invaluable data upon which system-level numerical models can be evaluated.
- Expansion of the experimental evaluation of surface infrastructure components beyond those within the component test program at UCSD. For example, small diameter pipes are readily utilized within the surface infrastructure and thus similar cyclic component tests would be valuable to advancing knowledge regarding the seismic behavior of such components.
- Additional investigations of surface subsystems where large relative seismic displacement is expected. For example, natural gas pipelines crossing rivers above ground, though as noted not as common, still pose risks to failure of the system during in the event of large relative movement of for example a supporting bridge. Such investigations could be readily performed using numerical parametric studies.
- As noted, the present study was focused on a subset of the most critical components of the surface infrastructure in an effort to develop the research methodology while also contributing to the development of seismic fragility curves for such systems. Additional analysis of select surface components of the distribution system are warranted, most notably vertical risers and meter sets are prevalent throughout the distribution system and thus advancing understanding of their seismic vulnerability is essential.

GLOSSARY AND LIST OF ACRONYMS

Term	Definition
Abaqus	FEA software (Smith, 2009)
Accelerometer	A sensor for measuring acceleration
ACI	American Concrete Institute
AGA	American Gas Association
API	American Petroleum Institute
ASTM	American Society for Testing and Materials
b	Material parameter for isotropic hardening
b_k	Hardening Ratio
C	Material parameter for kinematic hardening
CEC	California Energy Commission
City Gates	A type of M&R station in between transmission and distribution lines
Component	Individual parts of a subsystem. For example: a pressure vessel, straight pipes, elbows, tees, reducers, bolted flange joints.
CPUC	California Public Utility Commission
CSSC	California Seismic Safety Commission
DIC	Digital Image Correlation
Distribution pipeline	Low-pressure pipeline delivering natural gas to users
DM	Damage Measure
DoC	Department of Conservation
DoT	Department of Transportation
E	Modulus of elasticity (or Young modulus)
E_0	Initial stiffness
EDP	Engineering Design Parameter
EIA	Energy Information Administration
Elbow	A pipe fitting installed between two lengths of pipe or tubing to allow a change of direction, usually a 90° or 45° angle
EPA	Environmental Protection Agency

Term	Definition
FEA	Finite Element Analysis
FEMA	Federal Emergency Management Agency
f_u	Ultimate strength
f_y	Yield strength
HP	High pressure
HSS	Hollow structural steel
H_t	Height of the wellhead tree
Hz	Hertz
IM	Intensity Measure
IP	In-plane
LBNL	Lawrence Berkeley National Laboratory
LCI	Lettis Consultants International
L_p	Length of the pipe
LVDT	Linear variable differential transformer. An electromechanical sensor that transforms mechanical motion to displacement
M&R	Metering and pressure Regulating stations
Moment	Force multiplied by distance arm
NHERI	Natural Hazards Engineering Research Infrastructure
NP	No pressure
OP	Out-of-plane
OpenSees	Opensource software for seismic analysis (Mazzoni et al. 2006)
OSHA	Occupational Safety and Health Administration
PEER	Pacific Earthquake Engineering Research Center
PG&E	Pacific Gas and Electric Company
PSA	Pseudo Spectral Acceleration
PVP	Pressure Vessels and Piping
Q	Material parameter for isotropic hardening
R_0	Hardening parameter for Steel4 material in OpenSees
r_1	Hardening parameter for Steel4 material in OpenSees

Term	Definition
r_2	Hardening parameter for Steel4 material in OpenSees
R^2	Goodness-of-fit parameter
Reducer	A fitting that connects pipes of different sizes
RMS	Root Mean Square
Rot_OS	Rotation obtained by OpenSees
Rot_P	Rotation obtained by predicting equations
Service risers	Vertical pipes connecting the service laterals to the meter set
SG	Strain Gauge
Shake table	A special equipment that can simulate ground motions similar to earthquakes
Storage field	Area dedicated to store natural gas
Storage field facility	Facility for the processing of natural gas in storage fields
Straight tee	Tee where the three connected pipes have the same diameter (also known as equal tee, equivalent tee)
Strain	A number that describes relative deformation
Subsystem	Part of a system that can be analyzed as a unit from a dynamic standpoint but it cannot function as a unit.
System	Part of the facility that can perform a specific function.
Tee	A T-shaped pipe fitting with three openings used to combine or divide fluid flow (also known as T-joint/ tee joint/ tee fitting)
Transmission pipelines	High-pressure pipeline transporting natural gas along large distances
Valve	Element of the system used to regulate flow
UC Berkeley	University of California - Berkeley
UC San Diego	University of California, San Diego
UMEC	University Mechanical and Engineering Contractors, a piping manufacturer
UNR	University of Nevada, Reno
White noise	Random signal having equal intensity at different frequencies
WTP	Wellhead Tree and Piping

Term	Definition
Δ_0	Initial displacement
Δ_m	Target displacement
ε_u	Ultimate strain
ε_y	Yield strain
γ	Material parameter for kinematic hardening
μ	Mean
θ	Rotation
σ	Standard deviation
σ_0	initial yield stress
σ_y	yield stress

REFERENCES

Abbiati G., Bursi O. S., Caracoglia L., Di Filippo R., and La Salandra, V. (2016). Probabilistic Seismic Response of Coupled Tank-Piping Systems. Pressure Vessels and Piping Conference, 50466 (V008T08A015), doi: 10.1115/PVP2016-63292.

ACI-318 (2019). Building Code Requirements for Structural Concrete and Commentary. American Concrete Institute, doi: 10.14359/51716937.

AGA (n.d.). Natural Gas Delivery System Material. American Gas Association. Retrieved March 22, 2022, from https://www.aga.org/natural-gas/delivery/natural-gas-delivery-system-materials-/.

Bursi O. S., Reza M. S., Abbiati G., and Paolacci F. (2015). Performance-based earthquake evaluation of a full-scale petrochemical piping system. Journal of Loss Prevention in the Process Industries, 33 (10-22), doi: 10.1016/j.jlp.2014.11.004.

Butenweg C., Bursi O. S., Paolacci F., Marinković M., Lanese I., Nardin C., and Quinci G. (2021). Seismic performance of an industrial multi-storey frame structure with process equipment subjected to shake table testing. Engineering Structures, 243(112681), doi: 10.1016/j.engstruct.2021.112681.

Cademartori M., Morassi C., Siano R., Faravelli M., and Brunesi E. (2019). Seismic risk analysis of pressure vessels. Feb-fresenius Environmental Bulleting, 1025.

Chatziioannou K., Huang Y., and Karamanos S. A. (2021). Simulation of Cyclic Loading on Pipe Elbows Using Advanced Plane-Stress Elastoplasticity Models. Journal of Pressure Vessel Technology, 143(2), doi: 10.1115/1.4047876.

Chen W., Haroun M. A., and Liu F. (1996). Large amplitude liquid sloshing in seismically excited tanks. Earthquake engineering & structural dynamics, 25-7(653-669), doi: 10.1002/(SICI)1096-9845(199607)25:7<653::AID-EQE513>3.0.CO;2-H.

Clough D. P. (1977). Experimental evaluation of seismic design methods for broad cylindrical tanks. PhD Thesis, University of California, Berkeley.

Cornell, C.A. (1968), Eng Seis Risk Analysis, Bull. Seismo. Soc. Am., V58(5), 1583-1606, doi: 10.1785/BSSA0580051583.

CPUC (n.d.). Natural Gas and California. California Public Utility Commission. Retrieved March 10, 2022, from https://www.cpuc.ca.gov/industries-and-topics/natural-gas/natural-gas-and-california.

CSSC (2002). Improving Natural Gas Safety in Earthquakes. California Seismic Safety Commission. Retrieved April 7, 2022, from https://ssc.ca.gov/wp-content/uploads/sites/9/2020/08/cssc_2002-03_natural_gas_safety.pdf.

D'Amico M., and Buratti N. (2019). Observational seismic fragility curves for steel cylindrical tanks. Journal of Pressure Vessel Technology, 141(1), doi: 10.1115/1.4040137.

Di Carluccio A., Fabbrocino G., Salzano E., and Manfredi G. (2008). Analysis of pressurized horizontal vessels under seismic excitation. 18th The World Conference on Earthquake Engineering.

Di Filippo R., Abbiati G., Sayginer O., Covi P., Bursi O. S., and Paolacci F. (2019). Numerical surrogate model of a coupled tank-piping system for seismic fragility analysis with synthetic ground motions. Pressure Vessels and Piping Conference, 59018(V008T08A029).

DoC (n.d.). Underground Natural Gas Storage. Department of Conservation. Retrieved March 10, 2022, from https://www.conservation.ca.gov/calgem/Pages/UndergroundGasStorage.aspx.

EIA (2022). Underground Natural Gas Working Storage Capacity. Energy Information Administration. Retrieved March 10, 2022, from https://www.eia.gov/naturalgas/storagecapacity/.

EIA (2021). California State Energy Profile. Energy Information Administration. Retrieved March 10, 2022, from https://www.eia.gov/state/analysis.php?sid=CA#114.

EIA (2007). Natural Gas Compressor Stations on the Interstate Pipeline Network: Developments Since 1996. Energy Information Administration. Retrieved March 10, 2022, from https://www.eia.gov/naturalgas/archive/ngcompressor.pdf.

Eidinger J. M. (2021) Seismic fragility of natural gas transmission pipelines and wells. – Revision 4. G&E Engineering Systems.

Eidinger J., and Tang A. (2012). Christchurch, New Zealand Earthquake Sequence of Mw 7.1 September 04, 2010 Mw 6.3 February 22, 2011 Mw 6.0 June 13, 2011: Lifeline Performance.

Elfass S., Pantoli E., McCallen D., Hutchinson T. C. (2022). Shake Table Testing of a Surface Natural Gas Piping Subsystem. A Report for the "Performance-based Earthquake Engineering Assessment Tool for Natural Gas Storage and Pipeline Systems" Project. PEER Report 2022/##, Pacific Earthquake Engineering Research Center, University of California, Berkeley, CA.

EPA (2003). Directed Inspections and Maintenance at Gate Stations and Surface Facilities. Environmental Protection Agency. Retrieved March 10, 2022, from https://www.epa.gov/sites/default/files/2016-06/documents/ll_dimgatestat.pdf.

EPA (1996). Methane Emission From the Natural Gas Industry. Environmental Protection Agency. Retrieved March 10, 2022, from https://www.epa.gov/sites/default/files/2016-08/documents/10_metering.pdf.

Eshghi S., and Razzaghi M. S. (2004). The behavior of special structures during the Bam earthquake of 26 December 2003. Journal of Seismology and Earthquake Engineering, 5-4(197-207).

FEMA (2007). FEMA-461 - Interim Testing Protocols for Determining the Seismic Performance Characteristics of Structural and Nonstructural Components. Federal Emergency Management Agency, Washington DC. https://www.atcouncil.org/pdfs/FEMA461.pdf.

Hutabarat, D., O'Rourke, T.D., Bray, J.D., Bain, C., Lindvall, S. (2022). Performance-Based Earthquake Engineering Assessment Tool for Natural Gas Storage and Pipeline Systems, Underground Pipeline Fragilities. Pacific Earthquake Engineering Research (PEER) Center Report, in preparation.

Jaimes M. A., and Candia G. (2018). Toppling of rigid electric equipment during earthquakes. Engineering Structures, 168(229-242), doi: 10.1016/j.engstruct.2018.04.083.

Karamanos S. A. (2016). Mechanical behavior of steel pipe bends: an overview. Journal of Pressure Vessel Technology, 138(4), doi: 10.1115/1.4031940.

Karamanos S. A., Tsouvalas D., and Gresnigt A. M. (2006). Ultimate bending capacity and buckling of pressurized 90 deg steel elbows. Journal of pressure vessel technology, 128-3(348-356), doi: 10.1115/1.2217967.

Karamanos S. A., Giakoumatos E., and Gresnigt A. M. (2003). Nonlinear response and failure of steel elbows under in-plane bending and pressure. Journal of Pressure Vessel Technology, 125-4(393-402), doi: 10.1115/1.1613949.

Korndörfer J., Hoffmeister B., and Feldmann M. (2017). Seismic fragility of horizontal pressure vessels – effects of structural interaction between industrial components. 6th ECCOMAS thematic conference on computational methods in structural dynamics and earthquake engineering.

Krawinkler H., Parisi F., Ibarra L., Ayoub A., and Medina, R. (2001). Development of a testing protocol for woodframe structures, 102. Retrieved April 7, 2022, from https://www.researchgate.net/profile/Ricardo-Medina-3/publication/245911208_Development_of_a_testing_protocol_for_wood_frame_structures/links/5ad91be4458515c60f5a6790/Development-of-a-testing-protocol-for-wood-frame-structures.pdf

La Salandra V., Di Filippo R., Bursi O. S., Paolacci F., and Alessandri S. (2016). Cyclic response of enhanced bolted flange joints for piping systems. Pressure Vessels and Piping Conference , 50466(V008T08A024), doi: 10.1115/PVP2016-63244.

Lund L.V., O'Rourke T.D., Cooper T., Matsuda E., Tang A., Pickett M, Edwards C., Hayden B., and Strand C. (1995) Lifelines. Earthquake Spectra, 11_supplement2(143-244).

Mazzoni S., McKenna F., Scott M. H., and Fenves G. L. (2006). OpenSees command language manual. Pacific Earthquake Engineering Research (PEER) Center, 264, 137-158.

McMaster Carr. (n.d.). Retrieved on April 7, 2022, from https://www.mcmaster.com/tees/shape~tee/material~steel/connection-style~butt-weld/pipe-size~4/schedule~80/.

Moslemi M., and Kianoush M. R. (2012). Parametric study on dynamic behavior of cylindrical ground-supported tanks. Engineering Structures, 42(214-230), doi: 10.1016/j.engstruct.2012.04.026.

Moss D. R., and Basic M. (2012). Pressure vessel design manual. Doi: https://doi.org/10.1016/C2010-0-67103-3

Nakamura I. (2019). Numerical Investigation on Strength of Tee Pipes Under In-Plane/Out-of-Plane Cyclic Loading. Pressure Vessels and Piping Conference, 59018(V008T08A027), doi: 10.1115/PVP2019-93559.

Nakamura I., and Kasahara N. (2017). Excitation tests on elbow pipe specimens to investigate failure behavior under excessive seismic loads. Journal of Pressure Vessel Technology, 139(6), doi: 10.1115/1.4037952.

Nakamura I. (2013). Seismic safety capacity of a piping system with pipe supports based on the shake table test. Pressure Vessels and Piping Conference, 55744(V008T08A029), doi: 10.1115/PVP2013-97852.

O'Rourke M. J., and So P. (2000). Seismic fragility curves for on-grade steel tanks. Earthquake spectra, 16-4(801-815), doi: 10.1193/1.1586140.

OSHA (n.d.). Pressure Vessels. Occupational Safety and Health Administration. Retrieved March 28, 2022, from https://www.osha.gov/pressure-vessels.

Pantoli E., Hutchinson T. C., Elfass S., McCallen D., (2022). Cyclic tests on steel tees and elbows. A Report for the "Performance-based Earthquake Engineering Assessment Tool for Natural Gas Storage and Pipeline Systems" Project. PEER Report 2022/##, Pacific Earthquake Engineering Research Center, University of California, Berkeley, CA.

Papatheocharis T., Diamanti K., Varelis G. E., Perdikaris P. C., and Karamanos S. A. (2013). Experimental and numerical investigation of pipe T-junctions under strong cyclic loading. Pressure Vessels and Piping Conference, 55744 (V008T08A017), doi: 10.1115/PVP2013-97626.

Payne T. (2000). Nonlinear behavior of steel beams. Dam Safety Office, Department of the Interior, Bureau of Reclamation.

Rockpoint Gas Storage. Lodi. Retrieved March 2021, from https://www.rockpointgs.com/Businesses/Lodi

Rongere F., Eimon F. (2019) Quantification of Methane Emissions from M&R Stations. Retrieved March 10, 2022, from https://www.gti.energy/wp-content/uploads/2019/09/CH4-14-Sept18-Ford-Eimon-Presentation.pdf.

Ryu H. W., Kim H. T., Kim Y. J., and Kim J. W. (2018). Determination of combined hardening parameters to simulate deformation behavior of C (T) specimen under cyclic loading. Procedia Structural Integrity, 13(1932-1939), doi: 10.1016/j.prostr.2018.12.268.

Sall J., Stephens M. L., Lehman A., and Loring S. (2017). JMP start statistics: a guide to statistics and data analysis using JMP. Sas Institute.

Smith M. (2009). Abaqus/Standard User's Manual, Version 6.9.

SoCalGas (2017). Good neighbors and gas storage. Retrieved March 29, 2022, from https://www.youtube.com/watch?v=Tv5rNPCQPjM.

SoCalGas (2017b). SoCalGas - Safety Enhancements with Infrared Fence-line Monitoring. Retrieved July, 14, 2022 from https://www.youtube.com/watch?v=tTEaDXJunTw.

SoCalGas (2016a). Well Inspection at Aliso Canyon Storage Facility. Retrieved March 10, 2022, from https://www.youtube.com/watch?v=mTRlZkWD3VE&list=PL6NB0IZNGUDti_qSc1898lFRlhULOHeHo&index=30.

SoCalGas (2016b). How Underground Natural Gas Storage Works. Retrieved March 17, 2022, from https://www.youtube.com/watch?v=3FSMpCazwUA.

Suzuki K. (2008). Earthquake damage to industrial facilities and development of seismic and vibration control technology. Journal of System design and dynamics, 2-1(2-11), doi: 10.1299/jsdd.2.2.

US DoT (2018). Underground natural gas storage: geologica formations. Retrieved June 24, 2022 from https://www.phmsa.dot.gov/pipeline/underground-natural-gas-storage/pictures.

US DoT (n.d.). Natural gas pipeline systems. U.S. Department of Transportation. Retrieved March 16, 2022, from https://primis.phmsa.dot.gov/comm/NaturalGasPipelineSystems.htm?nocache=8431.

Varelis G. E., Karamanos S. A., and Gresnigt A. M. (2013). Pipe elbows under strong cyclic loading. Journal of Pressure Vessel Technology, 135(1), doi: 10.1115/1.4007293.

Wang C., Hubbard P.; Xu T., and Soga K. (2022). Performance-Based Earthquake Engineering Assessment Tool for Natural Gas Storage and Pipeline Systems, Task 4E Final Report – Sensor and Monitoring Technologies. California Energy Commission. Publication Number: CEC-500-202X-XXX.

Watakabe T., Tsukimori K., Otani A., Moriizumi M., and Kaneko N. (2014). Study on Strength of Thin-Walled Tee Pipe for Fast Breeder Reactors Under Seismic Loading. Pressure Vessels and Piping Conference, 46070(V008T08A032), doi: 10.1115/PVP2014-28619.

Wieschollek M., Hoffmeister B., and Feldmann M. (2013). Experimental and numerical investigations on nozzle reinforcements. Pressure Vessels and Piping Conference, 55744(V008T08A014), doi: 10.1115/PVP2013-97430.

Wieschollek M., Diamanti K., Pinkawa M., Hoffmeister B., and Feldmann M. (2013). Guidelines for seismic design and analysis of pressure vessels. Pressure Vessels and Piping Conference, 55744(V008T08A015), doi: 10.1115/PVP2013-97435.

Witt P. (2018). Health concerns about Playa Del Rey gas storage facility. Retrieved March 14, 2022, from https://www.thecorsaironline.com/corsair/2018/5/9/locals-raise-concerns-about-playa-del-rey-gas-storage-facility.

Yokel F. Y., and Mathey R. G. (1992). Earthquake resistant construction of gas and liquid fuel pipeline systems serving, or regulated by, the Federal Government (No. FEMA 233). Retrieved April 7, 2022, from https://nehrpsearch.nist.gov/static/files/NIST/PB94161999.pdf.

Yoshizaki K., Hamada M., and O'Rourke T. D. (2000). Large deformation behavior of low-angle pipeline elbows subjected to in-plane bending. 12th World conference on earthquake engineering, paper, 1508.

Zakavi S. J., Shiralivand B., and Nourbakhsh M. (2017). Evaluation of combined hardening model in ratcheting behavior of pressurized piping elbows subjected to in-plane moments. Journal of Computational & Applied Research in Mechanical Engineering, 7-1(57-71), doi: 10.22061/JCARME.2017.640.

Zsarnoczay, Adam. (2015). Steel4 Material. Obtained March 18, 2022, from https://opensees.berkeley.edu/wiki/index.php/Steel4_Material.